Durability Aspects of Polymer Electrolyte Membrane Fuel Cells

Dissertation Author: Vijay Anand Sethuraman, University of South Carolina (2006)

Abstract

In order for the successful adoption of proton exchange membrane (PEM) fuel cell technology, it is imperative that durability is understood, quantified and improved. A number of mechanisms are known to contribute to PEMFC membrane electrode assembly (MEA) performance degradation. In this dissertation, we show, via experiments, some of the various processes that degrade the proton exchange membrane in a PEM fuel cell; and catalyst poisoning due to hydrogen sulfide (H_2S) and siloxane.

The effect of humidity on the chemical stability of two types of membranes, [i.e., perfluorosulfonic acid type (PFSA, Nafion® 112) and biphenyl sulfone hydrocarbon type, (BPSH-35)] was studied by subjecting the MEAs to open-circuit voltage (OCV) decay and potential cycling tests at elevated temperatures and low inlet gas relative humidities. The BPSH-35 membranes showed poor chemical stability in *ex situ* Fenton tests compared to that of Nafion® membranes. However, under fuel cell conditions, BPSH-35 MEAs outperformed Nafion® 112 MEAs in both the OCV decay and potential cycling tests. For both membranes, (i) at a given temperature, membrane degradation was more pronounced at lower humidities and (ii) at a given relative humidity operation, increasing the cell temperature accelerated membrane degradation. Mechanical stability of these two types of membranes was also studied using relative humidity (RH) cycling.

Hydrogen peroxide (H_2O_2) formation rates in a proton exchange membrane (PEM) fuel cell were estimated by studying the oxygen reduction reaction (ORR) on a rotating ring disc electrode (RRDE). Fuel cell conditions were replicated by depositing a film of Pt/Vulcan XC-72 catalyst onto the disk and by varying the temperature, dissolved O_2 concentration and the acidity levels in $HClO_4$. The $HClO_4$ acidity was correlated to ionomer water activity and hence fuel cell humidity. H_2O_2 formation rates showed a linear dependence on oxygen concentration and square dependence on water activity. The H_2O_2 selectivity in ORR was independent of oxygen concentration but increased with decrease in water activity (i.e., decreased humidity).

Presences of trace impurities (such as CO, H_2S, NH_3, etc.) in the fuel also affect PEMFC durability. Among these impurities, H_2S causes significantly higher performance loss and irreversible catalytic poisoning. A concise mechanism for the poisoning kinetics of H_2S on composite solid polymer electrolyte Pt (SPE-Pt) electrode was validated experimentally by charge balances and theoretically by a model, which predicted the oxidation current as a function of the applied potential. H_2S dissociatively adsorbed onto SPE-Pt electrode as linear and bridge bonded sulfur (S) species and, under favorable potentials, underwent electro-oxidation to sulfur and then to sulfur dioxide (SO_2). Fraction of the adsorbed S species remained as 'hard-to-oxidize' adsorbents and caused irreversible loss of catalytic activity. Deactivation of bridge sites occurred first followed by the loss of linear sites. A method to estimate the catalytic sites irreversibly lost due to sulfur poisoning was developed.

Details

Subject	Chemical engineering; Energy
Classification	0542: Chemical engineering 0791: Energy
Identifier / keyword	Applied sciences; Durability; Fuel cells; Hydrogen peroxide; Hydrogen sulfide; Polymer electrolyte membrane fuel cells; Proton exchange

	membranes
Title	Durability aspects of polymer electrolyte membrane fuel cells
Author	Sethuraman, Vijay Anand
Number of pages	185
Publication year	2006
Degree date	2006
School code	0202
Source	DAI-B 67/12, Dissertation Abstracts International
Place of publication	Ann Arbor
Country of publication	United States
ISBN	978-1-109-84063-6
Advisor	Weidner, John W.
University/institution	University of South Carolina
University location	United States -- South Carolina
Degree	Ph.D.
Source type	Dissertations & Theses
Language	English
Document type	Dissertation/Thesis
Dissertation/thesis number	3245437
ProQuest document ID	305276158
Document URL	https://www.proquest.com/docview/305276158?accountid=13965
Copyright	Database copyright ProQuest LLC; ProQuest does not claim copyright in the individual underlying works.
Database	Dissertations & Theses @ University of South Carolina ProQuest Dissertations & Theses Global

DURABILITY ASPECTS OF

POLYMER ELECTROLYTE MEMBRANE FUEL CELLS

by

Vijay Anand Sethuraman

Bachelor of Technology
Central Electrochemical Research Institute, 2000

Submitted in Partial Fulfillment of the

Requirements for the Degree of Doctor of Philosophy in the

Department of Chemical Engineering

College of Engineering and Information Technology

University of South Carolina

2006

Major Professor
Chairman, Examining Committee
John W. Weidner

Committee Member
John W. Van Zee

Committee Member
Christopher T. Williams

Committee Member
Donna A. Chen

Committee Member
Michael A. Matthews

Dean of The Graduate School
Christine Ebert

INFORMATION TO USERS

The quality of this reproduction is dependent upon the quality of the copy submitted. Broken or indistinct print, colored or poor quality illustrations and photographs, print bleed-through, substandard margins, and improper alignment can adversely affect reproduction.

In the unlikely event that the author did not send a complete manuscript and there are missing pages, these will be noted. Also, if unauthorized copyright material had to be removed, a note will indicate the deletion.

ProQuest Information and Learning Company
300 North Zeeb Road
P.O. Box 1346
Ann Arbor, MI 48106-1346

Dedicated to amma, appa and raji

Acknowledgements

I thank my advisor Professor John W. Weidner for selecting me to join his research group and advising me for the past five and a half years. I also thank him for arranging a year long internship at United Technologies Corporation (UTC). Besides being a proponent of keeping things simple, John is perhaps the most optimistic person I have ever come across in my life. He was, is, and will be a great source of inspiration throughout my academic and non-academic life.

I also thank my committee members Professors Donna A. Chen, Christopher T. Williams and John W. Van Zee for their valuable input and suggestions throughout the course of my graduate research.

I thank the following staff members of the department for making everything easier for me: Ms. Diane Gooding, Ms. Marcia Rowen, Ms. Kay Dorrell, Mr. Brian Loggans, Mr. Jim Little, and Ms. Loretta Hardcastle.

I also thank the staff of the International Programs for Students at the University of South Carolina for their amazing support throughout my graduate student life.

I thank my family in India for their unwavering support through letters, e-mails and phone calls during my stay here in the United States. I thank Dr. V. Yegnaraman, Central Electrochemical Research Institute, for teaching me electrochemistry during my undergraduate years.

I thank the following NSF-REU students who helped me in obtaining valuable data used in this dissertation: Mr. Saahir Khan (Stanford University), Mr. Jonathan Thompson (Clemson University) and Ms. Leslie A. Wise (Kansas University).

I thank the following UTC employees: Dr. Lesia V. Protsailo, for providing me the opportunity to do a year long internship at UTC Power. She was always cheerful even when I missed an important deadline or didn't turn in results on time; Dr. Andrew T. Haug for his invaluable suggestions and numerous discussions on fuel cell durability; Dr. Sathya Motupally for his overall guidance; Mr. Michael Fortin for teaching me a lot about fuel cell durability experimentation; Ms. Marianne Pemberton for helping me with the RDE experimentation; Ms. Shruti Modi for helping me with the Fenton tests; Mr. Jon Odell for helping me with the single sided membrane electrode assembly build and testing them. I thank Professor James E. McGrath and his group at Virginia Tech. for providing the BPSH-35 membranes.

I thank the National Science Foundation – Industry/University Cooperative Research Center for Fuel Cells (NSF-I/UCRC) for supporting the anode poisoning work. I thank the United States Department of Energy for supporting the Advanced Cathode Catalyst and High Temperature Membrane program (DE-FC36-02AL).

Abstract

In order for the successful adoption of fuel cell technology, it is imperative that durability is understood, quantified and improved. A number of mechanisms are known to contribute to PEMFC membrane electrode assembly (MEA) performance degradation. These include catalyst poisoning, dissolution and sintering; ionomer and membrane poisoning and degradation; carbon corrosion, etc. Fundamental understanding of these degradation mechanisms will lead to the intelligent design of new materials and to extend their lifetime. Development and standardization of accelerated *ex situ* and *in situ* techniques to characterize and predict material properties as a function of various operating conditions is one of the challenges currently faced by fuel cell material developers. In this dissertation, we show, via experiments, some of the various processes that degrade the proton exchange membrane in a PEM fuel cell; and catalyst poisoning due to hydrogen sulfide (H_2S) and siloxane.

The effect of humidity on the chemical stability of two types of membranes, [i.e., perfluorosulfonic acid type (PFSA, Nafion® 112) and biphenyl sulfone hydrocarbon type, (BPSH-35)] was studied by subjecting the MEAs to open-circuit voltage (OCV) decay and potential cycling tests at elevated temperatures and low inlet gas relative humidities. The BPSH-35 membranes showed poor chemical stability in *ex situ* Fenton tests compared to that of Nafion® membranes. However, under fuel cell conditions, BPSH-35 MEAs outperformed Nafion® 112 MEAs in both the OCV decay and potential cycling tests. For both membranes, (i) at a given temperature, membrane degradation was more pronounced at lower humidities and (ii) at a given relative humidity operation, increasing the cell temperature accelerated membrane degradation. Mechanical stability of these

two types of membranes was also studied using relative humidity (RH) cycling. Due to decreased swelling and contraction during wet-up and dry-out cycles, Nafion® 112 lasted longer than BPSH-35 membranes in the RH cycling test. Membrane decay mechanism was devised supported by experimental evidences.

Hydrogen peroxide (H_2O_2) formation rates in a proton exchange membrane (PEM) fuel cell were estimated by studying the oxygen reduction reaction (ORR) on a rotating ring disc electrode (RRDE). Fuel cell conditions were replicated by depositing a film of Pt/Vulcan XC-72 catalyst onto the disk and by varying the temperature, dissolved O_2 concentration and the acidity levels in $HClO_4$. The $HClO_4$ acidity was correlated to ionomer water activity and hence fuel cell humidity. H_2O_2 formation rates showed a linear dependence on oxygen concentration and square dependence on water activity. The H_2O_2 selectivity in ORR was independent of oxygen concentration but increased with decrease in water activity (i.e., decreased humidity). Potential dependent activation energy for the H_2O_2 formation reaction was estimated from data obtained at different temperatures.

MEAs with built-in reference electrodes were developed. Using such electrodes, the isolated effect of supported Pt, PtCo and PtIrCo catalysts on membrane durability was studied. Electrodes with PtIrCo were found to be more durable than those with PtCo which in turn were more durable than those with Pt.

Presences of trace impurities (such as CO, H_2S, NH_3 etc.) in the fuel also affect PEMFC durability. Among these impurities, H_2S causes significantly higher performance loss and irreversible catalytic poisoning. A concise mechanism for the poisoning kinetics of H_2S on composite solid polymer electrolyte Pt (SPE-Pt) electrode

was validated experimentally by charge balances and theoretically by a model, which predicted the oxidation current as a function of the applied potential. H_2S dissociatively adsorbed onto SPE-Pt electrode as linear and bridge bonded sulfur (S) species and, under favorable potentials, underwent electro-oxidation to sulfur and then to sulfur dioxide (SO_2). Fraction of the adsorbed S species remained as 'hard-to-oxidize' adsorbents and caused irreversible loss of catalytic activity. Deactivation of bridge sites occurred first followed by the loss of linear sites. A method to estimate the catalytic sites irreversibly lost due to sulfur poisoning was developed.

The seals and tubing in a fuel cell system are currently made of Silicone based materials. The effect of silicone on the catalytic activity of Pt for oxygen reduction and hydrogen adsorption was studied using di-phenyl siloxane as a source compound at a RDE. Di-phenyl siloxane did not affect the catalytic activity of Pt when it was injected into the electrolyte. However, it blocked the oxygen reduction reaction when it was premixed with the catalyst. Proton transport was not blocked in either case. We postulate that di-phenyl siloxane induces hydrophobicity and causes local water starvation thereby blocking oxygen transport. Hence, the slow leaching of silicone seals in a fuel cell could cause silicon deposition on the electrode, which will irreversibly degrade fuel cell performance by blocking oxygen transport to the catalyst sites.

Keywords: Anode Poisoning, Durability, PEM Fuel Cell, Hydrocarbon Membrane, Hydrogen Sulfide, MEA, Membrane Electrode Assembly, Nafion®, PEMFC, Proton Exchange Membrane, Pt, Pt Alloys, Seals, Silicone

Table of Contents

List of Tables

List of Figures

1. General Introduction

1.1 Background

According to the Energy Information Administration (EIA) of the U. S. Department of Energy, global peak production of cheap crude oil doesn't occur until 2035. However, most of the researchers in the energy industry suggest that the global production of cheap crude oil could peak before 2010. [1] This forecasts the dawn of a solar-hydrogen economy, an economy based primarily on solar power (in all its forms, including wind power and hydroelectric power) and using hydrogen as a convenient way to store and transport energy. Hydrogen has the potential to end the industrial world's reliance on oil and a hydrogen based economy would reduce the carbon-dioxide emissions and mitigate the effects of global warming. Since hydrogen is so plentiful and exists everywhere on this planet, every human being could be "empowered", creating the first truly democratic energy regime in the history of mankind.

Fuel cells form the structural and fundamental unit of such an economy. Fuel cells are electrochemical energy conversion devices that convert chemical energy of a fuel gas/liquid directly to electrical energy and heat without the need for direct combustion as an intermediate step, resulting in much higher conversion efficiencies than conventional thermo-mechanical methods. In a typical fuel cell, fuel stream (i.e., hydrogen, methanol etc.) is continuously fed to the anode side (the negative electrode,

where it gets oxidized) and an oxidant (i.e., oxygen) is continuously fed the cathode side (the positive electrode, where it gets reduced).

1.1.1. Proton Exchange Membrane Fuel Cells (PEMFCs)

Proton Exchange Membrane Fuel Cells (PEMFCs) are a group of fuel cells that use solid polymer membranes as the electrolyte for the conduction of ions. Hydrogen and methanol are usually used as the fuel for this type of fuel cells. Even though proton is the mobile ion in both fuel modes, the fuel cell operating on hydrogen is usually called proton exchange membrane fuel cell and the fuel cell operating on methanol is called direct methanol fuel cell. Figure 1-1 shows the schematic of a single PEMFC operating on hydrogen. The reactions that take place in a PEM fuel cell are given below,

$$\text{Anode:} \qquad \mathrm{H_2 \rightarrow 2H^+ + 2e^-} \qquad [1\text{-}1]$$

$$\text{Cathode:} \qquad 4H^+ + 4e^- + O_2 \rightarrow 2H_2O \qquad [1\text{-}2]$$

$$\text{Overall:} \qquad \mathrm{2H_2 + O_2 \rightarrow 2H_2O} \qquad [1\text{-}3]$$

As can be seen in Figure 1-1, the proton exchange membrane only allows protons to pass from the anode side to the cathode side. The PEM also prevents the gases from diffusing from one side to the other. The anode, the cathode and the membrane together constitute the membrane electrode assembly (MEA). In the most complete form, an MEA consists of seven layers: a proton exchange membrane, three-phase anode and cathode catalyst layers, two gas diffusion layers (GDLs), and two sets of sealing gaskets, as shown in Figure 1-2.

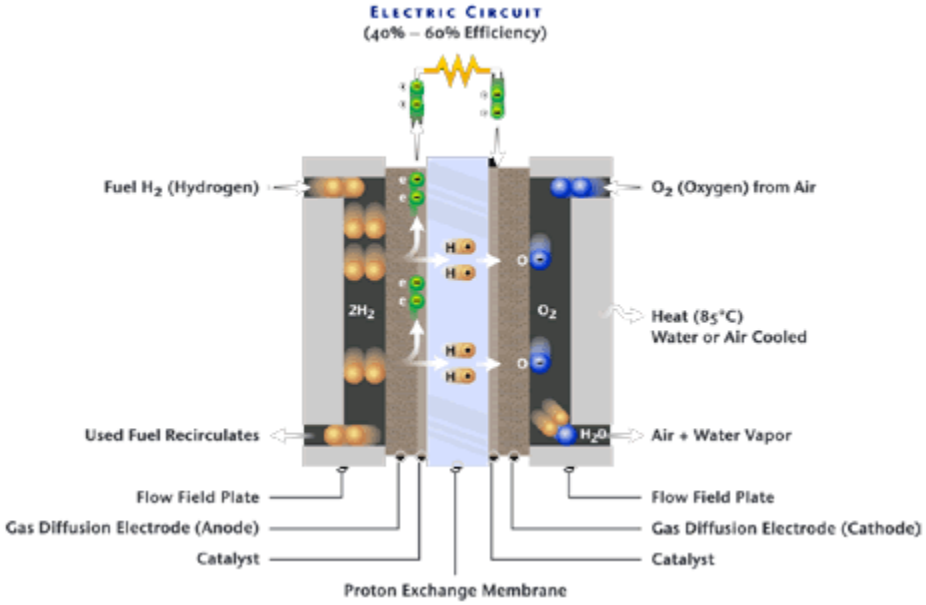

Figure 1-1. Schematic of a fuel PEM fuel cell operating on H_2 and O_2.

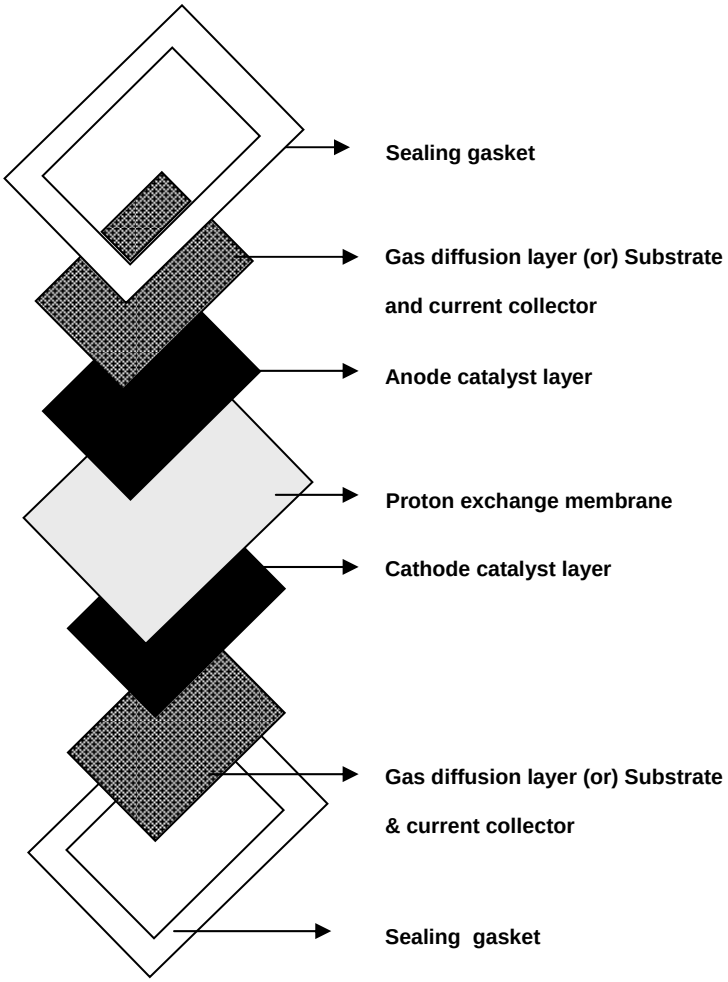

Figure 1-2. A seven layer MEA consists of a proton exchange membrane, three-phase anode and cathode catalyst layers, two gas diffusion layers, and two sealing gaskets.

DuPont's Nafion® is currently the standard for PEM fuel cells. Nafion® is made of a polytetrafluoroethylene (PTFE) backbone with perfluorinated-vinyl-polyether side chains containing sulphonic acid end groups. When these membranes become hydrated, the protons become highly mobile. The catalyst layers on the anode and cathode are composite structures consisting of the proton conducting polymer (*e.g.,* Nafion®) and a carbon supported metal catalyst. Catalyst layer thicknesses vary between 10 and 20 μm depending on catalyst loading levels. Platinum is by far the best catalyst for both the anode and the cathode. However, the choice of the anode catalyst and loading levels also depends on the fuel source. When operating on pure hydrogen relatively little Pt is needed since the hydrogen oxidation reaction is facile and the resulting overpotential is small. If the fuel is a reformate (*i.e.,* a mixture of H_2, CO_2, N_2 and impurities such as CO) or methanol, then catalysts such as a PtRu, PtRh or PtNi alloys can be used to minimize the adverse affect of CO poisoning.

The oxygen reduction reaction (ORR) is the more limiting reaction in a well performing fuel cell. Therefore, reducing the activation overpotential for ORR is a crucial factor in improving the fuel cell performance. Increasing the cell temperature and pressure, increasing the reactant concentration (i.e. operating on pure oxygen), increasing the electrode roughness and the catalyst loading are some of the ways to deal with the performance loss due to the sluggish ORR kinetics. For example, for a PEM fuel cell fueled by hydrogen and oxygen operating at 80ºC and 1 atmosphere, the loss due to the ORR at 0.5 A/cm^2 is 160 mV.

The performance of a PEMFC is measured in terms of a VI curve. A typical VI curve in terms of all the common losses is given in Figure 1-3.

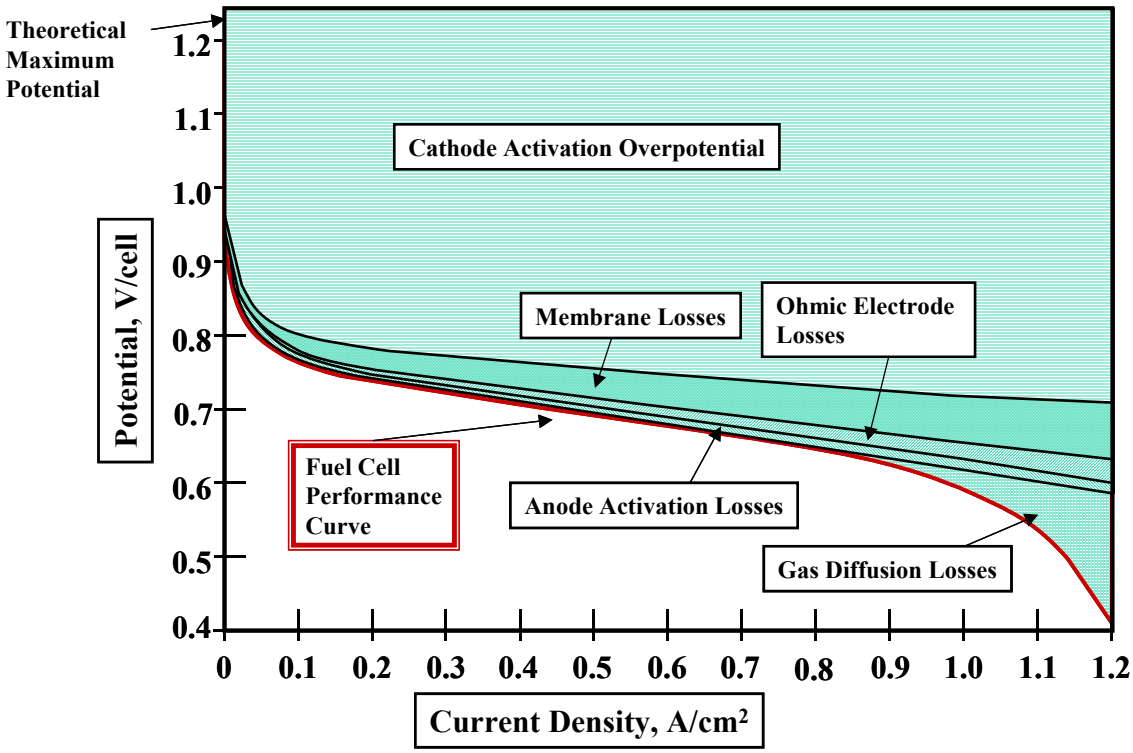

Figure 1-3. Fuel cell performance curve. Different kind of losses subtracted from the theoretical potential gives rise to the shape of the final current-voltage performance curve.

PEM fuel cells offer many advantages over other fuel cell types. Due to their low temperature operation, they have very fast start-up times (seconds) compared to PAFCs (minutes), MCFCs and SOFCs (hours). This fast start-up time also means a faster response time to change in load (power output). Their higher power density, efficient operation, environment friendliness and low cost of manufacturing make them the best choice for portable and vehicular applications. However they have limitations such as cost, fuel availability (hydrogen production and storage), membrane limitations (temperature of operation, water and thermal management) and reformate issues (CO, H_2S poisoning).

1.1.2. Durability of PEMFCs

US Department of Energy's (DOE) projected performance requirements[2] for the year 2010 are 5,000 hours (with 20,000 start/stops) at $45/kW for automotive stacks and upwards of 40,000 hours at $400-$750/kW for stationary power plants. Contemporary fuel cell research addresses the following durability concerns: a. Irreversible loss of catalytic activity due to anode impurities, b. Ionomer and membrane degradation, c. Carbon corrosion, d. Cathode catalyst dissolution and e. Degradation of seals.

1.1.2.1. Anode Durability

Though pure hydrogen is the ideal fuel for the PEM fuel cells, hydrogen storage and transportation is very difficult. Therefore, natural gas, methanol, gasoline, propane and diesel fuel are being proposed to be used as fuels so that they are reformed to produce a hydrogen-rich fuel stream. These fuels go through two main systems before they are converted to a clean hydrogen-rich stream: a reformer, which converts the fuel

(usually a reaction with steam or air) to produce a hydrogen rich reformate, and a clean-up system that removes all the impurities that are harmful to the fuel cell system. The hydrogen-rich fuel stream thus produced consists of 20% carbon dioxide, 1000 ppm – 1% carbon monoxide, 40% nitrogen and trace quantities of ammonia and hydrogen sulfide. Carbon monoxide[3, 4], ammonia[5], hydrogen sulfide[6] and carbon di-oxide[7] have been shown to cause performance losses. Of these, hydrogen sulfide, even when present as low as 500 ppb, causes irreversible performance loss due to sulfur deposition[8]. Avoidance of sulfur impurities is the only mitigation strategy to counter this problem.

1.1.2.2. Ionomer and Membrane Degradation

Membrane degradation can be classified into mechanical, thermal and chemical/electrochemical categories. Mechanical failures occur in the form of cracks, punctures, pinhole blisters or tears during fabrication of membrane electrode assemblies as well as during fuel cell operation. Frequent start-stops of fuel cell cause swelling and drying of membrane resulting in mechanical stresses in the membrane. Thermal degradation of membranes occurs at high temperatures (> 150 ºC). Wilkie et al.[9] proposed a mechanism for the thermal degradation of Nafion® involving cleavage of the C-S bond to form SO_2 and $OH^{\bullet}$ radical, and a carbon based radical which further disintegrates while degrading the membrane. The stability of the membrane during freeze-thaw cycles is important for their use in automobiles. McDonald et al.[10] reported significant decrease in percent elongation of a Nafion® 112 MEA at failure after 385 freeze-thaw cycles between -40 and +80 ºC. They suggested that a decrease in chain entanglement and aggregation of hydrophilic areas may open up the molecular structure leading to a decrease in strength. Freeze-thaw cycles also cause volume changes

associated with the freezing and melting of water trapped in the membrane. Chemical degradation of membrane is currently believed to occur via the attack of peroxy and hydroperoxyl radicals formed in the fuel cell electrodes. Depending on the type of membrane, radical attack can occur at the α-carbon of an aromatic group, at ether links, or branching points of the polymer. Any H-containing terminal bonds present in the polymer can be attacked by radicals.

1.1.2.3. Carbon Corrosion

PEM fuel cells are constructed with high surface-area platinum particles (~50 m^2/g) dispersed on high surface area carbon supports (~240 m^2/g)[11]. Carbon is thermodynamically unstable at typical operating conditions of the air electrode. The equilibrium potential for carbon oxidation to carbon di-oxide is 0.207 V relative to reversible hydrogen electrode (RHE) at 25 ºC[12]. PEM fuel cell cathodes generally operate at potentials in the range of 0.5-0.9 V vs. RHE, more anodic than the equilibrium potential for carbon corrosion. But stable performance after prolonged operation at typical operating temperatures (~70 ºC) suggests that rates of carbon corrosion are very low even in the presence of Pt and water. Meyers et al.[13] presented electron microprobe images of as-received and post-cycling MEAs. In that they showed that the cathode electrode significantly thinned due to exposure at high potentials. Reiser et al.[14] proposed that a non-uniform distribution of hydrogen along the fuel cell electrode could divide the cell into two regions, where the fuel-rich region drives a reverse current in the fuel starved region via the highly conductive bi-polar plates. A non-uniform distribution of hydrogen could occur during start-up and shut-down operations and also during local fuel (H_2) starvation. Carbon corrosion can be mitigated with uniform fuel distribution of fuel

across the cell during regular operation and with control of the cathode potentials[15] during transient start-up and shut-down operations.

1.1.2.4. Cathode Catalyst Dissolution

In 1993, Wilson et al.[16] reported 60% loss in active surface area due to Pt particle growth after 4000 hours of continuous operation at 80 ºC on hydrogen/air and at maximum power. Since then, there have been several publications on the durability of Pt and Pt alloy cathode catalysts.[17] Pt alloys as cathode catalysts have attracted wide attention because of their higher catalytic activity without sacrificing stability. However, the dissolution of transition metals in Pt alloys could result in a decrease of catalyst activity for ORR. Metal cations from the dissolution could easily exchange with a proton of PFSA membrane decreasing the ionic conductivity of the ionomer. These metal cations also migrate and deposit inside the membrane when they come into contact with a reductant such as molecular H_2 diffusing from the anode side.

1.1.2.5. Degradation of Seals

Durability of seals is not a well researched subject in the fuel cell community. Silicone based materials are widely used in seals and gaskets in fuel cell stacks. Schulze et al.[18] noted alteration on the color of the membranes where the seal material was in contact after fuel cell operation. Using X-ray photoelectron spectroscopy (XPS), they detected residues of silicone on the surface of the membrane and catalysts. Using scanning electron microscope and energy dispersive X-ray (SEM/EDX) analysis, they observed enrichment of silicone residues on Pt. They speculated that the deposition of Si on the catalyst may change the hydrophobic/hydrophilic characteristics of the electrodes.

1.2. Objectives and Outline of Dissertation

The objectives of this thesis were:

1. To compare the performance of two types of membranes - , i.e., perfluorosulfonic acid type (PFSA, Nafion 112®) and biphenyl sulfone hydrocarbon type, (BPSH) with accelerated durability tests.
2. To delineate a membrane durability mechanism supported by the experimental data.
3. To show the dependence of humidity and temperature on PEM fuel cell durability.
4. To show that the selectivity towards hydrogen peroxide formation in the oxygen reduction reaction is humidity dependent.
5. To understand the poisoning kinetics of hydrogen sulfide on supported Pt catalysts.

Chapter 2: Effect of Temperature and Humidity on the Durability of Perfluorosulfonic Acid and Hydrocarbon Membranes

In this chapter, we compare the performance of Nafion® 112 with BPSH membrane via accelerated durability tests such as open circuit voltage decay, load cycling, Fenton test, humidity cycling. Nafion® 112 showed better chemical stability than BPSH membrane in Fenton tests. However, inside a fuel cell, BPSH outperformed Nafion® 112 in both the OCV decay and load cycling tests. We present a membrane degradation mechanism supported by the experimental data. Summary of this mechanism is given below as processes that are always occurring simultaneously during the life of the fuel cell:

a. The presence of a very high potential (~ OCV) on the cathode causes catalyst dissolution from the catalyst layer. For example, Pt leaves the support as Pt^{2+}.
b. The dissolved catalyst then migrates into the membrane because of the concentration gradient.
c. This Pt^{2+} migration front comes into contact with H_2 diffusing from the anode. Pt^{2+} hence reduces to Pt and the result is a chemical deposition of Pt inside the membrane. The Pt in the membrane acts as a site for the formation of hydroxyl radicals, which attack the membrane. The membrane loses its structure, becomes progressively thin causing increase in gas crossover. The resulting mixed potential causes performance drop and in extreme cases leads to short-circuit of electrodes.
d. Hydrogen peroxide formation occurs on anode (at OCV) and on both electrodes under load conditions. H_2O_2 migrates into the membrane and produces hydroxyl radicals on Pt in the membrane.

BPSH has excellent gas crossover properties compared to Nafion®. This prevents peroxide formation on with electrodes, chemical platinization of the membrane and subsequent attack.

Chapter 3: Effect of Water Activity and Oxygen Concentration on Hydrogen Peroxide Formation on Pt on Carbon

In this chapter we show that the selectivity towards the 2 electron transfer reaction to hydrogen peroxide in the oxygen reduction reaction is sensitive to water activity. In the presence of water, the selectivity shifts to the 4 electron transfer

reaction to water formation. In the absence of water, the fraction of peroxide formation increases.

Chapter 4 Effect of Supported Pt Alloys on Membrane Durability

Pt alloys were investigated for their hydrogen peroxide kinetics using RRDE technique. We report an increased peroxide formation rates on Pt alloys than on Pt. However, when these alloys were used as cathode catalysts, they significantly increased the life of the proton exchange membrane. This is because of lower dissolution and passivation rates exhibited by alloys than Pt.

Chapter 5 Effect of Di-phenyl Siloxane on Catalytic Activity of Pt on C

In this chapter we show the effect of di-phenyl siloxane on the catalytic activity of Pt using RRDE technique. Si is a major element in seals, gaskets and tubing materials in a PEMFC system. Seal durability is currently the major issue in achieving the DoE durability targets. Using di-phenyl siloxane as a source compound, poisoning effect of seal degradation products on Pt activity was studied. Preliminary results suggest that di-phenyl siloxane blocked oxygen transport wherever it adsorbed and caused local water starvation. However, proton conduction was not blocked.

Chapter 6 Hydrogen Sulfide Kinetics on PEM Electrodes

In this chapter we present a poisoning mechanism for hydrogen sulfide on Pt supported on carbon and validate it experimentally using charge balances and theoretically with a model that predicts the oxidation current as a function of the applied potential. H_2S causes irreversible loss of catalytic activity (from a fuel cell

standpoint). A method to determine the amount of sites lost irreversibly due to H_2S poisoning is discussed.

1.3. References

1. C. J. Campbell and J. H. Laherrere, *Scientific American*, , p. 80, March 1998.

2. United States Department of Energy, Energy Efficiency and Renewable Energy: Hydrogen, Fuel Cells and Infrastructure Technologies Program, Website - http://www.eere.energy.gov/hydrogenandfuelcells/

3. M. Murthy, M. Esayian, A. Hobson, S. MacKenzie, W-K. Lee and J. W. Van Zee, *J. Electrochem. Soc.,* **148**, A1141 (2001).

4. M. Murthy, M. Esayian, W-K. Lee and J. W. Van Zee, *J. Electrochem. Soc.,* **150**, A29 (2003).

5. H. J. Soto, W-K. Lee, J. W. Van Zee and M. Murthy, *Electrochem. Solid State Letters*, **6**, A133 (2003).

6. R. Mohtadi, W-K. Lee, S. Cowan, J. W. Van Zee and M. Murthy, *Electrochem. Solid State Letters,* **6**, A272 (2003).

7. T. Gu, W-K. Lee, J. W. Van Zee and M. Murthy, *J. Electrochem. Soc.,* **151**, A2100 (2004).

8. V. A. Sethuraman, S. Balasubramanian, L. A. Wise and J. W. Weidner, *Electrochemical Society Transactions,* **1** (8), 111 (2006).

9. C. A. Wilkie, J. R. Thomsen and M. L. Mittleman, *J. Appl. Poly. Sci.*, **42**, 901 (1991).

10. R. C. MacDonald, C. K. Mittelsteadt and E. L. Thompson, *Fuel Cells*, **4**, 208 (2004).

11. S. S. Kocha, in *Handbook of Fuel Cells – Fundamentals, Technology and Applications, Fuel Cell Technology and Applications,* **3**, Chapter 43, W. Vielstich, H. A.

Gasteiger and A. Lamm, Editors, John Wiley and Sons, Ltd., West Sussex, England (2003).

12. M. Pourbaix, *Atlas of Electrochemical Equilibria in Aqueous Solutions,* p. 453, National Association of Corrosion Engineers, Houston, Texas (1979).

13. J. P. Meyers and R. M. Darling, *J. Electrochem. Soc.,* **153**, A1432 (2006).

14. C. A. Reiser, L. Bregoli, T. W. Patterson, J. S. Yi, J. D. Yang, M. L. Perry and T. D. Jarvi, *Electrochem. Solid State Letters*, **8**, A273 (2005).

15. C. A. Reiser, D. Yang and R. Sawyer, *U. S. Pat. Appl.* 2002/0076583.

D. Yang, M. M. Steinbugler, R. D. Sawyer, L. L. Van Dine, and C. A. Reiser, *U. S. Pat. Appl.* 2003/0129462.

C. A. Reiser, D. Yang and R. Sawyer, *U. S. Pat. Appl.* 2003/0134164.

C. A. Reiser, D. Yang and R. Sawyer, *U. S. Pat. Appl.* 2003/0134165.

R. J. Balliet and C. A. Reiser, *U. S. Pat. Appl.* 2004/0001980.

T. A. Bekkedahl, L. J. Bregoli, R. D. Breault, E. A. Dykeman, J. P. Meyers, T. W. Patterson, T. Skiba, C. Vargas, D. Yang and J. S. Yi, *U. S. Pat. Appl.* 2004/0081866.

R. J. Balliet, C. A. Reiser, T. W. Patterson and M. L. Perry, *U. S. Pat. Appl.* 2004/0126628.

J. A. S. Bett, N. E. Cipollini, T. D. Jarvi and R. D. Breault, *U. S. Pat. Appl.* 2004/0126644.

16. M. S. Wilson, F. H. Garzon, K. E. Sickafus and S. Gottesfeld, *J. Electrochem. Soc.,* **140**, 2872 (1993).

17. J. St-Pierre, D. P. Wilkinson, S. Knights and M. L. Bos, *J. New Mater. Electrochem. Systems,* **3**, 99 (2000).

T. R. Ralph and M. P. Hogarth, *Platinum Met. Rev.*, **46**, 3 (2002).

T. Okada, in *Handbook of Fuel Cells: Fundamentals, Technology, and Applications*, Vol. 3, Chapter 37, W. Vielstich, A. Lamm and H. A. Gasteiger, Editors, John Wiley & Sons, New York (2003).

T. Okada, Y. Ayato, M. Yuasa and I. Sekine, *J. Phys. Chem. B*, **103**, 3315 (1999).

T. Okada and G. Xie, *Electrochim. Acta*, **43**, 3741 (1998).

18. M. Schulze, T. Knöri, A. Schneider and E. Gülzow, *Journal of Power Sources*, **127**, 222 (2004).

2. Durability Studies of PFSA & Hydrocarbon Membranes

2.1. Abstract

The effect of humidity on the chemical stability of two types of membranes, [i.e., perfluorosulfonic acid type (PFSA, Nafion® 112) and biphenyl sulfone hydrocarbon type, (BPSH-35)] was studied by subjecting the membrane electrode assemblies (MEAs) to open-circuit voltage (OCV) decay and potential cycling tests at elevated temperatures and low inlet gas relative humidities. The BPSH-35 membranes showed poor chemical stability in *ex situ* Fenton tests compared to that of Nafion® membranes. However, under fuel cell conditions, BPSH-35 MEAs outperformed Nafion® 112 MEAs in both OCV decay and potential cycling tests. For both membranes, (i) at a given temperature, membrane degradation was more pronounced at lower humidities and (ii) at a given relative humidity operation, increasing the cell temperature accelerated membrane degradation. Mechanical stability of these two types of membranes was also studied using relative humidity (RH) cycling. Due to decreased swelling and contraction during wet-up and dry-out cycles, Nafion® 112 lasted longer than BPSH-35 membranes in the RH cycling test.

[V. A. Sethuraman, J. W. Weidner, A. T. Haug, and L. V. Protsailo, "Effect of Humidity on the Durability of PFSA and Hydrocarbon Membranes", manuscript to be submitted to the *Journal of the Electrochemical Society*.]

2.2. Introduction

Current engineering requirements for automotive fuel cells demand stack operation at higher temperatures (>100 ºC) and low relative humidities (< 25 % RH). Elevated temperature operation offers better tolerance to CO from the reformer, faster oxygen reduction reaction kinetics and better water and thermal management enabling easier system integration. Lower relative humidity operation offers quicker start-ups and better freeze-cycle management. The current benchmark membrane for proton exchange membrane (PEM) fuel cells is Nafion®, a perfluorinated sulfonated copolymer made by DuPont. Nafion® copolymers exhibit good thermal and chemical stability, as well as very high proton conductivity under hydrated conditions at temperatures below 90 °C. However, applications of these membranes are limited at high temperatures and low relative humidities due to their loss of conductivity[1]. These limitations have led to the search for new polymer electrolytes for proton exchange membranes. Extensive reviews of polymer-based proton exchange membranes have recently been published.[2, 3] In search for new polymer electrolytes for use in PEM fuel cells, it is a common practice to functionalize aromatic polymers with proton conducting groups. Among the promising candidates for an alternative high temperature and low humidity PEM are derived from poly(arylene ether sulfone)s,[4] well-known engineering thermoplastic material (particularly when devoid of aliphatic units) that display excellent thermal and mechanical properties. Sulfonated poly(arylene ether sulfone)s synthesized by attaching sulfonic acid groups in polymer modification reactions (post-sulfonation route) have been investigated since the pioneering work of Noshay and Robeson[5], who developed a mild sulfonation procedure for the commercially available bisphenol-A-based-poly(ether

sulfone). Since these sulfonated polymers exhibited protonic conduction, they were used in desalination membranes for reverse osmosis.

McGrath and his group synthesized aromatic, film-forming, highly sulfonated-poly(arylene ether sulfone) copolymers via direct copolymerization for use in PEM fuel cells.[6] The 4,4' -biphenyl-based poly(arylene ether sulfone) copolymers have been most extensively studied by them and have developed the acronym BPSH-XX to represent bi-phenol in acidic form. The XX represents the molar fraction of sulfonic acid units in the copolymer repeat unit. These aromatic ionomers are copolymers that are comprised largely of repeating thermally stable aromatic rings, which are stiffer, longer, and have higher glass transition temperatures than Nafion® and yet are designed to produce ductile films. They have shown that direct copolymerization has many advantages, such as enhanced stability; control of ion-contaminating sites; a whole variety of molecular structures; and the ability to make higher molecular weights, which translate to improved mechanical properties.[2] These polymers showed much higher yield strength and modulus than the analogous perfluorinated copolymers.

Membrane degradation in the PEM fuel cell environment has been discussed[7] as having chemical and mechanical components. In this work, the chemical and mechanical stability of two types of membranes, [i.e., perfluorosulfonic acid type (PFSA, Nafion 112®) and biphenyl sulfone hydrocarbon (or H^+) type, (BPSH-35)] is studied.[8] Chemical stability was studied using *ex situ* Fenton test[9, 10] and *in situ* OCV decay[11] and potential cycling tests at elevated temperatures and low relative humidities. Mechanical stability of these two membranes was studied by relative humidity cycling at elevated temperature. (Figure 2-1)[12].

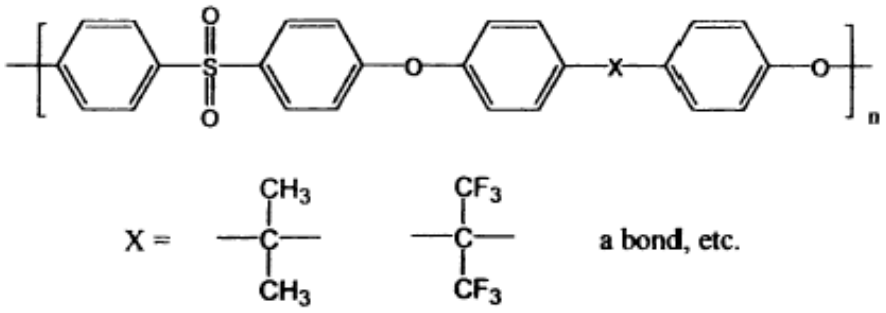

Structure 2.1 Structure of poly(arylene ether sulfone)

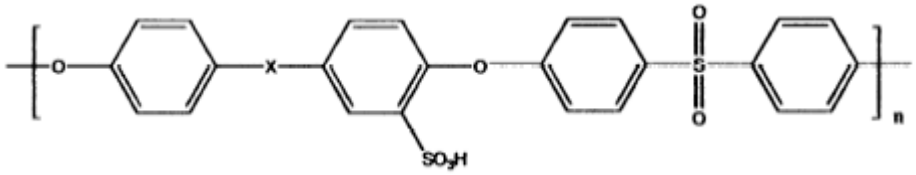

Structure 2.2 Structure of sulfonated-poly(arylene ether sulfone)

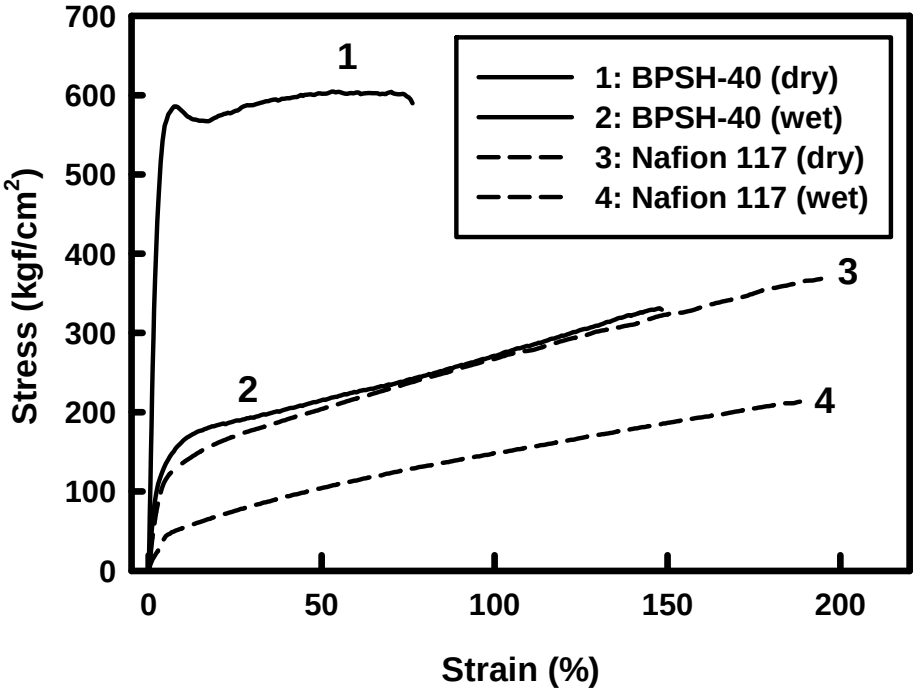

Figure 2-1. Comparison of humidity dependent stress-strain behavior of BPSH-40 and Nafion® 117 membranes.

2.3. Experimental

2.3.1. Fuel Cell

Commercially available Pt/C catalyst (TEC10E50E 46.7% Pt on Ketjen Black carbon, Tanaka Kikinzoku Kogyo KK, Japan) was mixed with Nafion® (5% aqueous solution, 1100 EW; Solution Technology Inc., Mendenhall, PA) ionomer and the resulting catalyst-ionomer ink (79% catalyst, 21% Nafion) was coated onto Teflon® based (EI DuPont de Nemours and Company) decals. These catalyst-coated decals were dried at room temperature and atmospheric pressure for 30 minutes and then dried in vacuum for 30 minutes. Catalyst-coated membranes (CCMs), 6.5 cm x 6.5 cm, were then made by hot pressing the catalyst-coated Teflon decals onto both sides of Nafion® 112 membranes (proton form) at 130 °C and 4500 lbs for 300 seconds. Reinforced silicon, un-reinforced silicon and Teflon pads were used as supports for this process. The CCMs had a Pt loading of ~0.4 mgPt/cm^2 on both anode and cathode sides.

One such CCM was assembled into a fuel cell (25 cm^2 hardware, Fuel Cell Technologies Inc., NM). Wet-proofed Toray® paper with micro-porous layer (243 μm total; Toray Industries, Japan) was used as gas diffusion media (GDM). Gaskets were chosen in such a way that they allowed for 21% compression on the GDMs at 30 in-lbs of torque on the bolts. The fuel cell had non-porous modular serpentine flow channels on the anode side and interdigitated flow channels (IDFF) on the cathode side. The assembled fuel cell was tested for throughput, gas crossover and overboard leaks and then conditioned with H_2/O_2 in a fuel cell test stand (Habco Inc., CT) at 80 °C and 101 kPa

(absolute). Several current-voltage curves were measured in hydrogen and oxygen with 30 and 25% utilizations respectively until a steady high performance was reached.

2.3.2. Open Circuit Voltage Decay

After the cell was conditioned, it was put on an open-circuit with H_2/O_2 as feed gases on the anode/cathode sides respectively. The OCV decay was monitored over the life of the cell until it failed. A fuel cell with an open circuit potential of 0.8 V or less, or a hydrogen crossover current of 10 mA/cm^2 or more was considered to be a failure. The temperatures of the saturators were adjusted to vary the humidity of inlet gases. The pressure of the fuel cell system was set such that the gases had a fixed partial pressure regardless of their humidity. The OCV decay test was briefly interrupted every 24 hours for performing some diagnostics (described below) to evaluate the condition of the fuel cell. This experiment (OCV decay) was carried out for different temperatures and relative humidities. However, a new cell was used for each OCV decay experiment.

2.3.3. Potential Cycling

Potential cycling was performed using a potentiostat (M273A, Princeton Applied Research Inc., TN) in which the fuel cell was cycled between open circuit and a fixed current of 25 mA/cm^2 for 1 minute each.

2.3.4. Membrane Humidity Cycling

A membrane with no catalyst was built into a fuel cell apparatus with microporous-less gas diffusion layers and appropriate gaskets on both sides. 100% humidified N_2 (at 1000 cc min^{-1} total at STP; UHP, Praxair) was fed to both sides of the membrane for an hour followed by the same rate of bone-dry N_2 for the next hour. This

induced periodic mechanical stresses to the membrane. Gas crossover (at $\Delta P = 3psi$) was measured and water samples were collected at regular intervals to diagnose the state of the membrane. The cell was cycled until the gas crossover measured more than 500 cc min^{-1}.

2.3.5. Hydrogen Crossover Measurements

Molecular hydrogen crossing over from the anode side to the cathode side of the membrane was measured using a potential sweep between 0 and 500 mV vs. DHE on the cathode with N_2 flowing over it. While the magnitude of the oxidation-current in the voltammogram gave an indication of the amount of H_2 crossing over, the slope of current-voltage curve gave an indication of the electrical resistance across the two electrodes (commonly known as 'short'). A well-shorted electrode would mean that the electrodes were well insulated electronically (i.e., zero slope) and a poorly shorted electrode would mean that the electrodes were physically in contact with each other (i.e., infinite slope). This diagnostic played a significant role in this durability study because a high H_2 crossover was an indication of membrane degradation or expanding pinholes and a poor short was an indication of carbon strands from either electrodes in physical contact with each other. Water samples were collected once every 4 hours during the first 16 hours of the OCV decay and load cycling experiments. After that, they were collected every 24 hours. These water samples were analyzed for the presence of fluorine and sulfur using a Dionex ICS-200 ion chromatography system.

2.3.6. Measurement of Linear Expansion due to Swelling

Nafion® 112 and BPSH-35 membrane samples were cut into 2 cm by 2 cm pieces. They were placed in a vacuum oven at 25 ºC for 30 minutes. Their initial dimensions were measured immediately after taking them out of the vacuum oven at 25 ºC using a Mitutoyo digital caliper (i.e., length, width) and screw gauge (thickness). The membrane samples were then immersed in water at 25 ºC and left for there 30 minutes. The samples were then taken out and their dimensions were measured again and recorded. The samples were then placed in boiling water for a period of 10 minutes and their dimensions recorded afterwards. The increase in thickness due to swelling was estimated by subtracting the measured thickness after boiling at 80 ºC from the initial thickness measured at 25 ºC.

2.3.7. Fenton Test

A Nafion® 111 membrane (H^+ form, DuPont Fluoroproducts, NC) sample measuring ~2" by ~2" was cut and heated in a clean glass vial containing water at 80 ˚C for two hours to remove any surface impurities and solvents. The water was later drained from the vial and the membrane was dried in vacuum at 80 ˚C for four hours. The dry weight of the membrane was then measured. This weight was used to prepare ferrous sulfate solution such that it contained 25mg Fe/g Nafion® in 500 ml water. $FeSO_4.7H_2O$ (98.1% assay, Fischer Scientific Company, NJ) was used for this purpose. The dried Nafion® membrane was placed in this solution for 15 hours in a N_2 atmosphere. This process impregnated Fe ions into the membrane. After this impregnation process, the membrane was dried in vacuum at 80 ˚C for four hours. The dry weight of the membrane impregnated with Fe ions was measured.

The Fe impregnated membrane was placed in a Teflon® container containing 100 ml of 3% hydrogen peroxide aqueous solution (30%, VWR International) at 80 ˚C. Since hydrogen peroxide decomposes in the presence of a metal, this solution was replaced once every 24 hours and the leachate was saved for fluorine analysis. After 96 hours, the membrane was dried in vacuum at 80 ˚C for four hours. The weight loss, if any was recorded. This process was repeated with a sample of hydrocarbon membrane. The leachate was analyzed for fluorine using a Dionex ICS-200 ion chromatography system.

2.5. Membrane Degradation

During accelerated durability tests such as OCV decay and potential cycling, the membrane loses its physical structure and disintegrates over a period of time. The drop in OCV, an increase in the hydrogen crossover current and optical images of failed MEAs indicates that the membrane thinning occurs over a period of time. Figure 2-2 represents a schematic of reactant flows across a catalyst coated membrane. The presence of a very high potential (~ OCV) on the cathode side of the membrane causes Pt dissolution from the cathode catalyst layer as Pt^{2+} and migration into the membrane because of concentration gradient. Pt^{2+} species in the membrane is reduced by molecular H_2 crossing over from the anode side resulting in the platinization of membrane. Similar platinization of membranes has been reported in the literature. Takenaka and Torikai[13] reported a chemical procedure for the metallization of membrane in which an anionic metal ion in a solution in contact with one face of PEM is reduced by a reductant which diffuses through the membrane from a solution in contact with the opposite face. Fedkiw et al.[14] reported a two-step impregnation-reduction method in which the membrane (Nafion® in this case) was ion-exchanged with a pre-cursor metal salt followed by an

exposure to a reductant. Similar chemical platinization occurs in a PEM fuel cell membrane, where the Pt^{2+} ions act as the source for Pt and H_2 crossing over from the anode act as a reductant. The chemical platinization occurs in the membrane at a distance X_0 from the cathode-membrane interface. This distance is dictated by the relative molecular diffusional fluxes of O_2 and H_2 from the cathode and anode sides respectively. Figure 2-3 shows Pt map on a cross-section of a post-test MEA. The white band in the membrane region is metallic Pt. There is no Pt in the neat vicinity of the cathode-membrane interface because of a high oxygen concentration and very low to zero availability of molecular hydrogen (reductant).

The lower potential on the anode side of the membrane together with oxygen crossing over from the cathode side drives the peroxide formation reaction. The peroxide thus formed disintegrates to $OH^{\bullet}$ radicals on the Pt in the membrane. The $OH^{\bullet}$ radicals thus formed attack the membrane and produces HF. Direct radical formation can also occur in that $OH^{\bullet}$ radicals are formed directly from the crossover O_2 under the influence of the right potential. This makes the membrane thin over a period of time and is reflected in terms of fluorine emission, OCV decrease (due to higher mixed-potential), increased hydrogen crossover current, and physical shorting.

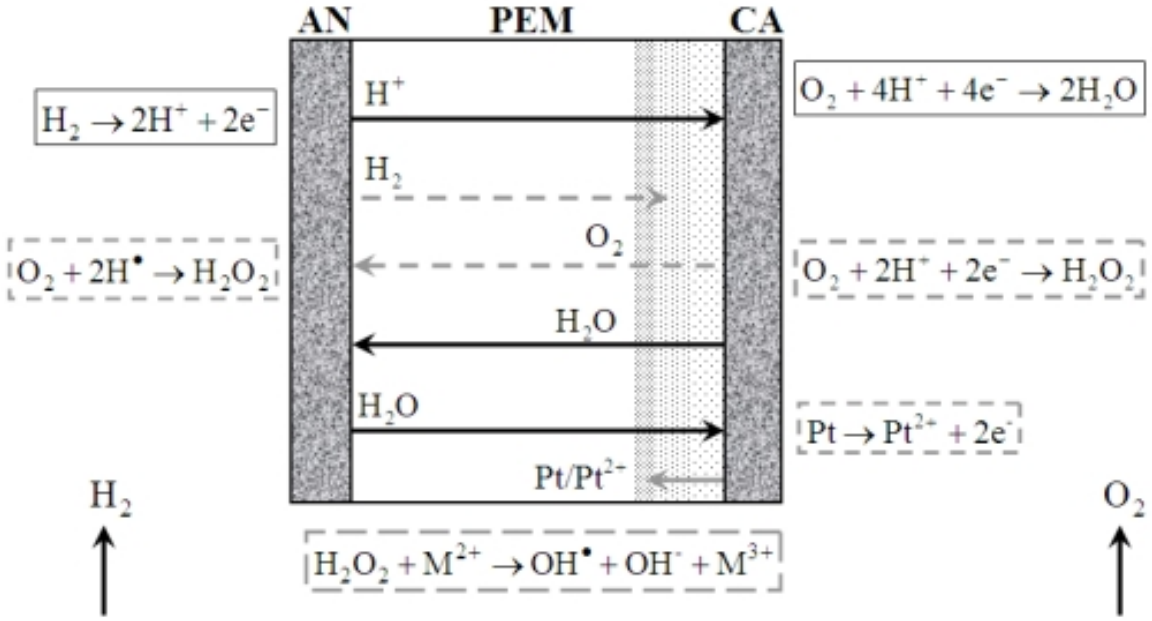

Figure 2-2. Schematic of reactant fluxes across a catalyst coated membrane. The reactions given in solid boxes are benign while the reactions given in dashed boxes cause membrane degradation.

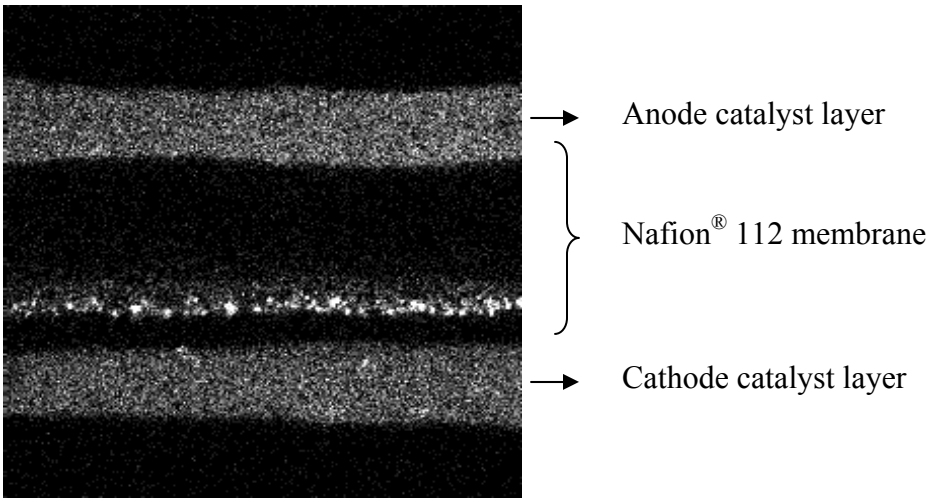

Figure 2-3. Electron microprobe analysis (EMPA) for elemental Platinum in a Nafion® 112 based MEA after 2800 cycles between 0.87 and 1.05 V (30 seconds each) in H_2/N_2 at 120 °C and 50% RH conditions. Anode and cathode had ~ 46% Pt/C catalyst with a 0.4 mg_{Pt}/cm^2 loading. The figure shows the Pt map on a cross-section of the post-test MEA.

2.6. Results and Discussion

2.6.1. Chemical Stability

In the light of the membrane degradation mechanism presented above, there needs to be a concentration of Pt ions and/or chemical platinization of membrane for catalyzing the hypothesized hydroxyl radical generation reaction. Fenton tests involve artificially impregnating the membranes with a known concentration of metal ions followed by testing them in peroxide solution. The results from these tests indicated a poor chemical stability for BPSH membranes. Figure 2-5 shows % weight loss after Fenton tests on BPSH-35 and Nafion® 112 membranes. The membrane samples were impregnated with 25 mg $FeSO_4$/g membrane and soaked in 3% H_2O_2 solution. BPSH-35 turned yellow soon after the start of the Fenton test and split into pieces after 16 hours (Figure 2-4). The sample disintegrated completely after 24 hours. Nafion® 112 sample, on the other hand, showed much higher chemical stability and lost 16% (by weight) after 96 hours. The weight loss estimated by gravimetric procedure correlated well with fluorine content from the leachate.

Figure 2-4 Image of BPSH membrane in 3% H_2O_2 solution after 16 hours of Fenton testing.

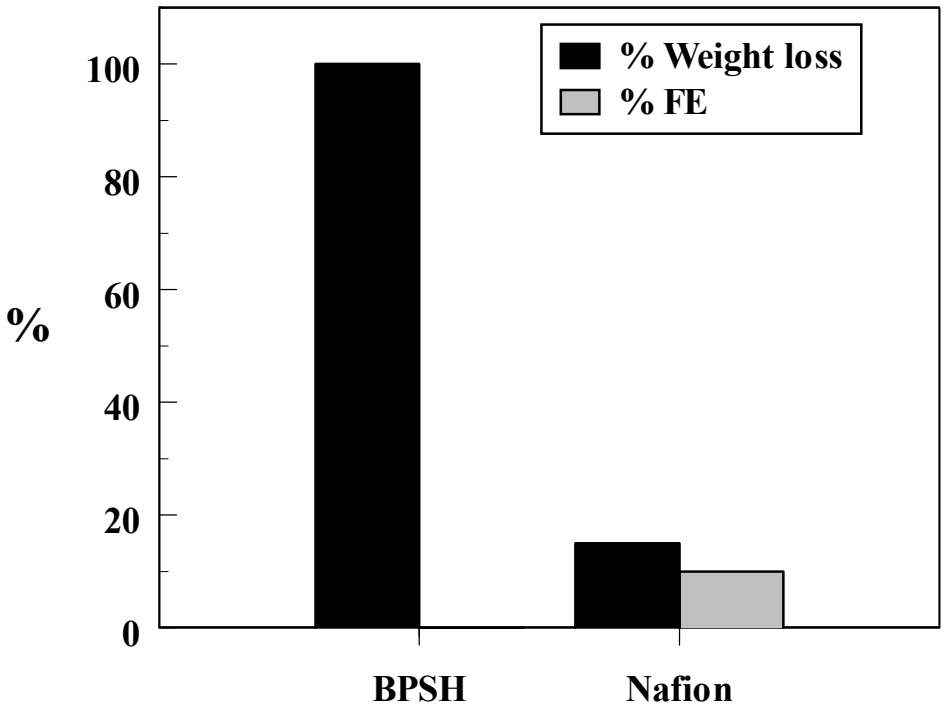

Figure 2-5. Percent weight loss and fluorine emission obtained from Fenton tests on BPSH and Nafion membranes after 24 and 96 hours respectively.

In order to obtain a measurable weight loss from the Fenton tests on BPSH-35 samples, the impregnation loading was systematically reduced coupled with a reduction in the concentration of H_2O_2 solution. At 1 mg $FeSO_4$/g membrane loading, 4.75% weight loss was observed after 4 hours. BPSH-35 samples with no impurity impregnation also disintegrated in 3% H_2O_2 solution after 125 hours. This is in accordance with previously observed[15] stability of Nafion® membrane in Fenton solution test media. The performance of a polymer in Fenton test is a measure of its chemical stability in strong oxidizing environments. To understand these Fenton results from PEM fuel cell standpoint, it can be said that if Pt migrates into BPSH membrane, it will cause degradation in the presence of peroxide molecules generated *in situ*.

Figure 2-6 shows the result of the OCV decay test on a Pt/KB coated Nafion® 112 membrane operating on H_2/O_2 at 25% relative humidity for three different temperatures. The inset shows membrane life as a function of temperature at 25% relative humidity operation with H_2/O_2 feed. The open-circuit voltage profiles have spikes because the cell was periodically stopped for performing hydrogen crossover measurements. Since these diagnostics involved scanning the cathode between 50 and 1150 mV vs. DHE, they resulted in the reduction of Pt oxides to Pt on the cathode. This temporary increase in the availability of metallic Pt increased the open-circuit potential when the OCV decay test was resumed. The voltage decayed back to the voltage prior to interruption once oxides were reformed. The overall OCV decay rates were found to be independent of the number of times the cell was stopped for diagnostics. The cell operating at 120 °C failed in less than 25 hours while the cells operating at 100 °C and 80 °C failed respectively after 56 and 498 hours.

Figure 2-7 shows the result of the OCV decay test on a Pt/KB coated Nafion® 112 membrane operating on H_2/O_2 at 100 °C for three different gas humidities. The cell operating at 25% RH failed after 56 hours while the cells operating at 50% and 75% RH failed after 75 and 175 hours respectively. Healy et al.[10], Knights et al.[16], and Endoh et al.[17] all observed higher degradation under low humidity conditions. Data trends from Figure 2-6 and Figure 2-7 indicate that membrane degradation significantly increases when a combination of high temperature and low humidity conditions exist. At least two phenomena explain this behavior: (1) the water dependent glass transition temperature of Nafion® and (2) the humidity and temperature dependent peroxide formation rates as reported earlier.[18] Nafion® is a homopolymer and exhibits three glass-transitions according to Yeo and Eisenberg[19]: an α transition at 111 °C due to the movement of the PTFE backbone, a β transition at 23 °C due to the relaxation of the ionic regions and a γ transition at -110 °C due to local short range motions of fluorocarbons in the PTFE backbone. Later findings by Kyu and Eisenberg[20] on the sensitivity of the α peak to the change in the water content of the membrane suggest that this assignment of α and β peaks be reversed. This humidity dependent α transition plays an important role in the viscoelastic behavior and hence the glass transition temperature of Nafion®. The lower the water content, the lower the glass transition temperature with bone dry Nafion® approaching the reported $T_{g,\alpha}$ = 111 °C. Furthermore, X-ray diffraction (XRD) studies of Nafion® showed that the characteristic peak (18º diffraction angle) greatly diminished under low humidification conditions[21], suggesting low humidification could decrease the crystallinity of Nafion®. O_2 and H_2 diffusion coefficients for completely dry Nafion® membrane were reported by Sakai et al.[22] to be two orders of magnitude greater than that

for fully humidified Nafion® membrane. Therefore, the initial lower OCV at lower humidity conditions is due to gas crossing the membrane and depolarizing the opposite electrode. The relatively faster OCV decay at lower humidity conditions is due to increased rate of H_2O_2,[18] $OH^{\bullet}$ and $OOH^{\bullet}$[23] generation at lower humidity conditions.

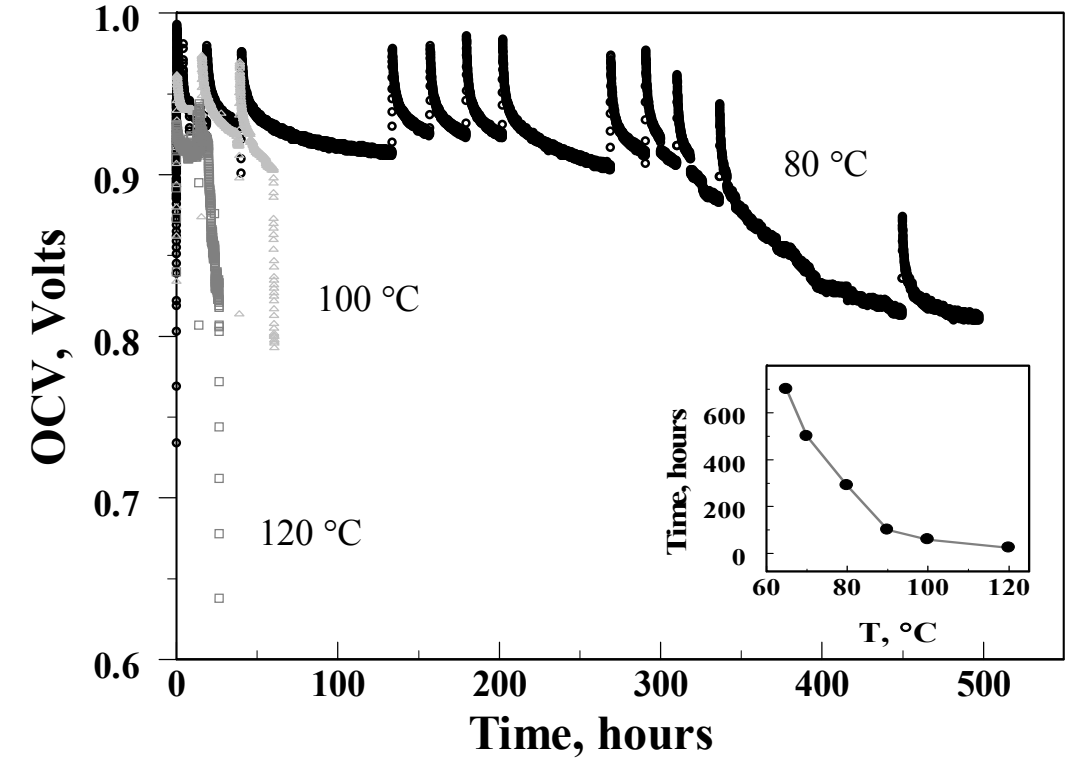

Figure 2-6. Open circuit voltage decay for Nafion® 112 MEA operating on H_2/O_2 and 25% RH at 80, 100 and 120 °C. Inset: Nafion® 112 MEA life at open-circuit voltage decay till failure at 25% RH for various temperatures. Failure at OCV decay test would mean an OCV of 0.8 V or below.

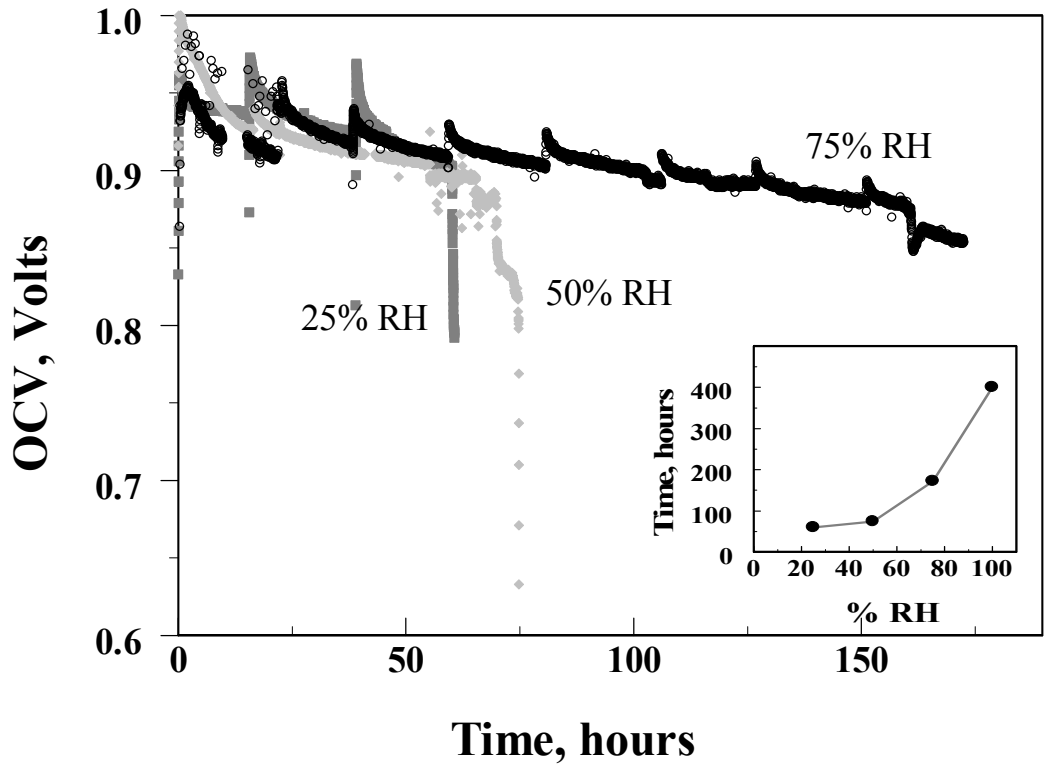

Figure 2-7. Open circuit voltage decay for Nafion® 112 MEA operating on H_2/O_2 at 373 K and 150 kPa for the following inlet gas humidities: 25%, 50% and 75% RH. Inset: Nafion® 112 MEA life at open-circuit voltage decay tests till failure at 100 °C for different relative humidities.

The OCV decay profiles show two slopes: (1) a slow decay followed by (2) a rapid fall. The slow decay in OCV is due to material loss from the membrane and its gradual thinning. The rapid fall in the OCV is due to (1) pin-hole formation resulting in extremely high gas crossover rates and/or (2) shorting between carbon electrodes due to complete loss of membrane mass. Evidence for the former can be seen in Figure 2-9 where the rapid fall in OCV coincides with rise in hydrogen crossover current. The difference between the former and the latter slopes was more pronounced at lower humidities. The OCV decay rate was measured as the ratio of the difference between the initial OCV and the OCV prior to the rapid fall to the time between these two OCVs. The OCV decay rates are summarized in Table 2-1 for different temperatures and relative humidities. At 100 ºC and 25% RH operation, the OCV decay rate measured from a BPSH-35 cell (Figure 2-9) is approximately three times lower than a similar Nafion® 112 cell.

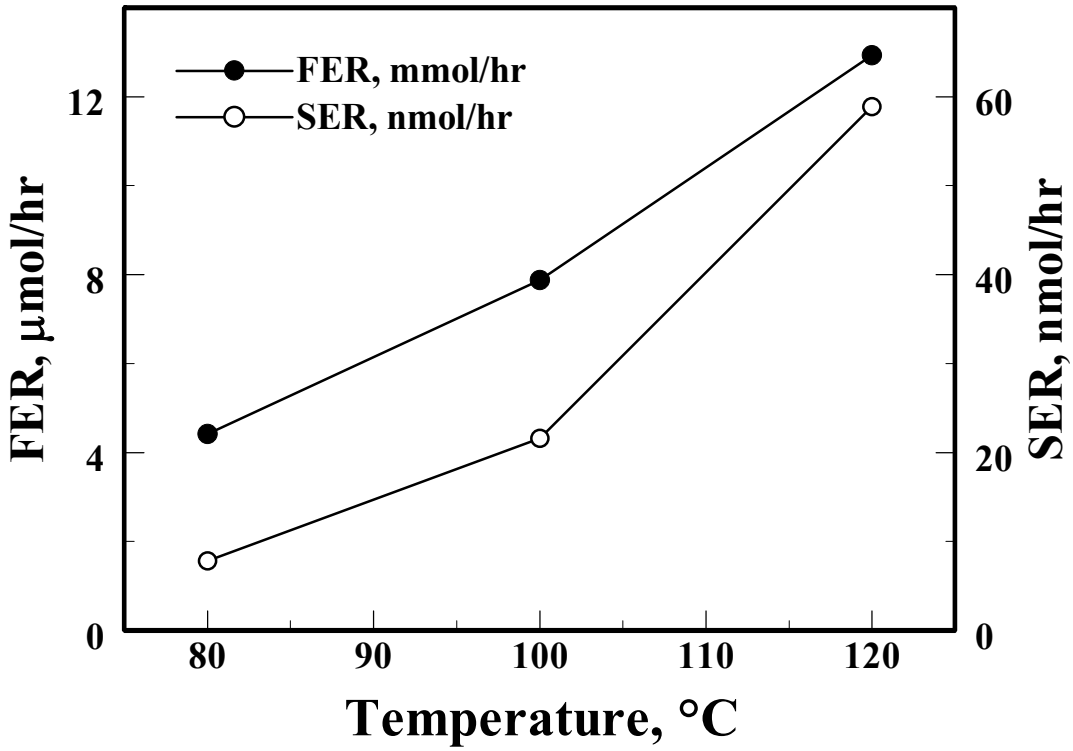

Figure 2-8. Total ,average fluorine [●] and sulfur [○] emission rates for a Nafion® 112 membrane during open circuit voltage decay as a function of temperature. All three cells were operated at 25% RH.

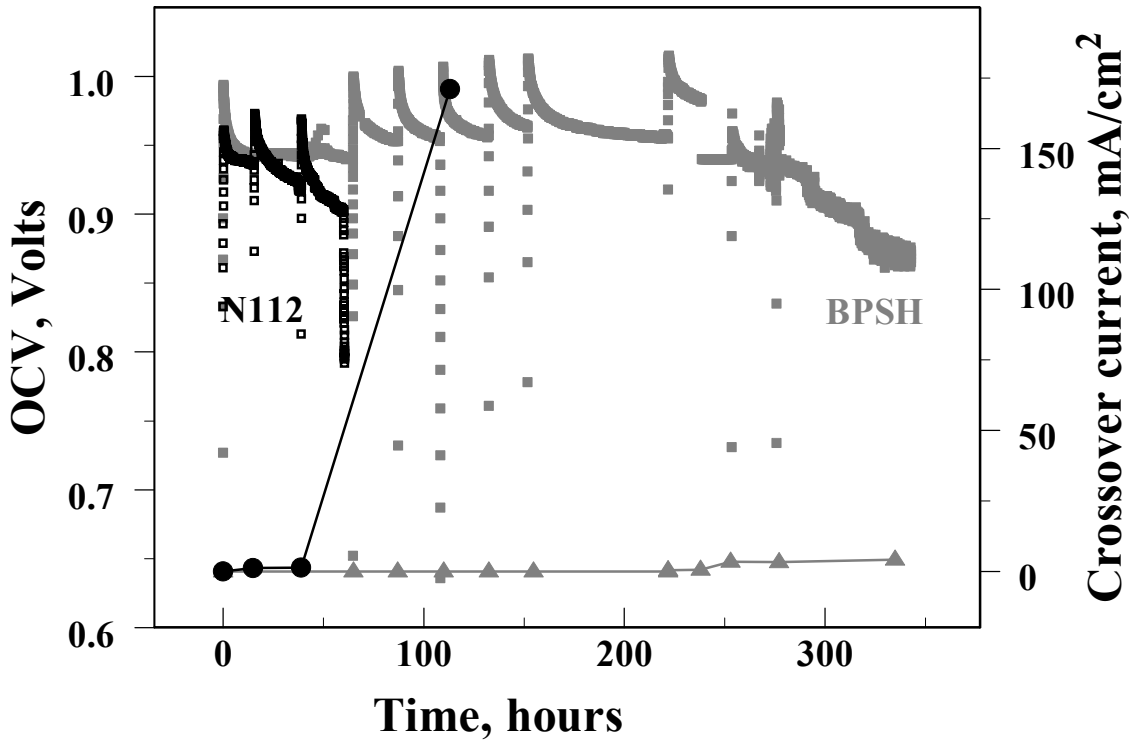

Figure 2-9. Open circuit voltage decay (□, ■) and hydrogen crossover current (●, ▲) for Nafion® 112 (□, ●) and BPSH (■, ▲) membranes at 100 ºC and 25% inlet gas relative humidity.

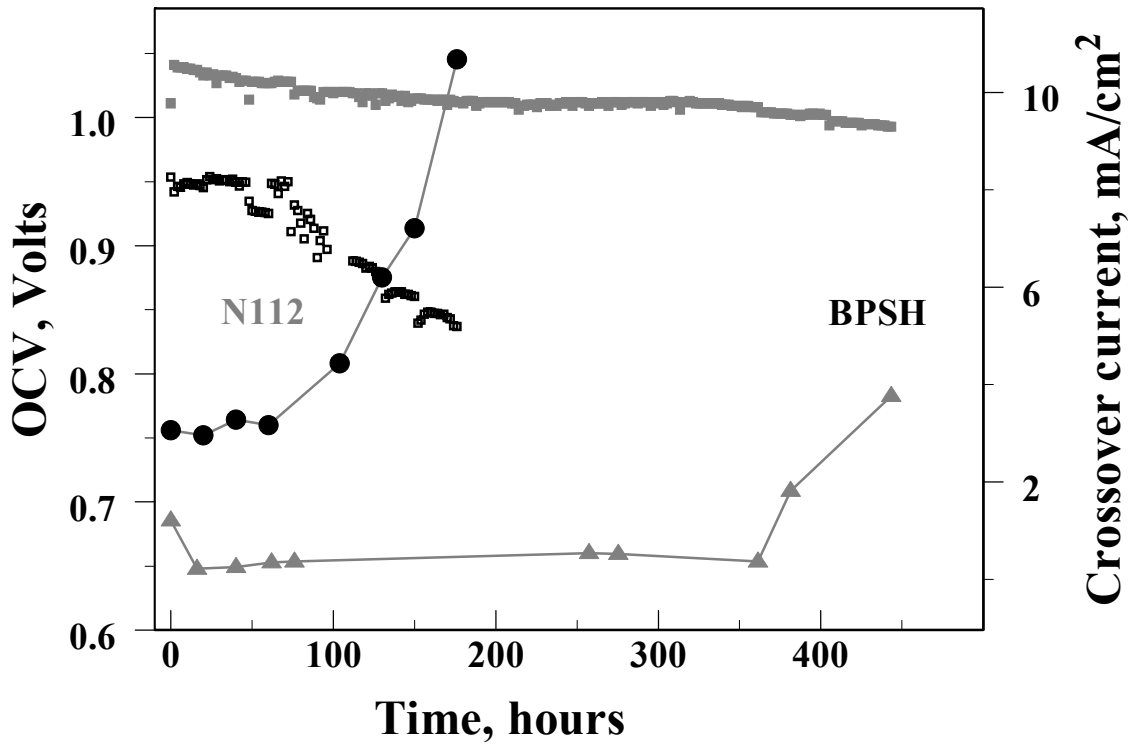

Figure 2-10. Open circuit voltage (□, ■) and hydrogen crossover current (●, ▲) for Nafion® 112 (□, ●) and BPSH (■, ▲) membrane during potential cycling (duty cycle = 0.5) between open circuit and 25 mA cm^{-2} (1 minute each) at 100 ºC, 150 kPa and 25% RH on H_2/O_2.

Figure 2-9 and Figure 2-10 show the comparison between the performances of Nafion® 112 and BPSH-35 membranes during the OCV decay experiment and potential cycling experiments, respectively, at 100 °C and 25% relative humidity conditions. Only the OCV data is shown for the case of potential cycling test in Figure 2-7. The OCV decay rate of BPSH cell was less than that of Nafion® 112 cell in both cases. Unlike OCV decay test, there is no rapid fall in OCV at any point during the potential cycling tests. At 100 ºC and 25% RH operation, Nafion® 112 lasted three times (~175 hours) longer during the potential cycling test than during OCV decay test (~60 hours). This result seems counter-intuitive because potential cycling should degrade the cell faster than maintaining at open circuit potential. Potential cycling an oxygen cathode create potentials that favor peroxide formation, i.e., the cathode routinely experiences potentials in the 0.4-0.7 V vs. NHE window. Also unlike OCV decay test, potential cycling eliminates continuous passivation of Pt, i.e., less PtO^- and $PtOO^-$ leads to more Pt dissolution thereby increasing the concentration of Pt^{2+} in the cathode. However, during potential cycling, water production at the cathode during load intervals increases the local water activity. This increase in local water activity decreases both peroxide production and Pt dissolution. Secondly, potential cycling interrupts oxygen crossover to the anode because oxygen is consumed during load intervals. Therefore the net flux of O_2 to the anode side would be lower during potential cycling than during the OCV decay test. Lower O_2 flux would mean lower peroxide production at the anode. Thirdly, the cathode experiences lesser time at Pt dissolution potentials. Comparison between these two membranes in terms of H_2 crossover across the membrane is also shown in these figures.

Similar to the OCV decay profile, the H_2 crossover current also do not show a sudden increase at any time during the potential cycling test.

The OCV decay rate of a cell is a measure of the chemical stability of its MEA. The membranes typically fail during the OCV decay test due to material loss resulting in overall thinning of the membrane or pinhole formation, both of which cause gas crossover and electrical shorting. The total fluorine and sulfur emission rates, defined as the ratio of total moles of fluorine or sulfur emitted to the total membrane life, exhibits linear dependence versus temperature at low humidity operation. Both gas crossover and electrical shorting lead to a drop in the OCV. The loss of fluorine and sulfur as measured in the exhaust water (Figure 2-8) confirm that the Nafion® membrane is losing mass and post-test images from the cycling tests (Figure 2-11) reveal that significant thinning occurred to the Nafion® membrane during these accelerated tests. Nafion® 112 lost 30 μm (60%) of its thickness in 100 hours of potential cycling between open circuit and 25 mA cm^{-2} at 100 ºC and 25% RH. However, BPSH-35 membrane did not thin during the same test for over 300 hours. It is very clear from these in-cell accelerated chemical stability tests that BPSH-35 outperforms Nafion® 112. Though Fenton tests indicate that the BPSH-35 membranes degrade strongly in the presence of trace iron contamination, they don't translate to their stability in the OCV decay tests. Conversely, good chemical stability exhibited by Nafion® 112 membranes during Fenton tests did not translate to their in-cell stability.

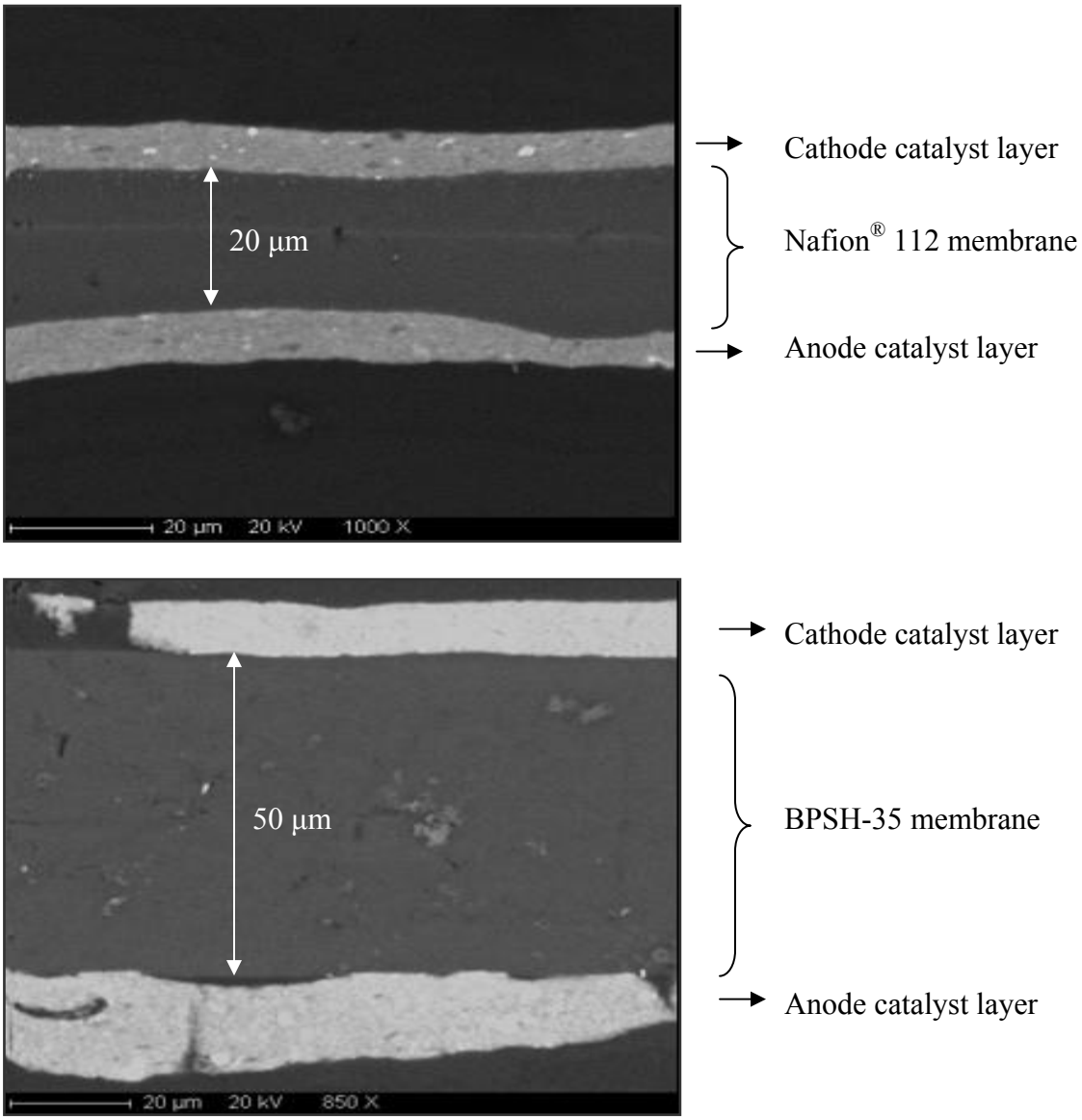

Figure 2-11. Post-test cross-sectional images of Nafion and BPSH-35 MEA's. The MEAs were cycled between open circuit and 25 mA/cm^2 for 1 minute each at 100 °C and 25% RH on H_2/O_2.

2.6.1.2. Peroxide formation rates at either electrodes

If the membrane degradation occurs via peroxy-radical attack, as reported by Cleghorn et al.[24], then the reason for the above performances could be because of the gas permeation properties of these membranes. Oxygen permeability, measured using electrochemical monitoring technique, is much higher for a Nafion® 112 membrane than a BPSH-35 membrane of equivalent thickness. This is shown in Figure 2-12. Gas permeation property of a membrane has two major implications to its durability in a PEM fuel cell – the transport of oxygen from the cathode side to the anode side and the transport of hydrogen from the anode side to the cathode side of a fuel cell. While the former affect hydrogen peroxide production the latter plays a significant role in Pt deposition inside the membrane.

H_2O_2 formation occurs at the anode at OCV conditions because of the existence of a favorable local potential (~0 V vs. NHE) and at both anode and cathode at load conditions. Since oxygen crossover rates are about 11 times lower for a BPSH-35 membrane compared to Nafion® 112 membrane, with the anode catalyst being the same, the former produces 11 times lower peroxide at its anode side than the latter at all conditions. It was shown earlier[18] that H_2O_2 formation in a fuel cell is very sensitive to humidity and temperature. This partly explains why Nafion® 112 showed poor chemical stability during in-cell tests at high temperatures and lower humidities.

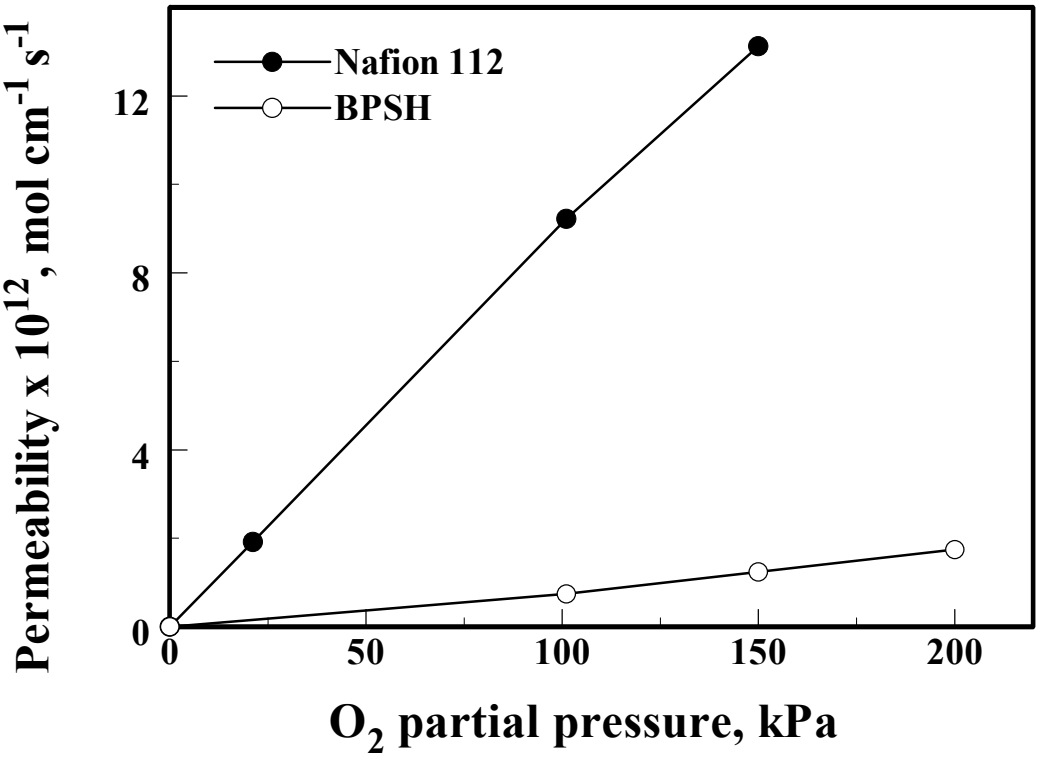

Figure 2-12. Oxygen permeability for Nafion® 112 and BPSH membranes measured using the electrochemical monitoring technique at 25 °C for different oxygen partial pressures.

2.6.1.2. Pt dissolution and migration into the membrane

Secondly, lower hydrogen transport from the anode side to the cathode side affects Pt deposition in the membrane. At high potentials normally experienced at the cathode during OCV conditions, Pt dissolves[25] from the support as Pt^{2+} and diffuses into the membrane because of concentration gradient. Molecular H_2 crossing over from the anode side acts as a reductant and reduces the Pt^{2+} species chemically, which results in the chemical deposition of metallic Pt inside the membrane. Similar chemical platinization of Nafion® had been reported earlier by Fedkiw et al.[14, 26] and Takenaka et al.[13] The presence of Pt inside the membrane catalyzes the formation of hydroxyl radicals which attack the membrane[27]. Assuming the rates of Pt dissolution and Pt^{2+} migration are same for both BPSH-35 and Nafion® 112 membranes, the former owing to its lower H_2 crossover has lower concentration of Pt inside the membrane than the latter.

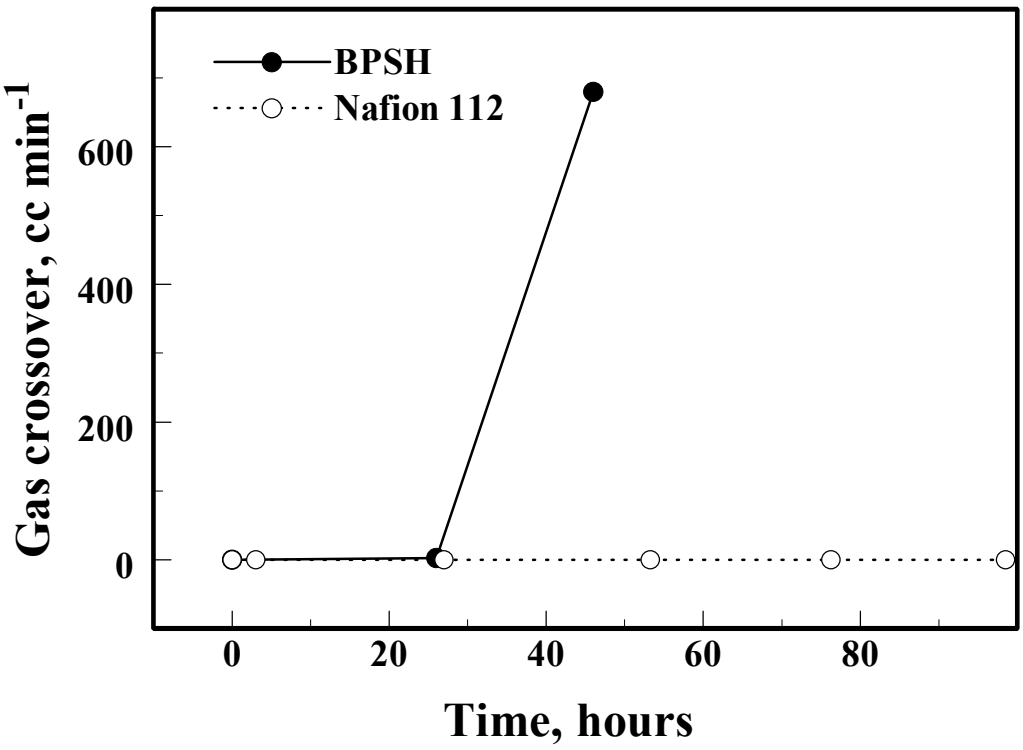

Figure 2-13. Gas crossover at 3 psig differential nitrogen pressure across the membrane measured during the humidity cycling test on Nafion® 112 and BPSH membranes. The relative humidity was cycled between 100% for one hour and 0% for one hour at 100 ºC and 150 kPa.

2.6.2. Mechanical Stability

Mechanical stability of the membranes was tested by alternating completely dry feed gas and fully saturated (100% RH) feed gas at 1 hour intervals. This induced mechanical stresses in the membrane because of repeated swelling and contraction. Figure 2-13 shows gas crossover measured at 3 psig at various time intervals during this RH cycling. Nafion® 112 showed better mechanical stability than BPSH-35 membrane. This is in accordance with an earlier report by Mathias et al.[28] on higher mechanical stability for Nafion® than a hydrocarbon membrane. This is because of BPSH membrane's increased expansion and contraction during wet-up and dry-out cycles. BPSH-35 membranes failed because of cracks along the edge of the gasket-membrane interface, where the stresses are maximal during expansion and contraction during RH cycling. Linear expansion in all three dimensions between completely dry and wet conditions was measured for Nafion® and BPSH membranes and is tabulated in Table 2-2.

2.7. Conclusions

In situ chemical and mechanical stabilities and their dependence on temperature and humidity must be considered when evaluating membranes for PEM fuel cells. Though BPSH membranes showed poor chemical stability in *ex situ* Fenton tests, they outperformed Nafion® 112 membranes in OCV decay and potential cycling tests in fuel cell conditions. The superior *in situ* chemical stability exhibited by BPSH membranes is partly because of their lower gas crossover rates than Nafion® 112 membranes. Gas permeation property plays a very important role in membrane durability. Lower oxygen crossover rates to the anode results in lower anode peroxide formation rates; and lower

hydrogen crossover rates to the cathode results in lesser Pt deposition inside the membrane. Though the correct mechanism for membrane degradation is not entirely known, the process seems to be a strong function of gas humidity and local water activity. Gas humidity affects the mechanical durability of the membranes especially if the fuel cell operation calls for frequent start-stop cycles. The frequent wet-up and dry out cycles cause mechanical stresses on the membrane. It is desirable for a membrane to have lower water uptake, which translates to better dimensional stability.

Table 2-1. Voltage decay rates for Nafion® 112 and BPSH-35 membranes measured during the OCV decay experiments.

Membrane	Temperature, K	% Relative Humidity	OCV decay rate, mV/h
Nafion® 112	353	25	0.358
	373	25	1.82
		50	1.064
		75	0.498
	393	25	4.02
BPSH-35	373	25	0.507

Table 2-2. Percent linear expansion in x, y and z directions for Nafion® 112 and BPSH membranes.

Membrane	Linear expansion x - direction, %	Linear expansion y - direction, %	Swelling upon boiling, %
BPSH – 35	25	15	41.2
Nafion® 112	10	3.1	11.4

2.8. References

1. J. P. Myers, "Development of High Temperature Membranes and Improved Cathode Catalysts", *DoE Hydrogen, Fuel Cells and Infrastructure Technologies Review*, May 2004.

2 . M. A. Hickner, H. Ghassemi, Y. S. Kim, B. R. Einsla and J. E. McGrath, *Chem. Rev.,* **104**, 4587 (2004).

3. J. A. Kerres, *J. Membrane Sci.,* **185**, 3 (2001).

4. J. J. Dumais, A. L. Cholli, L. W. Jelinski, J. L. Hedrick and J. E. McGrath, *Macromolecules*, **19**, 1884 (1986).

5. A. Noshay and L. M. Robeson, *J. Applied Polymer Science*, **20**, 1885, (1976).

6. F. Wang, M. Hickner, Y. S. Kim, T. A. Zawodzinski and J. E. McGrath, *J. Membrane Science*, **197**, 231 (2002).

7. D. P. Wilkinson and J. St. Pierre, *Handbook of Fuel Cells – Fundamentals, Technology and Applications, Fuel Cell Technology and Applications,* **3**, Chapter 43, W. Vielstich, H. A. Gasteiger and A. Lamm, Editors, John Wiley and Sons, Ltd., West Sussex, England (2003).

8. BPSH-35 membranes were obtained from Professor James E. McGrath, Virginia Polytechnic Institute and State University, Blacksburg, VA 24061.

9. C. Walling, *Accts. Chem. Research*, **8**, 125 (1975).

10. J. Healy, C. Hayden, T. Xie, K. Olson, R. Waldo, M. Brundage, H. Gasteiger and J. Abbott, *Fuel Cells*, **5**, 302 (2004).

11. G. Escobedo, T. H. Madden and R. B. Moore. *DOE Hydrogen Program FY 2005 Progress Report*, 761, (2005).

12. L. V. Protsailo, "Development of High-Temperature Membranes and Improved Cathode Catalysts", *DoE Hydrogen Program FY 2005 Progress Report*, p. 743 (2005).

13. H. Takenaka, E. Torikai, Y. Kawami and N. Wakabayashi, *Int. J. Hydrogen Energy*, **7**, 397 (1982).

14. P. S. Fedkiw and W. Her, *J. Electrochem. Soc.,* **136**, 899 (1989).

15. A. B. LaConti, M. Hamdan, R. C. MacDonald, in *Handbook of Fuel Cells: Fundamentals, Technology and Applications,* W. Vielstich, A. Lamm and H. Gasteiger, Editors, **3**, p. 647, John Wiley and Sons, Chichester, England (2003).

16. S. D. Knights, K. M. Colbow, J. St-Pierre and D. P. Wilkinson, *J. Power Sources*, **127**, 127 (2004).

17. E. Endoh, S. Terazono, H. Widjaja and Y. Takimoto, *Electrochem. Solid State Letters,* **7**, A209 (2004).

18. V. A. Sethuraman, J. W. Weidner, A. T. Haug, S. Motupally and L. V. Protsailo, "Effect of Water Activity and Oxygen Concentration on H_2O_2 formation on Pt/C", manuscript to be submitted to *J. Electrochem. Soc.*, (2006).

19. S. C. Yeo and A. Eisenberg, *J. App. Polym. Sci.,* **21,** 875 (1977).

20. T. Kyu and A. Eisenberg, in *Perfluorinated Ionomer Membranes*, A. Eisenberg and H. L. Yeager, Editors, *Amer. Chem. Soc. Symp. Ser., **180***, Chapter 6, 79, A. C. S Publications, Washington, DC (1982).

21. C. Huang, K. S. Tan, J. Lin and K. L. Tan, *Chem. Phys. Letters,* **371**, 80 (2003).

22. T. Sakai, H. Takenaka and E. Torikai, *J. Electrochem. Soc.,* **133**, 88 (1986).

23. A. Panchenko, *Dipl.-Chem.*, Institute für Phzsikalische Chemie der Universität Stuttgart, October 2004.

24 . S. Cleghorn, J. Kolde and W. Liu, in *Handbook of Fuel Cells – Fundamentals, Technology and Applications, Fuel Cell Technology and Applications,* **3**, p. 566, W. Vielstich, H. A. Gasteiger and A. Lamm, Editors, John Wiley and Sons, Ltd., West Sussex, England (2003).

25 . P. J. Ferreira, G. J. la O', Y. Shao-Horn, D. Morgan, R. Makharia, S. Kocha and H. Gasteiger, *J. Electrochem. Soc.,* **152**, A2256 (2005).

26. R. Liu, W-H. Her and P. S. Fedkiw, *J. Electrochem. Soc.,* **139**, 15 (1992).

27. D. E. Curtin, R. D. Lousenberg, T. J. Henry, P. C. Tangeman and M. E. Tisack, *J. Power Sources*, **131**, 41 (2004).

28. M. F. Mathias, R. Makharia, H. A. Gasteiger, J. J. Conley, T. J. Fuller, C. J. Gittleman, S. S. Kocha, D. P. Miller, C. K. Mittelsteadt, T. Xie, S. G. Yan and P. T. Yu, *Electrochem. Soc. Interface,* **14** (3), 24 (2005).

3. Effect of Water Activity and Oxygen Concentration on Hydrogen Peroxide Formation on Pt/C

3.1. Abstract

Hydrogen peroxide (H_2O_2) formation rates in a proton exchange membrane (PEM) fuel cell were estimated by studying the oxygen reduction reaction (ORR) on a rotating ring disc electrode (RRDE). Fuel cell conditions were replicated by depositing a film of Pt/Vulcan XC-72 catalyst onto the disk and by varying the temperature, dissolved O_2 concentration and the acidity levels in $HClO_4$. The $HClO_4$ acidity was correlated to ionomer water activity and hence fuel cell humidity. H_2O_2 formation rates showed a linear dependence on oxygen concentration and square dependence on water activity. The H_2O_2 selectivity in ORR was independent of oxygen concentration but increased with decrease in water activity (i.e., decreased humidity). Potential dependent activation energy for the H_2O_2 formation reaction was estimated from data obtained at different temperatures.

[V. A. Sethuraman, J. W. Weidner, A. T. Haug, S. Motupally and L. V. Protsailo, "Effect of Water Activity and Oxygen Concentration on Hydrogen Peroxide Formation on Pt/C", submitted to the *Journal of the Electrochemical Society*, December 2006.]

3.2. Introduction

One of the mechanisms for catalyst/ionomer's chemical degradation in PEMFCs involves the formation of hydroxyl and hydroperoxyl ($OH^{\bullet}$ and $HO_2^{\bullet}$) radicals[1, 2] caused by hydrogen peroxide (H_2O_2) formation on the catalyst surface via reactions 3-1 - 3-3 and decomposition via reactions 3-4 - 3-5.

$$H_2 \xrightarrow{Pt} 2H\bullet \quad \textbf{3-1}$$

$$H\bullet + O_2 \longrightarrow OOH\bullet \quad \textbf{3-2}$$

$$OOH\bullet + H\bullet \longrightarrow H_2O_2 \quad \textbf{3-3}$$

$$H_2O_2 + M^{2+} \longrightarrow M^{3+} + \bullet OH + OH^- \quad \textbf{3-4}$$

$$\bullet OH + H_2O_2 \longrightarrow OOH\bullet + H_2O \quad \textbf{3-5}$$

These radicals react with the perfluorosulfonic acid (PFSA) type ionomer in the electrode and the membrane to produce hydrofluoric acid (HF)[3]. The sequence is listed below

$$R_p - CF_2COOH + OH\bullet \longrightarrow R_p - CF_2 + CO_2 + H_2O \quad \textbf{3-6}$$

$$2R_p - CF_2 + 2OH\bullet \longrightarrow R_p - CF_2OH + R_p - COF + HF \quad \textbf{3-7}$$

$$R_p - COF + H_2O \longrightarrow R_p - COOH + HF \quad \textbf{3-8}$$

The fluoride emission rate (FER) in the form of HF is a measure of membrane degradation given in reactions 3-7 and 3-8. Since two thirds of Nafion® is fluorine (on a mass basis), this chemical degradation results in mechanical instability in the membranes

causing pinholes and eventual failure. Since this degradation is initiated by the peroxide-radical attack, understanding H_2O_2 kinetics at the electro-catalyst/ionomer interface at low humidities and elevated temperatures from a PEM fuel cell context is vital towards explaining the increased degradation rate observed under such conditions. Though Liu and Zuckerford[4] have reported a method for *in situ* detection of H_2O_2 formation, it only served as a qualitative indicator of the existence of peroxide. *In situ* quantification of peroxide kinetics is very difficult owing to its instability.

Therefore, the objective of this investigation is to estimate H_2O_2 formation rates in a PEM fuel cell by studying the ORR on a rotating ring disc electrode (RRDE). Fuel cell conditions were replicated by depositing a film of Pt/Vulcan XC-72 catalyst onto the disk and by varying the temperature, dissolved O_2 concentration and the acidity levels in $HClO_4$. The $HClO_4$ acidity was correlated to ionomer water activity and hence fuel cell humidity.

Rotating ring disk electrode (RRDE) studies on supported Pt catalysts have been successfully used[5, 6, 7, 8, 9, 10] as a technique to quantify peroxide formation and for screening oxygen reduction catalysts. Paulus et al.[5, 7] reported the use of a *thin-film* RRDE method for characterizing oxygen reduction reaction (ORR) in supported high surface area catalysts and were able to quantify the amount of H_2O_2 produced during oxygen reduction reaction (ORR). They decreased the film thickness and improved the ionomer-catalyst film stability at higher rotation speeds, which resulted in uniform collection efficiencies and better peroxide measurements. Antoine et al.[8] reported a weak platinum particle size effect on H_2O_2 production during ORR and agreed with previously reported observations that H_2O_2 yields were higher for potentials less than 0.4 V vs. SHE.

Enayetullah et al.[9] studied ORR electrocatalysis on polycrystalline Pt microelectrode in various concentrations of Trifluoromethane sulfonic acid (TFMSA). They reported higher tafel slopes and lower activation energies for ORR in higher concentrations of TFMSA, which was attributed to lower water activity. Murthi et al.[10] studied ORR in supported Pt and Pt alloy catalysts in 1M and 6 M TFMSA as a way to study the effect of water activity. They reported higher peroxide yields in 6M TFMSA solution compared to a 1M solution.

3.3. Experimental

3.3.1. Rotating Ring Disc Electrode (RRDE)

For the RRDE studies, commercially available Pt/Vulcan catalyst (20% Pt on Vulcan XC-72R carbon, Johnson Matthey Inc., PA) was used. Catalyst coated glassy carbon electrodes were prepared as described by Schmidt et al.[11]. Aqueous suspensions of 1 mg catalyst ml^{-1} were obtained by pulse-sonicating 20 mg Pt/Vulcan catalyst with 20 ml triple-distilled, ultrapure water (Millipore Corporation) in an ice bath (70% duty cycle, 60W, 15 minutes). Sonication was done using a Braun-Sonic U Type 853973/1 sonicator. Glassy carbon disc served as the substrate for the supported catalyst and was polished to a mirror finish (0.05 μm deagglomerated alumina, Buehler®) prior to catalyst coating. An aliquot of 14 μl catalyst suspension was pipetted onto the carbon substrate, which corresponded to a Pt loading of ~14.1 μg Pt cm^{-2}. After evaporation of water for 30 minutes in N_2 atmosphere (15 in-Hg, vacuum), 14 μl of diluted Nafion solution (5% aqueous solution, 1100 EW; Solution Technology Inc., Mendenhall, PA) was pipetted on the electrode surface and further evaporated for 30 minutes in N_2 atmosphere (15 in-Hg,

vacuum). Nafion® was used to adhere the Pt/Vulcan particles onto the glassy carbon electrode (the ratio of H_2O/Nafion® solution used was ca. 100/1). Previous work by Paulus et al. indicate that this procedure yielded a Nafion® film thickness of ca. 0.1 μm and that the utilization of the Pt/Vulcan catalyst (based on H-adsorption charge) on the electrode with this film was ~100%.

The catalyst-Nafion® coated electrode was immersed in deaerated (UHP Nitrogen, Praxair) Perchloric acid ($HClO_4$, 70%, Ultrapure Reagent Grade, J. T. Baker) of varying concentrations for further synchronized chrono-amperometric and potentiodynamic experiments. Though a variety of supporting electrolytes are reported in the literature, anion adsorption on Pt is minimal for only few electrolytes[12]. Trifluoromethane sulfonic acid (TFMSA) and $HClO_4$ are some of the acids, anions of which exhibited minimal or no adsorption on Pt. All RRDE experiments were performed at atmospheric pressure. All solutions were prepared from ultrapure water (Millipore Inc., 18.2 MΩcm).

The electrochemical measurements were conducted in a standard electrochemical cell (RDE Cell®, Pine Instrument Company, NC) immersed in a custom-made jacketed vessel, temperature of which was controlled by a refrigerated/heating circulator (Julabo Labortechnik GMBH). A ring-disk electrode setup with a bi-potentiostat (Bi-Stat®, Princeton Applied Research Inc., TN) in conjunction with rotation-control equipment (Pine Instrument Company, NC). EC-Lab® software (version 8.60, Bio-logic Science Instruments, France) was used to control the bi-potentiostat. The Pt ring electrode was held at 1.2 V vs. SHE where the oxidation of peroxide is diffusion limited. The catalyst coated glassy carbon disc electrode (5 mm diameter, 0.1966 cm^2 area, DT21 Series, Pine

Instrument Company, NC) was scanned between 0 – 1.2 V vs. SHE to characterize H_2O_2 formation within the potential range relevant to fuel cell operating conditions. Potentials were determined using a Mercury-mercurous sulfate (Hg/Hg_2SO_4) reference electrode. All potentials in this study, however, refer to that of the standard hydrogen electrode (SHE). A high-surface area Pt cylindrical-mesh (5 mm diameter, 50 mm length) attached to a Pt wire (0.5 mm thick, 5 mm length) was used as the counter electrode.

3.3.2. Effect of Oxygen Concentration

The effect of oxygen concentration on ORR and H_2O_2 formation kinetics was studied by varying the concentration of oxygen in the gas bubbled through the electrolyte. The following three gases were used: oxygen (UHP grade, Praxair), Air (Industrial, Praxair) and 10.01% oxygen in nitrogen (Airgas). A gas flow meter (0-500 ml, Dwyer Instruments Inc., IN) was used to control the flow of the gas feed at ~100 ml min^{-1} into the electrolyte. The electrochemical cell was sealed during the experiments to keep air from affecting the concentration of dissolved oxygen in the electrolyte. The concentration of dissolved oxygen in the electrolyte was estimated using the solubility values for oxygen in pure liquid water at 25 ˚C and 101 kPa.[13]

3.3.3. Effect of pH

The effect of proton concentration on ORR and H_2O_2 formation kinetics was studied by varying the acidity of $HClO_4$ in the 2.0 – 0.1 M concentration window (~-0.301 – 1 pH, assuming K_a >>1 for $HClO_4$). Between solution changes, the electrochemical cell and its components were washed and boiled in DI water for 5 hours

to ensure accurate pH levels. The catalyst-Nafion® coated electrode was also cleaned in a sonicator before every experiment.

3.3.4. Collection Efficiency

Standard procedure[14] for the determination of collection efficiency of a ring-disc electrode was followed. The electrodes were prepared as described above. The experiment was carried out in an electrochemical cell in deaerated (UHP Nitrogen, Praxair) 0.1 M H_2SO_4 (96.5%, J. T. Baker) with 10 mmol l^{-1} $K_3Fe(CN)_6$ (99.7%, J. T. Baker. The disk electrode was swept at 1 mV s^{-1} [vs. SHE] while the Pt ring was held at a constant potential of 1.2 V [vs. SHE]. At this ring potential, the oxidation of $[Fe(CN)_6]^{4-}$, produced at the disk electrode, to $[Fe(CN)_6]^{3-}$, proceeds under pure diffusion control. The collection efficiency was determined as $N = I_{ring}/I_{disk} = 0.20$, which was independent of disk potential and consistent with the theoretical collection efficiency provided by the manufacturer of the ring-disc electrode.[15]

Figure 3-1 shows the ring and disc currents observed in electrolytes with two different acidities. While the symbols in (a) and (b) represent data, the lines in (b) represent disk current multiplied by the collection efficiency.

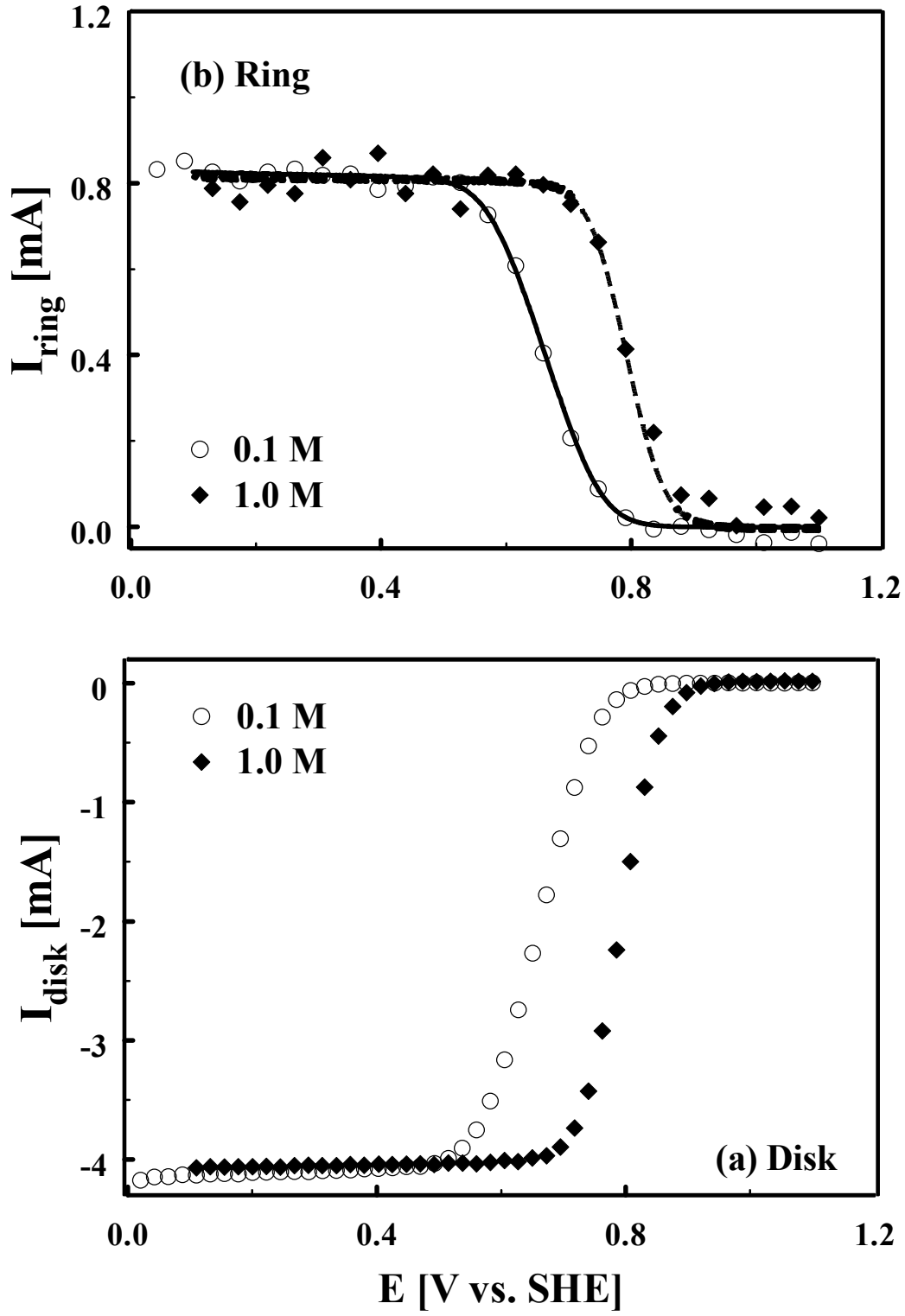

Figure 3-1. (a) Disk $\{[Fe(CN)_6]^{3-} + e^- \rightarrow [Fe(CN)_6]^{4-}\}$ and (b) Ring $\{[Fe(CN)_6]^{4-} \rightarrow [Fe(CN)_6]^{3-} + e^-\}$ currents at 25 ˚C for the determination of the collection efficiency on a

Pt/Vulcan XC-72R (14.1 μg Pt cm^{-2}) thin-film RRDE [2500 rpm] in 0.1 M [○] and 1.0 M [♦] H_2SO_4 supporting electrolyte with 20 mM $K_3Fe(CN)_6$. Positive sweeps at 1 mV s^{-1}; E_{ring} = 1.2 V vs. SHE. The lines in (b) indicated by —— [0.1 M H_2SO_4] and ----- [1.0 M H_2SO_4], correspond to their respective I_{disk} multiplied by N, where N is the collection efficiency equaling 20%.

3.4. Theory

At the disk, the following two reactions occur. Only the two-electron transfer reaction of O_2 reduction to H_2O_2, as captured by the Pt ring was analyzed in this work.

$$O_2 + 2H^+ + 2e^- \leftrightarrow H_2O_2 \qquad E^0 = 0.695V \ \ vs.\ SHE \qquad \textbf{3-9}$$

$$O_2 + 4H^+ + 4e^- \rightarrow 2H_2O \qquad E^0 = 1.23V \ \ vs.\ SHE \qquad \textbf{3-10}$$

At the ring, the H_2O_2 produced at the disk is oxidized via the reverse of reaction **3-9**. The fraction of H_2O_2 formation, $\chi_{H_2O_2}$, can be determined from the collection efficiency, ring and disk currents by the expression,,

$$\chi_{H_2O_2} = \frac{2I_{ring}/N}{I_{disk} + I_{ring}/N} \qquad \textbf{3-11}$$

The measured current density j on a film covered RDE for the first-order ORR kinetics was previously reported[16] to take the following expression, in terms of kinetic and mass-transport dependent currents,

$$\frac{1}{j} = \frac{1}{j_{kin}} + \frac{\delta_f}{n_e F D^f_{O_2} C^f_{O_2}} + \frac{1}{j_D} \qquad \textbf{3-12}$$

In this case, j is taken to be

$$j = \frac{I_{ring}}{N.A} \qquad \textbf{3-13}$$

j_{kin} is the current density in the absence of mass transfer effects and j_D is the diffusion current given by the Levich equation.

$$j_D = 0.62nFD^{*\ 2/3}_{O_2} C^*_{O_2} \nu^{-1/6} \omega^{1/2} \qquad \textbf{3-14}$$

The concentration of O_2 in the solution was calculated from the partial pressure of O_2 in the inlet gas and O_2 solubility data for pure liquid water at corresponding temperature and 101 kPa. The difference in O_2 solubility in pure liquid water and in $HClO_4$ (up to 2M) was assumed to be negligible. The kinetic current, j_{kin}, was accordingly estimated from the measured current j using the following expression obtained by solving equations 12 and 14,

$$j_{kin} = \frac{jnFD_{O_2}^{f} C_{O_2}^{f} D_{O_2}^{*\,2/3} C_{O_2}^{*} \omega^{1/2}}{nFD_{O_2}^{f} C_{O_2}^{f} D_{O_2}^{*\,2/3} C_{O_2}^{*} \omega^{1/2} - \delta_f j D_{O_2}^{*\,2/3} C_{O_2}^{*} \omega^{1/2} - 1.6\nu^{1/6} j D_{O_2}^{f} C_{O_2}^{f}} \qquad \textbf{3-15}$$

Therefore, H_2O_2 rates presented in this analysis are the ring currents adjusted for mass transfer effects.

The rate expression for H_2O_2 production in terms of the kinetic current can be written as,

$$j_{kin} = n_e F k_f C_{O_2}^{a} C_{H^+}^{b} \qquad \textbf{3-16}$$

$$k_f = k_{f,0} \exp\left[\frac{\alpha F \eta}{RT^0}\right] \qquad \textbf{3-17}$$

In equation 3-16, '*a*' and '*b*' are reaction orders with respect to O_2 and H^+ respectively. The kinetic rate constant k_f was estimated for different potentials by plotting H_2O_2 production rate as a function of oxygen concentration for various potentials. Since the electrode reaction rate was earlier shown by Damjanovic and Hudson[17] to be faster on an oxide-free Pt surface than on an oxide-covered surface, both the forward and the reverse scans were used to estimate the reaction rate constant. The potential dependence of this rate constant is given in equation 3-17.

The activation energies for hydrogen peroxide formation reaction on Pt/Vulcan XC-72R were evaluated at a fixed electrode potential using the Arrhenius equation[5, 18] shown below,

$$\left(\frac{\partial \log\left(j_{kin}\right)}{\partial\left(1/T\right)}\right)_E = \frac{E_a}{2.3R} \qquad \textbf{3-18}$$

This experimentally estimated activation energies for H_2O_2 formation on supported Pt catalysts were compared to the computationally estimated activation energies reported in the literature. Using density functional theory (DFT) based studies, Anderson and Albu[19], Sidik and Anderson[20] and Wang and Balbuena[21] have reported activation energies for H_2O_2 formation on Pt_1, Pt_2 and Pt_3 sites respectively.

Kinetic rate constants for H_2O_2 formation at elevated temperatures were estimated using the experimentally estimated activation energies. The following expression was used,

$$k_f^0 = k_{f,0}^0 \exp\left[\frac{E_a}{RT}\right] \qquad \textbf{3-19}$$

H_2O_2 production rates in a fuel cell anode as a function of relative humidities and cell temperature were then calculated using these kinetic parameters and experimentally measured O_2 crossover to the anode side.

3.5. Results and Discussion

3.5.1. H_2O_2 Kinetic Study Using RRDE

Figure 3-2 shows the peroxide formation rates, as indicated by the ring current, for different concentrations of dissolved oxygen in the electrolyte. It can be seen that the increases in the ring and the disc currents indicate a linear dependence of oxygen

concentration on the respective rates. It should be noted that hydrogen evolution starts in the neighborhood of ca. 25-50 mV vs. SHE. Hence, both ring and disc currents in the 25-50 mV region include a fractional contribution due to hydrogen evolution [$2H^+ + 2e^- \longrightarrow H_2$] and oxidation [$H_2 \longrightarrow 2H^+ + 2e^-$] respectively. This is noted by the decrease in the disk currents and an increase in the ring currents in the 25 – 50 mV potential region. Data obtained below 25 mV was not used in this analysis.

Figure 3-3 shows the fraction of peroxide produced in the ORR at the disk, as captured by the ring and shows no dependence on oxygen concentration.

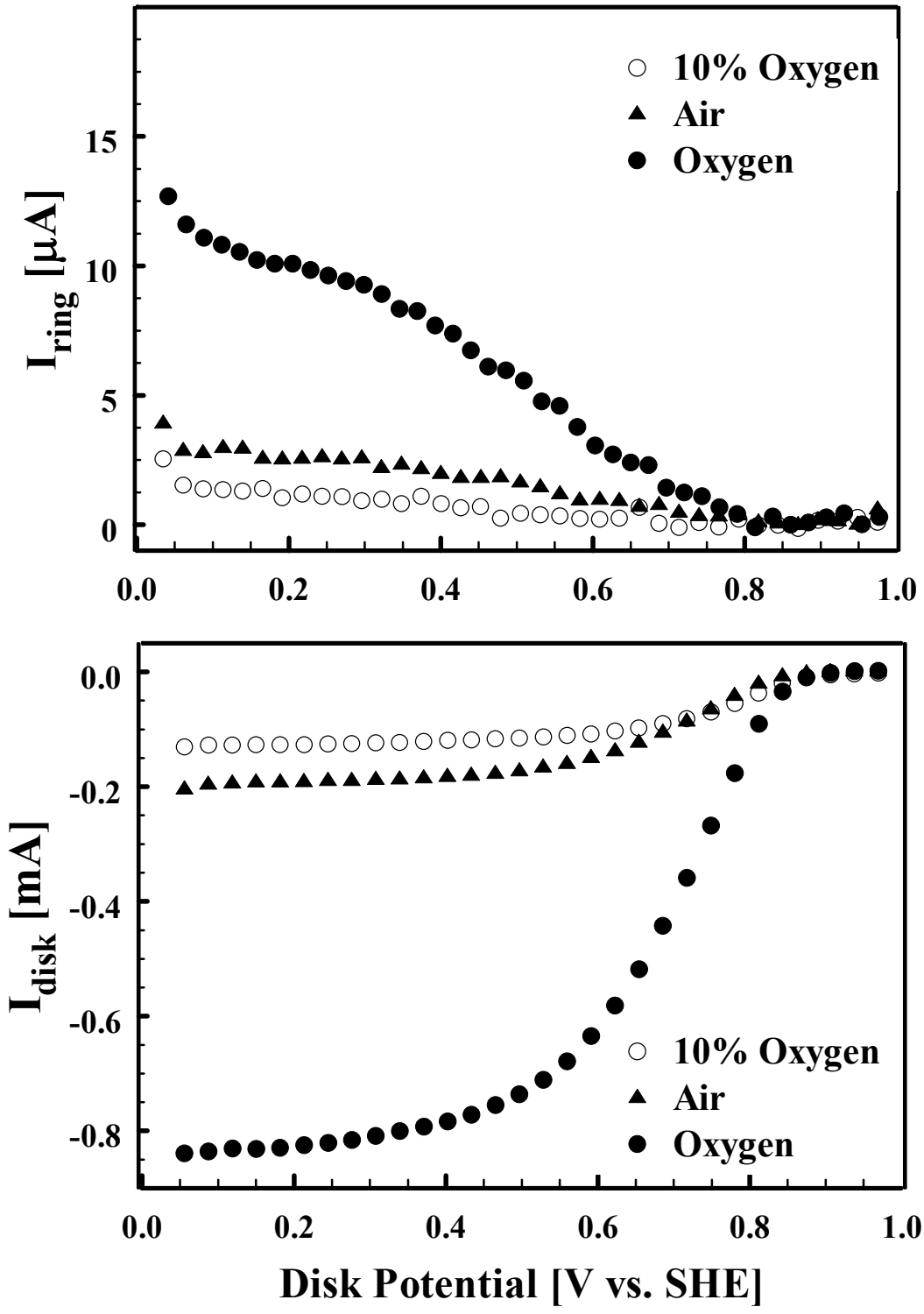
10% Oxygen
Air
Oxygen
I_{ring} [μA]
15
10
5
0
0.0
0.2
0.4
0.6
0.8
1.0
I_{disk} [mA]
0.0
-0.2
-0.4
-0.6
-0.8
Disk Potential [V vs. SHE]

Figure 3-2. (a) Polarization curves for the oxygen reduction reaction on a Pt/Vulcan XC-72R (14.1 μg Pt cm^{-2}) thin-film RRDE [2500 rpm] in 2.0 M $HClO_4$ solution [pH = -0.3] bubbled with 10% O_2 [○], Air [▲] and O_2 [●]. (b) Ring currents following the production of H_2O_2 [E_{ring} = 1.2 V vs. SHE].

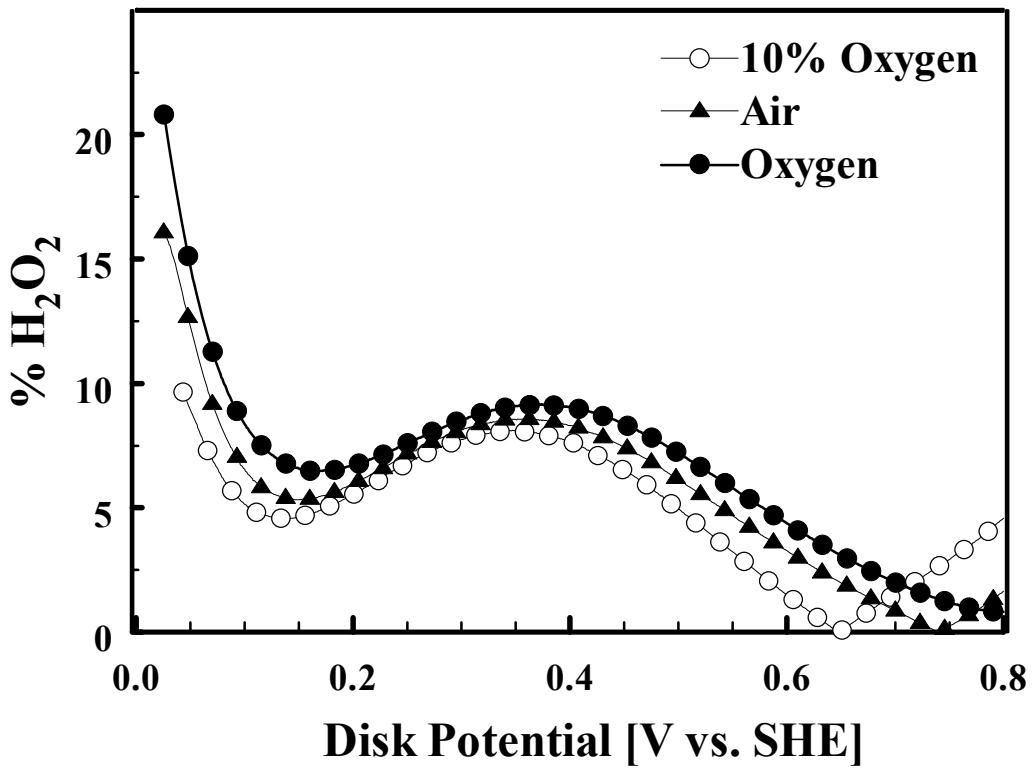

Figure 3-3. % H_2O_2, given by equation 3-11, formed during the oxygen reduction reaction on Pt/Vulcan XC-72R in 2.0 M $HClO_4$ solution [pH = -0.3] bubbled with 10% O_2 [○], Air [▲] and O_2 [△] at 25 °C. E_{ring} = 1.2 V vs. SHE, 1mV/s, 2500 rpm.

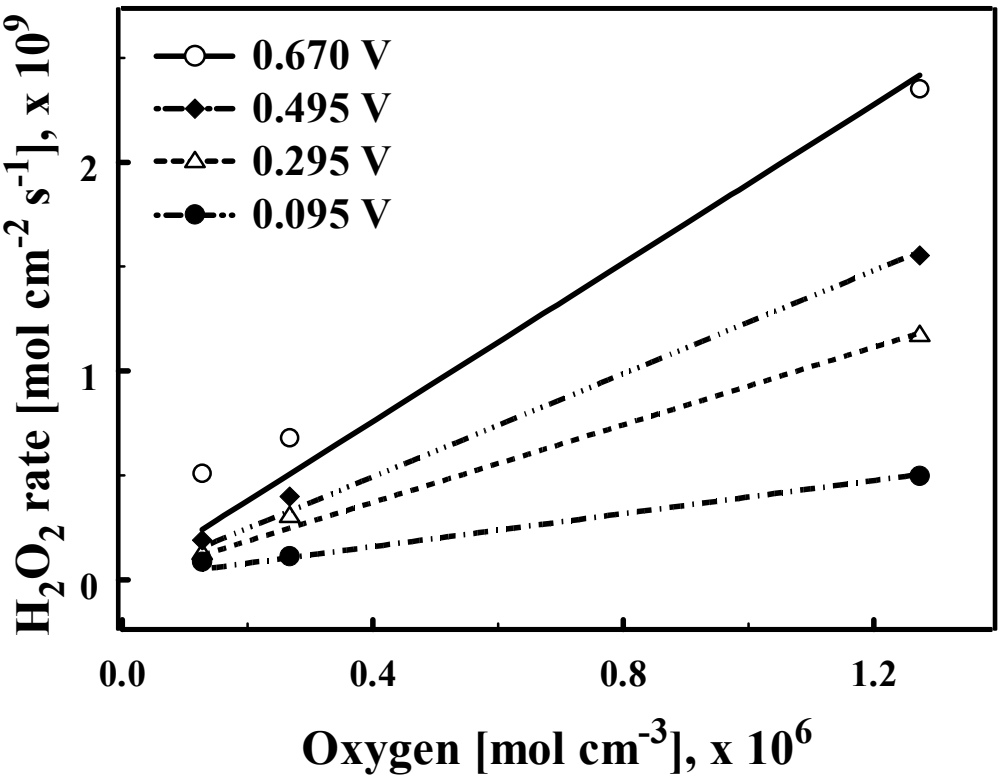

Figure 3-4. H_2O_2 formation rates [mol cm^{-2} s^{-1}] on Pt/Vulcan XC-72R in 2.0 M $HClO_4$ solution [pH = -0.3] as a function of dissolved oxygen concentration [mol L^{-1}] for the following four overpotentials: 0.695 V [○], 0.495 V [♦], 0.295 V [Δ] and 0.095 V [•]. The symbols represent data and the lines represent linear fits with zero intercepts.

Also, for all overpotentials, the ring currents and hence the rate of H_2O_2 formation as captured by the ring shows a linear dependence on oxygen concentration. This is shown in Figure 3-4. The data points were fit to a linear equation with zero intercept. Therefore the value for *a,* the reaction order with respect to O_2 in the H_2O_2 formation reaction is 1. The slopes represent the electrochemical rate constant k_f, as given by equation 3-17. In this figure, an overpotential of 0.670 V represents a potential of 0.025 V vs. SHE because the equilibrium potential for H_2O_2 formation is 0.695 V. Four representative overpotentials were chosen for this plot. The anode experiences the highest overpotential (for peroxide formation) at all times during fuel cell operation. The cathode experiences a significant drop in the local potential during load conditions and can approach and go negative of H_2O_2 equilibrium potential.

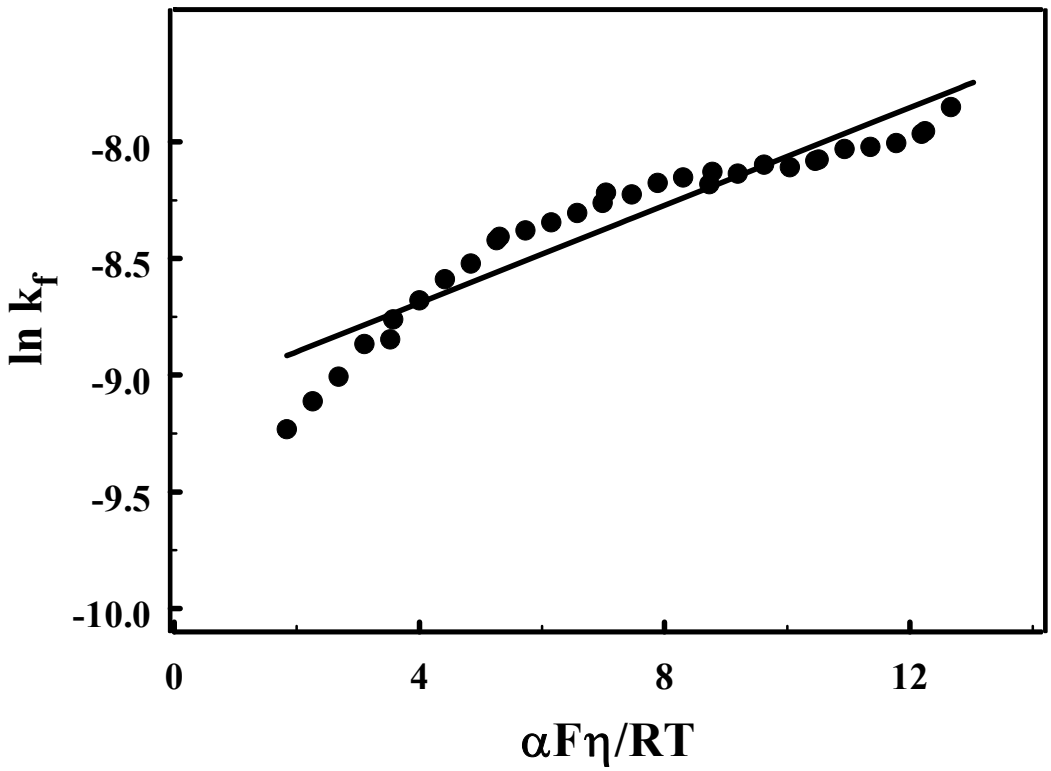

Figure 3-5. Electrochemical rate constant for H_2O_2 formation, kf, as a function of overpotential, $\eta = E_{app} - E^0$, $E^0 = 0.695$ V vs. SHE.

Figure 3-5 shows the potential dependence of the rate constants estimated from Figure 3-1. The slope of this plot represented k_f^0 (equation 3-17), which was used in conjunction with the activation energy to estimate reaction rates at higher temperatures. Though rate constants were calculated for every potential at a 5 mV interval in the 0.025 – 0.6 V potential window (based on Figure 3-1a), only few representative data points are shown in Figure 3-5. Figure 3-6 shows the ring currents and the fraction of H_2O_2 formed with different acidities. Perchloric acid systems in the 0.1 and 2.0 M concentration range equilibrated with pure O_2 were used to study the effect of proton concentration. Figure 3-6 shows an increased rate of H_2O_2 formation with increasing proton concentration. The effect of ClO_4^- concentration on this increased rate of peroxide formation is very minimal. Schmidt et al.[22] have shown that ClO_4^- has the least adsorptive effect on ORR kinetics. Since the disc currents were similar for all acid concentrations, the increased ring currents meant that selectivity towards peroxide formation was a function of proton concentration, which indirectly relates to water activity, i.e., a 2.0 M $HClO_4$ solution has less water than a 0.1 M solution. This correlates to the relative humidity of fuel cell gases and its effect on the local proton concentration.

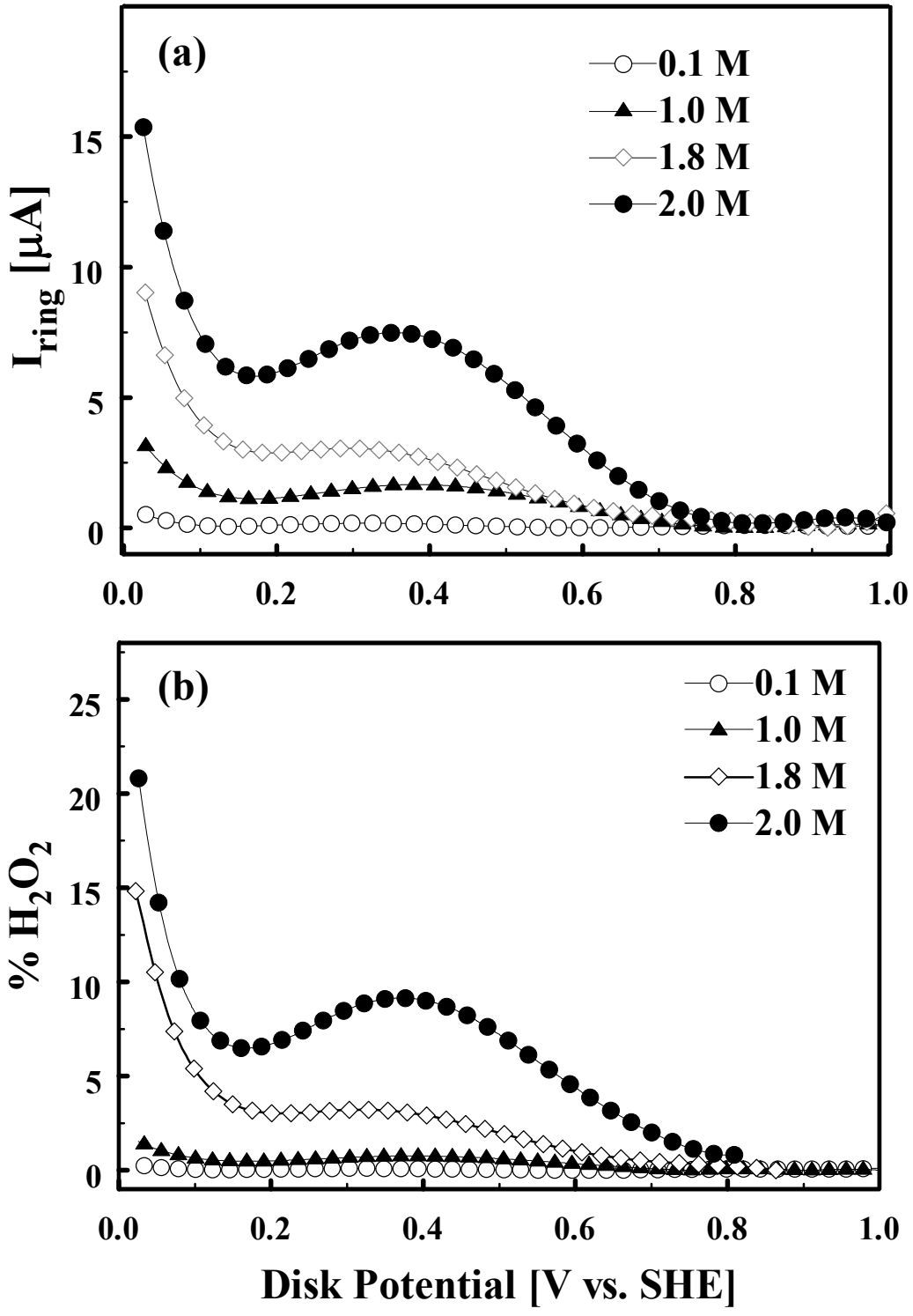

Figure 3-6. (a) Rate and (b) % of H_2O_2 formed during the oxygen reduction reaction on Pt/Vulcan XC-72R in 0.1 M [○], 1.0 M [▲], 1.8 M [◇] and 2.0 M [●] $HClO_4$ solution [pH = -0.3] bubbled with O_2 at 25 °C. E_{ring} = 1.2 V vs. SHE, 1mV/s, 2500 rpm.

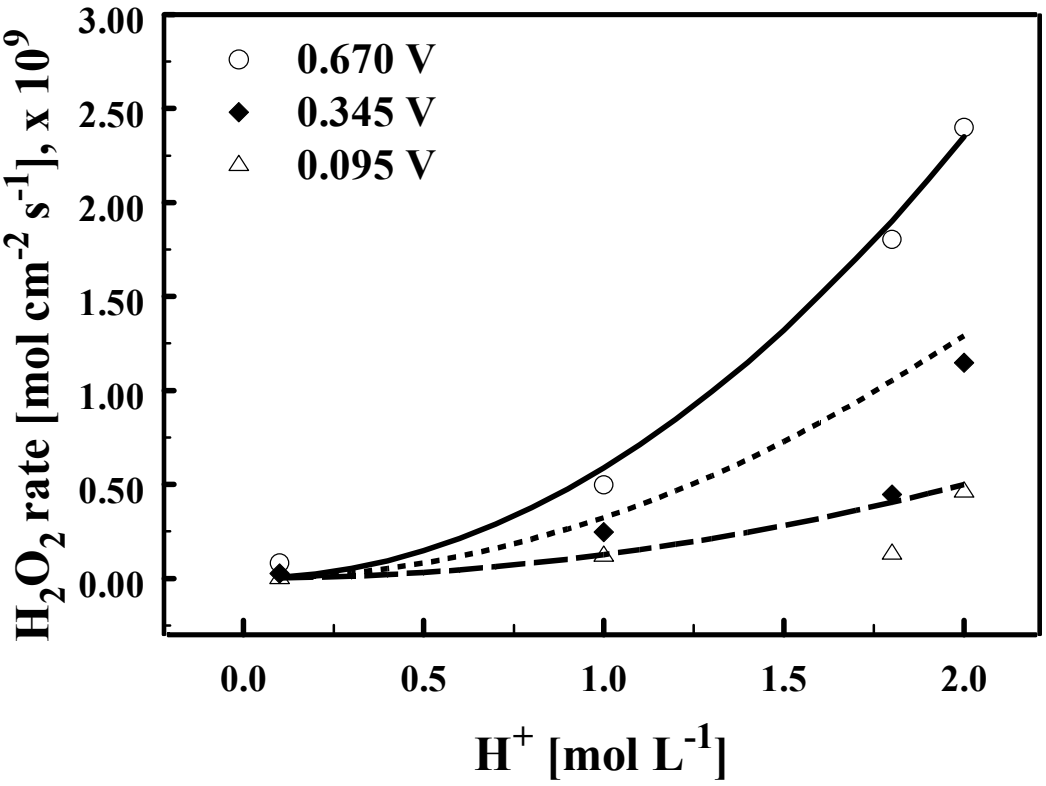

Figure 3-7. H_2O_2 formation rates [mol cm^{-2} s^{-1}] on Pt/Vulcan XC-72R in $HClO_4$ solution as a function of acidity [M] for the following three overpotentials: 0.695 V [○], 0.345 V [♦] and 0.095 V [Δ].

Figure 3-7 shows the dependence of H_2O_2 formation rate on proton concentration. This is consistent with Murthi et al.'s RRDE results in 1 and 6 M TFMSA. The points are measurements and lines are predictions according to equation 3-16. The rate constant obtained earlier via Figure 3-5 was used. The reaction order with respect to H^+ in the H_2O_2 formation reaction, b, was found to be 2 from this fit. The change in selectivity shown by the Pt catalyst in favor of the two-electron transfer at higher acid concentrations (or lower water activities) is a very interesting phenomenon and should be further investigated and explained.

3.5.2. Estimation of H_2O_2 Rates in PEMFCs

The H_2O_2 formation rates measured as a function of water activity, potential and temperature using RRDE experiments is used to estimate H_2O_2 formation rates fuel cell electrodes. The estimation procedure is presented separately for the cathode and the anode.

3.5.2.1. Cathode

Peroxide formation rate at the cathode is estimated via equation 3-16 , i.e. as a product of the rate constant and the local reactant concentrations. Peroxide formation at the cathode is possible only for fuel cells operating at considerable load conditions such that the local potential goes negative than the equilibrium potential for peroxide formation. For estimation of peroxide rates here, local potential at the cathode was taken to be 0.6 V (i.e., $\eta = 0.095$ V).

3.5.2.1.1. Local H^+ Concentration

Zawodzinski et al.[23] measured the absorption isotherm of Nafion® 117 membrane at 30 °C. Between water activity values of 0 and 1, the experimentally measured absorption isotherm was fit to the following polynomial[24],

$$\lambda = 0.043 + 17.81[a_w] - 39.85[a_w]^2 + 36.0[a_w]^3 \qquad \textbf{3-20}$$

In this equation, λ represents the number of water molecules per sulphonic acid group in the polymer and a_w represents the activity of water, which is the effective mole fraction of water given by p_0/p^*, where p^* is the vapor pressure of water, in bar. p^* was calculated from the Antoine correlation,

$$\ln p^* = A_1 - \frac{B_1}{T + C_1} \qquad \textbf{3-21}$$

The constants are A = 11.6832, B = 3816.44, C = -46.13.[25] Inside a fuel cell, this water activity is essentially the equilibrium relative humidity expressed as a fraction. The concentrations of H_2O and H^+ in the polymer are respectively expressed as,

$$C_{H_2O} = \frac{1000\rho\lambda}{EW} \qquad \textbf{3-22}$$

$$C_{H^+} = \frac{C_{H_2O}}{\lambda} \qquad \textbf{3-23}$$

In these equations, EW is the equivalent weight of the polymer (taken to be 1100) and ρ is the humidity-dependent density of the polymer given by,

$$\rho = \frac{1.98 + 0.0324\lambda}{1 + 0.0648\lambda} \qquad \textbf{3-24}$$

It was assumed that all sulphonic acid groups exist in a completely dissociated form. In other words, though Nafion® is a super acid catalyst, it was assumed to behave as a strong acid in the presence of water.

3.5.2.1.2. Local Oxygen Concentration

Oxygen solubility at the membrane-cathode catalyst layer interface, $C_{O_2}^c$, was estimated using the following relation,

$$C_{O_2}^c = \frac{P_{O_2}^m}{D_{O_2}^m} \qquad \textbf{3-25}$$

In this equation, $P_{O_2}^m$ and $D_{O_2}^m$ respectively represent the permeability and the diffusion coefficient of O_2 in Nafion® 112 membrane. $D_{O_2}^m$ values for different temperatures and relative humidities were obtained from Sakai et al.'s work[26].

Figure 3-8 shows the variation of λ and pH of Nafion® as a function of water activity. Since Nafion is a super-acid catalyst, even at vapor-saturated conditions [λ = 14], the pH is fairly below 0. This trend (not shown) is seen for $HClO_4$, also a strong acid. The acid was assumed to be completely dissociated i.e., Ka >>1.

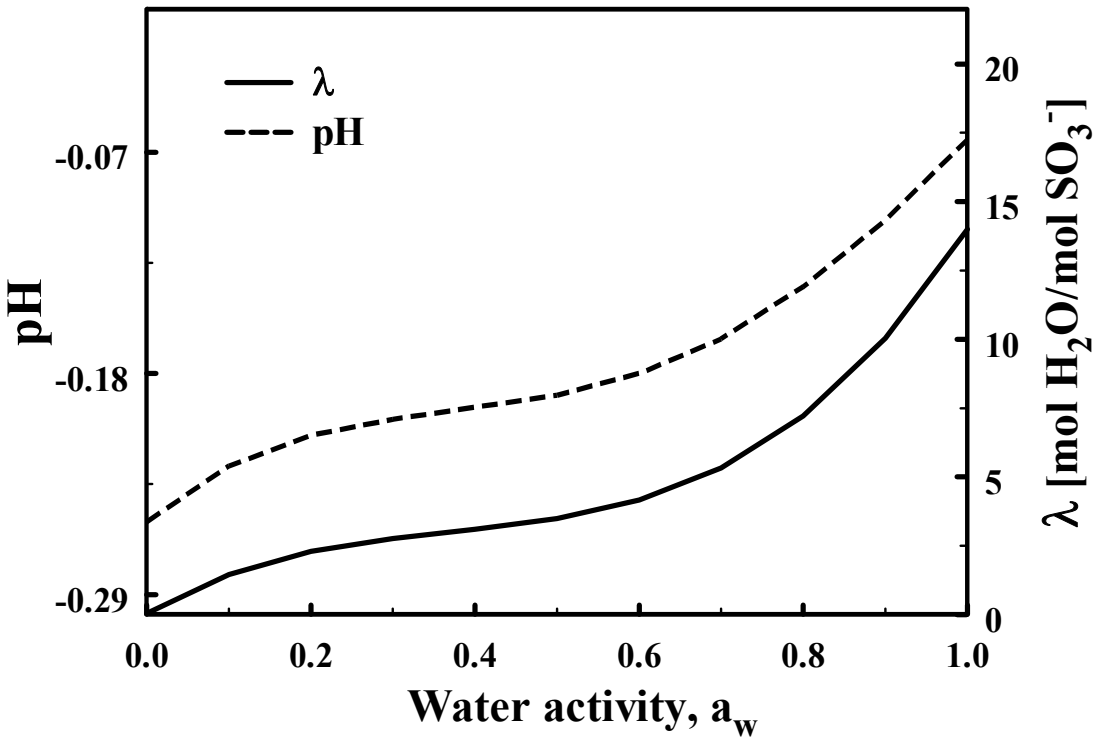

Figure 3-8. pH (-----) and λ (——) vs. water activity, aw, plots for Nafion®. λ is the amount of water per sulphonic acid group [mol basis] and aw is the effective mole fraction of water and is equal to the equilibrium relative humidity expressed as a fraction.

3.5.2.1.3 Activation Energy Estimation

Since rate constants were estimated at 25 °C using RRDE, they had to be projected to higher temperatures in order to be used to calculate peroxide formation rates in a fuel cell. Activation energies for H_2O_2 formation on supported Pt catalysts were estimated from kinetic currents obtained at 15 °C, 25 °C, 35 °C and 45 °C.

Figure 3-9 shows the Arrhenius plot of the kinetic current versus temperature for two different overpotentials. The estimated activation energies were compared to those calculated theoretically by Anderson and Albu [figure 2 in ref. 24] in Table 3-1. The activation energies agree reasonably well.

Figure 3-10 shows the peroxide rates at the cathode-membrane interface when the local potential at the cathode is 0.6 V and the gas feed is pure oxygen at 1 atm. Though the amount of peroxide formed at the cathode is only of the order of few micromoles at fully humidified conditions, the relative difference between dry and fully humidified conditions at 95 ºC is about an order of magnitude.

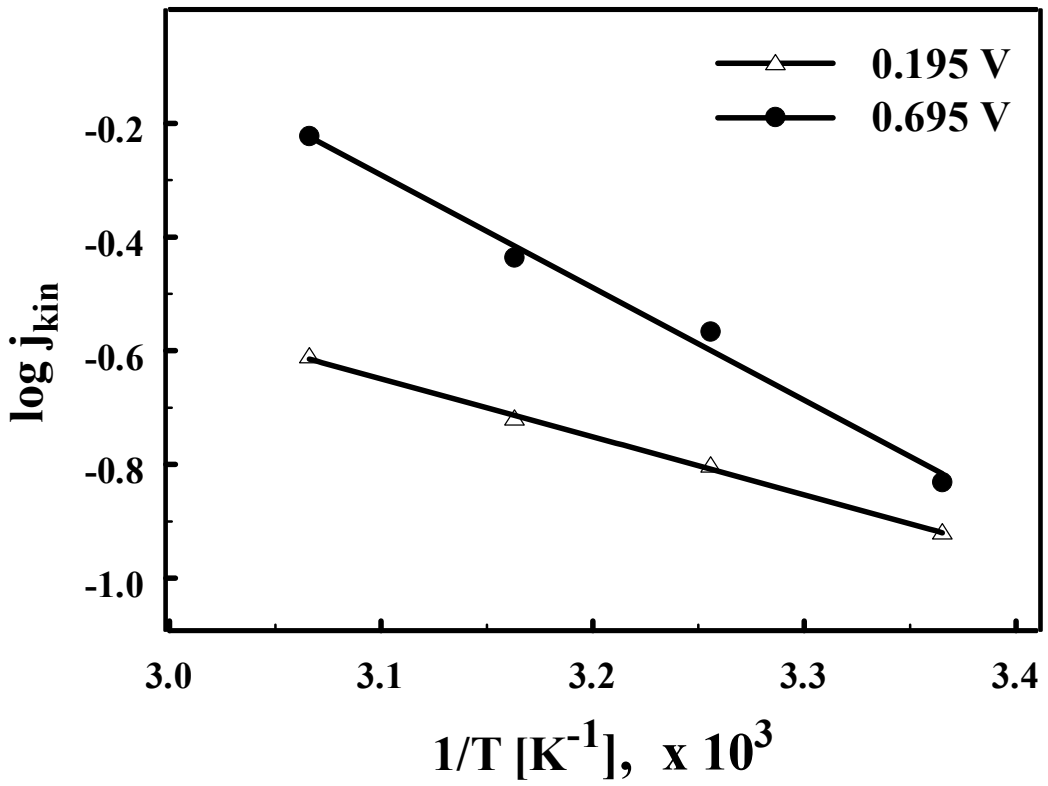

Figure 3-9. Arrhenius plots for H_2O_2 formation reaction on Pt/Vulcan XC-72R in 2M $HClO_4$ at overpotential of 0.195 V (-○-) and 0.695 V (-●-) vs. NHE.

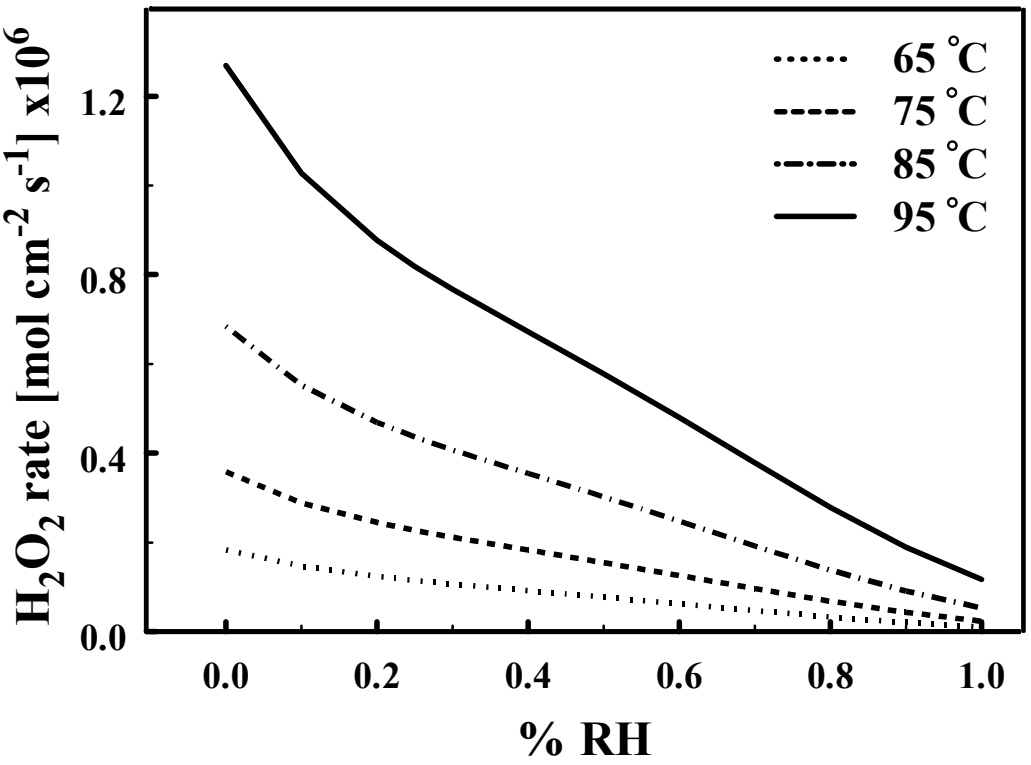

Figure 3-10. Rates of H_2O_2 formation [mol cm^{-2} s^{-1}] in the cathode side of a PEM fuel cell for different relative humidities and temperatures. Local potential at the cathode was assumed to be ~0.6 V vs. SHE, which translates to an overpotential of 0.095 V for H_2O_2 formation.

3.5.2.2. Anode

The potential profile across the membrane, measured *in situ* by Liu and Zuckerbrod [figure 19] and modeled by Burlatsky et al. at open circuit conditions, indicate that the potential at the anode-membrane interface is ~ 0 V. For the purpose of calculating H_2O_2 rates at the anode/membrane interface, a potential of ~0 V was assumed to exist at the interface. This translates to an overpotential of 0.695 V for the H_2O_2 formation reactions. Peroxide formation rate at the anode was estimated as the fraction of oxygen crossing over the membrane going to hydrogen peroxide.

3.5.2.2.1. Oxygen Flux Across Nafion 112®

Oxygen permeability through Nafion® depends greatly on the water content of the membrane. It has been shown by Sakai et al.[26] that O_2 diffusion rates in a completely dry Nafion® membrane has values similar to that in PTFE and approaches the limit of liquid water with increasing water content.

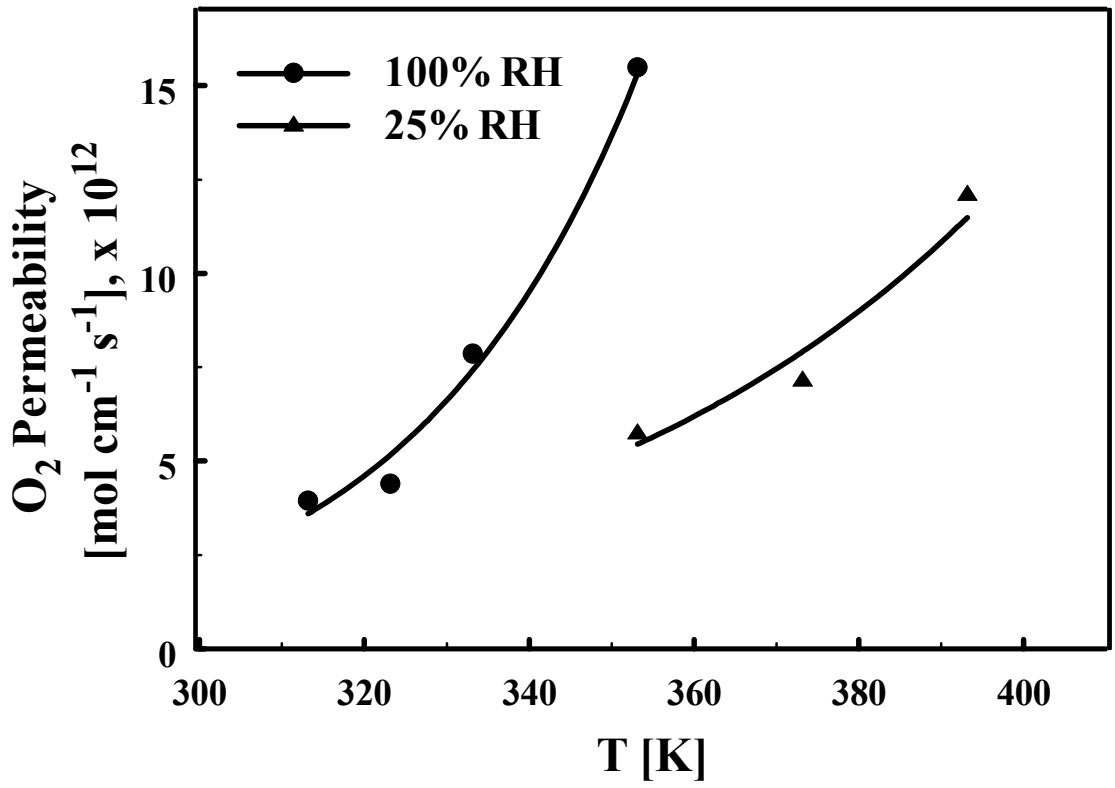

Figure 3-11. Oxygen permeability [mol cm^{-1} s^{-1}] rates in Nafion® 112 measured experimentally by electrochemical monitoring technique as a function of temperature for two different relative humidities, 25% and 100% RH. These rates were normalized to a 101 kPa O_2 feed.

Figure 3-11 shows experimentally measured O_2 permeability rates across a Nafion® 112 membrane as a function of temperature and relative humidity. The permeability rates were corrected for an O_2 feed at 101 kPa. These permeation rates estimated using electrochemical monitoring technique (EMT) are comparable to those estimated by gas chromatography (GC) method.[27] Between 25% and 100% relative humidity of the feed gas, the permeability rates differ by as much as an order of magnitude. Permeability rates for other temperatures and water contents were estimated using these values. Fraction of the oxygen that reaches the anode-membrane interface goes to peroxide and the rest may go to water. Hence, peroxide formation rates at the anode-membrane interface is,

$$R_{H_2O_2} = \chi_{H_2O_2} F_{O_2} \qquad \textbf{26}$$

$\chi_{H_2O_2}$, the fraction of oxygen that goes to peroxide, is a function of water activity and temperature. $\chi_{H_2O_2}$, however, is not a function of oxygen concentration (see Figure 3-3). F_{O_2}, oxygen flux across the membrane from the cathode to the anode can be written as,

$$F_{O_2} = \frac{D^m_{O_2}}{\delta}\left(C^c_{O_2} - C^a_{O_2}\right) \qquad \textbf{27}$$

$C^a_{O_2}$, the concentration of oxygen at the anode-membrane interface is zero.

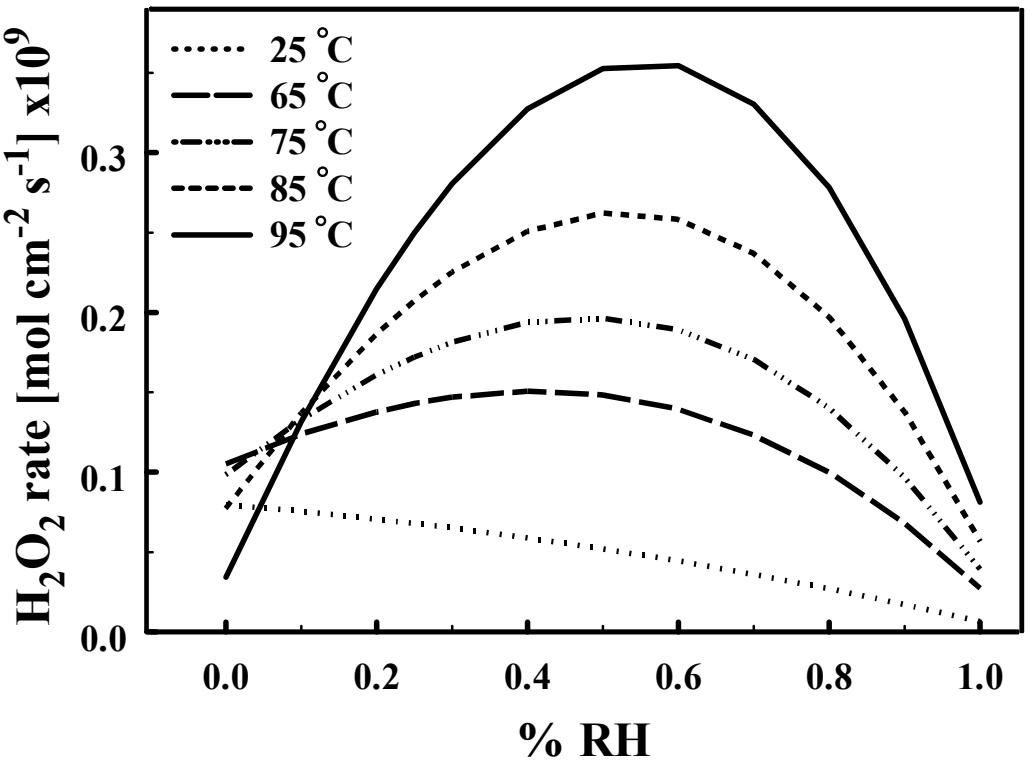

Figure 3-12. Rates of H_2O_2 formation [mol cm^{-2} s^{-1}] in the anode side of a PEM fuel cell for different relative humidities and temperatures. Local potential at the anode was assumed to be ~0 V vs. SHE, which translates to an overpotential of 0.695 V for H_2O_2 formation.

Figure 3-12 shows the H_2O_2 formation rates at the anode-membrane interface. This goes through a peak because oxygen permeability decreases with decreasing water activity whereas H_2O_2 selectivity increases with decrease in water activity. These anode and cathode H_2O_2 formation rates cannot be directly correlated with the fluoride emission rates because there are several intermediate reactions between H_2O_2 formation and actual membrane degradation. However quantification of H_2O_2 formation rates is important basic information to better understand membrane degradation rates. This quantification would help in validating a durability mechanism and ultimately in increasing PEMFC durability at elevated temperatures and low relative humidities.

3.6. Conclusions

Using RRDE, the fraction of H_2O_2 formed during ORR was studied on Pt/Vulcan XC-72 catalyst in $HClO_4$ solution. The RRDE measurements showed that H_2O_2 formation rates exhibit a linear dependence on O_2 concentration in the system and a non-linear dependence on acidity. Experimentally measured ring currents were corrected for mass transfer effects and used to obtain kinetic rate constants corresponding to H_2O_2 formation. Using a specially designed cell, EMT was used to measure O_2 permeability across Nafion® 112 membrane for different temperatures and relative humidities. Kinetic rate constants measured using RRDE were used in conjunction with experimentally measured O_2 crossover rates to estimate H_2O_2 formation rates in anode and cathode of a PEM fuel cell.

List of Symbols

a	reaction-order with respect to O_2 in the H_2O_2 formation reaction
a_w	water activity
A	disk area, cm^2
b	reaction-order with respect to H^+ in the H_2O_2 formation reaction
$C^*_{O_2}$	oxygen concentration in the bulk of the electrolyte, mol cm^{-3}
$C^f_{O_2}$	oxygen concentration in Nafion® film, mol cm^{-3}
$C^a_{O_2}$	oxygen concentration in Nafion® 112 membrane-anode catalyst layer interface, mol cm^{-3}
$C^c_{O_2}$	oxygen concentration in Nafion® 112 membrane-cathode catalyst layer interface, mol cm^{-3}
$D^*_{O_2}$	oxygen diffusion coefficient in the electrolyte, $cm^2\ s^{-1}$
$D^f_{O_2}$	oxygen diffusion coefficient in Nafion® film, $cm^2\ s^{-1}$
$D^m_{O_2}$	diffusion coefficient of O_2 in Nafion® 112 membrane, $cm^2\ s^{-1}$
E^0	equilibrium potential, 0.695 V vs. SHE at 25 ˚C and 101 kPa
E^*_a	activation energy for H_2O_2 formation, J mol^{-1}
E_{app}	applied potential, V vs. SHE
EW	equivalent weight of Nafion® polymer, 1100 g $equiv^{-1}$
F	Faraday constant, 96485 C mol^{-1}
I_{ring}	ring current, μA
I_{disk}	disk current, mA
j	total measured current, mA cm^{-2}

j_D	diffusion-limited current, mA cm^{-2}
j_{kin}	kinetic current, mA cm^{-2}
k_b	rate constant for H_2O_2 electro-oxidation, s^{-1}
k_f	rate constant for H_2O_2 formation, cm s^{-1} M^{-n}
N	collection efficiency, 20%
n	number of electrons transferred per O_2 molecule in H_2O_2 formation, 2
$P_{O_2}^m$	permeability of O_2 in Nafion® 112 membrane, mol cm^{-1} s^{-1}
R	universal gas constant, 8.314 J mol^{-1} K^{-1}
T	temperature, K
t	time, s

Greek

α	transfer co-efficient
δ	Pt/C electrode thickness, cm
δ_f	Nafion® film thickness, cm
ρ	density of Nafion®, g cm^{-3}
v	kinematic viscosity, cm^2 s^{-1}
η	overpotential, V vs. SHE
λ	moles of water per sulphonic acid group in Nafion®
$\chi_{H_2O_2}$	fraction of H_2O_2 produced at the disk
ω	electrode rotation rate, s^{-1}

Superscript	
0	standard state or equilibrium
a	anode
c	cathode
Subscript	
b	backward reaction
D	diffusion
disk	Pt/Nafion® coated disc electrode
f	Nafion® film or forward reaction
kin	kinetic
ring	Pt ring electrode

Table 3-1. Activation Energies for Peroxide Formation Reaction in 2M $HClO_4$ as a Function of Overpotential (η)[a].

Overpotential vs. SHE, V	**E_a, kJ/mol (This work)**	**E_a, kJ/mol (Anderson *et al.*)[a]**
0.595	128	103.29
0.495	121	94.6
0.395	98.98	85.91
0.295	76.43	79.15
0.195	53.34	67.57

[a] Overpotential, $\eta = E_{app} - E^0$, E^0 = 0.695 V vs. SHE.

[b] Obtained from the summation of activation energies reported in figure 2 for the reactions [9] and [10] in A. B. Anderson and T. V. Albu, *J. Electrochem. Soc.,* **147**, 4229 (2000).

Table 3-2. Parameters used in the analysis of measured current at the Pt ring[a].

Parameter	Value	Comments
a	1	Measured
A	0.164025 cm^2	Ref. 15
b	2	Measured
$C^*_{O_2}$	1.274 mol cm^{-3}	Ref. 13[a]
$D^*_{O_2}$	2.2 x 10^{-6} cm^2 s^{-1}	Ref. [28]
E^0	0.695 V vs. SHE	
EW	1100 g mol^{-1}	Ref. [29]
F	96485 C mol equiv.$^{-1}$	Ref. [30]
N	0.2	Measured
R	8.314 J mol^{-1} K^{-1}	Ref. 30
T^0	298 K	Measured
α	0.5	Assumed
δ_f	10^{-5} cm	Ref. 5
ρ	1 g cm^{-3}	Ref. 30
υ	0.009 cm^2 s^{-1}	Estimated
ω	2500 s^{-1}	Measured

[a] The mole fraction solubility X_1 of oxygen in water is given as $\ln X_1 = A_2 + \frac{B_2}{T^*} + C_2 \ln T^*$, where, $T^* = \frac{T}{100} K$. A_2 = -66.7354, B_2 = 87.4755 and C_2 = 24.4526.

3.7. References

1. A. B. LaConti, M. Hamdan and R. C. McDonald, *Handbook of Fuel Cells: Fundamentals, Technology and Applications*, **3**, W. Vielstich, A. Lamm and H. A. Gasteiger, John Wiley and Sons, New York, NY (2003).

2. E. Endoh, S. Terazono, H. Widjaja and Y. Takimoto, *Electrochem. Solid State Letters,* **7**, A209 (2004).

3. D. E. Curtin, R. D. Lousenberg, T. J. Henry, P. C. Tangeman and M. E. Tisack, in *Proceedings of the 2nd European Polymer Electrolyte Fuel Cell Forum*, Vol. 1, p. 25-35 (2003).

4. W. Liu and D. Zuckerbrod, *J. Electrochem. Soc.,* **152**, A1165 (2005).

5. U. A. Paulus, T. J. Schmidt, H. A. Gasteiger and R. J. Behm, *J. Electroanal. Chem.,* **495**, 134 (2001).

6. E. Claude, T. Addou, J.-M. Latour and P. Aldebert, *J. Applied Electrochemistry*, **28**, 57 (1998).

7. U. A. Paulus, A. A. Wokaun, G. G. Scherer, T. J. Schmidt, V. Stamenkovic, N. M. Markovic, and P. N. Ross, *Electrochim. Acta,* **47**, 3787 (2002).

8. O. Antoine and R. Durand, *J. Applied Electrochemistry,* **30**, 839 (2000).

9. M. A. Enayetullah, T. D. DeVilbiss and J. O'M. Bockris, *J. Electrochem. Soc.,* **136**, 3369 (1989).

10. V. S. Murthi, R. C. Urian and S. Mukerjee, *J. Phys. Chem. B*, **108**, 11011 (2004).

1 [11]. T. J. Schmidt, H. A. Gasteiger, G. D. Stäb, P. M. Urban, D. M. Kolb and R. J. Behm, *J. Electrochem. Soc.,* **145**, 2354 (1998).

[12]. T. J. Schmidt, U. A. Paulus, H. A. Gasteiger and R. J. Behm, *J. Electroanal. Chem.*, **508**, 41 (2002).

13. L. H. Gevantman, in *CRC Handbook of Chemistry and Physics*, 79th ed., D. R. Lide, Editor, p. 8-86, CRC Press, New York (1998-99).

14. W. J. Albery and M. L. Hitchman, *Ring-Disc Electrodes*, Clarendon Press, Oxford (1971).

15. *Rotated Ring-Disk Electrodes: DT21 Series*, Pine Instrument Company, Raleigh, NC 27617.

16. S. K. Zečević, J. S. Wainright, M. H. Litt, S. Lj. Gojković and R. F. Savinell, *J. Electrochem. Soc.,* **144**, 2973 (1997).

17. A. Damjanovic and G. Hudson, *J. Electrochem. Soc.,* **135**, 2269 (1988).

18. U. A. Paulus, A. Wokaun, G. G. Scherer, T. J. Schmidt, V. Stamenkovic, V. Radmilovic, N. M. Markovic and P. N. Ross, *J. Phys. Chem. B,* **106**, 4181 (2002).

19. A. B. Anderson and T. V. Albu, *J. Electrochem. Soc.,* **147**, 4229 (2000).

20. R. A. Sidik and A. B. Anderson, *J. Electroanal. Chem.,* **528**, 69 (2002).

21. Y. Wang and P. B. Balbuena, *J. Chem. Theory Comput.,* **1**, 935 (2005).

22. T. J. Schmidt, U. A. Paulus, H. A. Gasteiger and R. J. Behm, *J. Electroanal. Chem.,* **508**, 41 (2001).

23. T. Zawodzinski, M. Neeman, L. Sillerud and S. Gottesfeld, *J. Phys. Chem.,* **95**, 6040 (1991).

24. T. Fuller, *Ph. D. Dissertation*, University of California, Berkeley (1989).

25. R. C. Reid, J. M. Prausnitz and T. K. Sherwood, *The Properties of Gases and Liquids*, McGraw Hill Inc., New York (1977).

26. T. Sakai, H. Takenaka and E. Torikai, *J. Electrochem. Soc.,* **133**, 88 (1986).

27. K. Broka and P. Ekdunge, *J. Appl. Electrochem.,* **27**, 117 (1997).

28. Q. Guo, V. A. Sethuraman and R. E. White, *J. Electrochem. Soc.,* **151**, A983 (2004).

29. K. A. Mauritz and R. B. Moore, *Chemical Reviews,* **104**, 4535 (2004).

30. R. H. Perry and D. W. Green, *Perry's Chemical Engineer's Handbook*, 7th Edition, McGraw Hill (1997).

4. Effect of supported Pt Alloys on Membrane Durability

4.1 Abstract

The effect of Pt/KB, PtCo/KB and PtIrCo/KB catalysts on membrane durability in a PEM fuel cell was studied using single-sided membrane electrode assemblies (MEA) with built-in reference electrode. MEA with PtIrCo/KB had the least fluorine emission rate (FER) followed by PtCo/KB and Pt/KB.

4.2 Introduction

The stability of supported Pt catalysts is one of the important factors that affect PEMFC durability. Pt alloys as cathode catalysts have attracted wide attention to achieve high performance and to increase power density of PEMFCs. The dissolution of transition metal and Pt passivation are important concerns. Dissolution could result in a decrease of catalyst activity for ORR. More importantly, such dissolution could result in migration into the membrane because of a concentration gradient and exchange with the membrane because of stronger affinity of metal cations with the sulfonic acid group than protons.[1] Though extensive research had been done on the research and development of new alloy catalysts and understanding the mechanisms of oxygen reduction reaction (ORR)[2, 3, 4, 5, 6, 7, 8, 9, 10, 11], there is not much in the literature on their durability in fuel cell environment[12, 13, 14, 15]. Pourbaix diagrams[16] indicate that most transition metals such as Co, Cr, Fe, Ni, Mn, Cu, V, Ru and Ir are soluble between 0.3 V and 1.0 V vs. SHE and at a pH of around 0. In this work, we consider two such elements – namely Co and Ir. It

was shown by Yu et al.[17] that PtCo supported on Carbon is more stable than Pt/C. They evaluated the stability of PtCo/C catalysts under fuel cell operating conditions. Using potential cycling test between 0.87 V and 1.2 V vs. RHE, they were able to illustrate how Co dissolution might affect PEMFC performance. However, they found that co-dissolution neither detrimentally affected the cell voltage nor dramatically reduced membrane conductivity. Using similar durability experiments Protsailo et al.[18] later showed that PtIrCo/C significantly outperformed PtCo/C in terms of durability and performance. The downside was cost involved in labor and materials towards manufacturing such ternary catalysts. In this work, we analyze the effect of these two catalysts - PtCo/C and PtIrCo/C – on membrane durability in a PEM fuel cell environment. Using membrane electrode assembly (MEA) with built-in reference electrode, we were able to isolate the effect of either the anode or the cathode and the local potential. A test matrix with different combinations of gas feed, catalyst used and applied potential was made to isolate the effects of each of these. Preliminary results from one set of tests are presented here.

4.3 Experimental

4.3.1 Membrane Electrode Assembly with Reference Electrode

The effect of Pt alloy catalysts on membrane durability was studied using single sided MEAs designed with built-in reference electrodes. In order to reliably force a potential on an electrode (anode or cathode), a reference electrode was placed inside the membrane in such a way that it was electronically isolated from the anode and the cathode but was in contact with H_2 gas. Since it is impossible to place a Pt or Au foil or wire inside a thin membrane, the reference electrode was sandwiched between two

membranes. A perforated thinner membrane (Nafion® 111, in this case) electronically insulated the reference electrode from the anode Figure 4-1 shows the design of such an electrode. The working membrane in this case was thicker Nafion 117® membrane. For the reference electrode to work in a regular (two-sided) MEA, the flow-field should have an additional channel outside the projected electrode area so that the reference electrode has access to H_2.

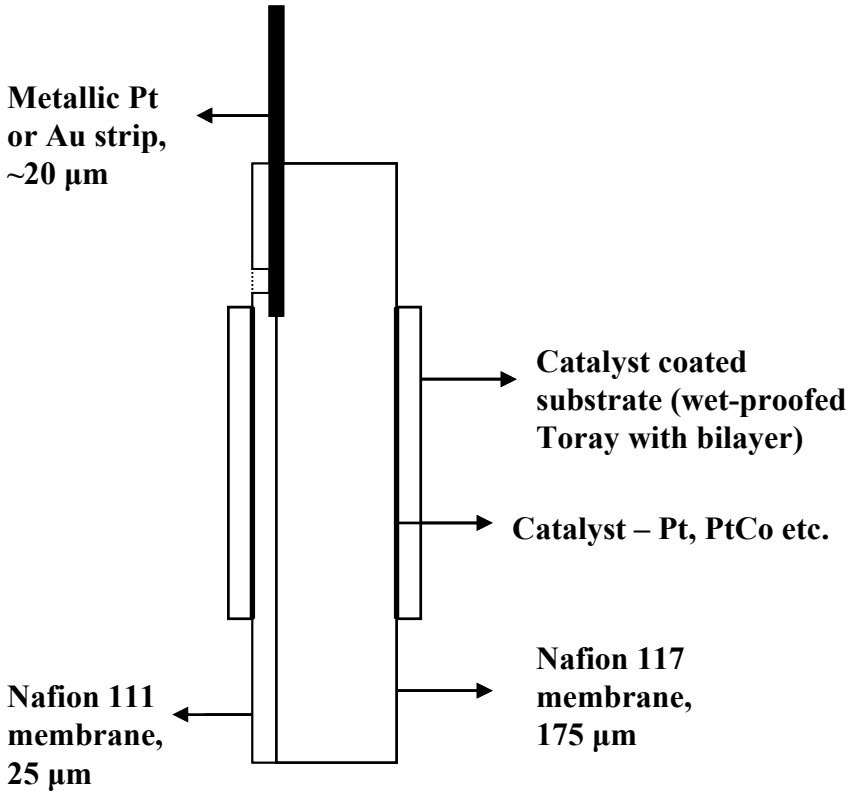

Figure 4-1. Normal MEA with reference electrode.

4.3.2 Single -sided Membrane Electrode Assembly

The same design as described above was used with electrode on only one side of the MEA. This design was an improvement over earlier durability experiments with single-sided MEA reported by Mittal et al.[19]. In that, they built single sided MEAs (MEAs with catalysts and substrate on one side and no catalyst or substrate on the other side) they measured the fluorine emission rates at open circuit conditions Their test matrix comprised of four such configurations with hydrogen and oxygen flowing on the anode and the cathode respectively and nitrogen flowing on either electrodes. In this work, with the inclusion of the reference electrode, a potential can be reliably forced upon the single sided electrode configuration. The effect of potential on membrane durability can now be studied.

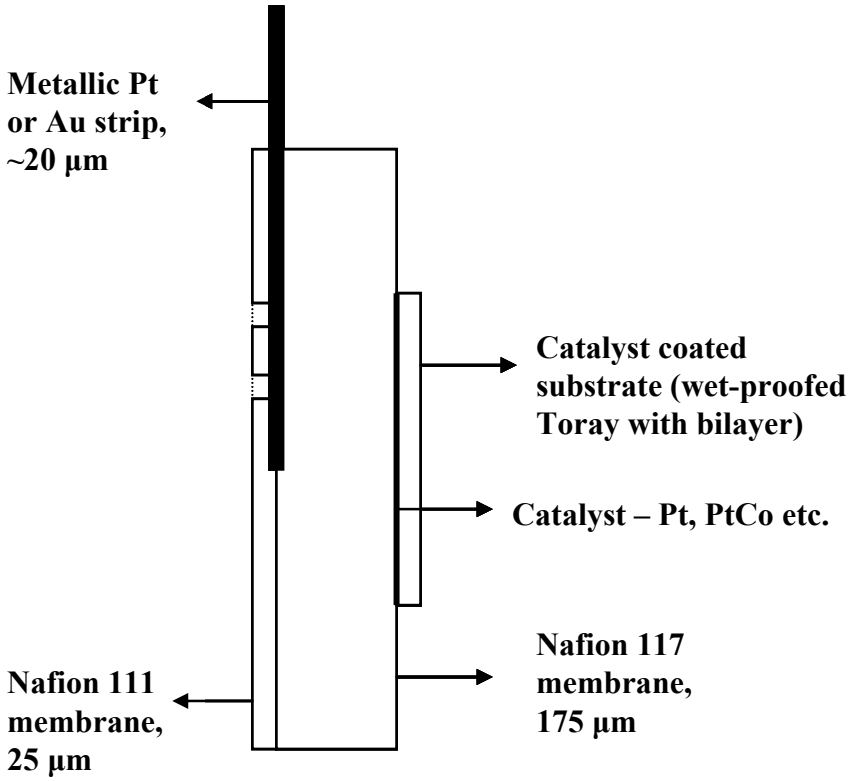

Figure 4-2. Schematic of a single-sided MEA with reference electrode for H_2O_2 experiments.

4.4 Results and Discussion

Since alloys produced more peroxide than Pt, they were tested for their effect on membrane durability in actual fuel cell conditions using single-sided MEAs with built in reference electrodes. H_2 flowing over Au foil served as reference electrode. Since the peroxide generation rates were observed at about 600 mV vs. SHE, a potential of 600 mV vs. H_2 on Au was applied on the single sided electrode with O_2 flowing over. The results from the single sided MEAs (Figure 4-3) showed that membranes coated with PtIrCo had the least fluorine emission rates. PtCo had the next lower FER followed by Pt. If membrane degradation occurs via peroxy radical attack as reported by Cleghorn et al.[20], alloys, due to their increased hydrogen peroxide generation rates[21] should cause more membrane degradation and hence more fluorine emission rates that Pt alone.

However, alloys are more stable than Pt in terms of dissolution. Figure 4-4 shows results from electron microprobe analysis for elemental Pt, CO and Ir from post test MEAs that were cycled on the cathode side between 0.87 and 1.05 V vs. RHE (2800 cycles, 1 minute at each potential, H_2 anode, N_2 cathode). Pt concentration in the membrane decreases in the order Pt > PtCo > PtIrCo. Therefore, alloys are more stable than Pt in terms of dissolution. Lower metal content in the membrane means lower radical generation regardless of the amount of hydrogen peroxide generated.

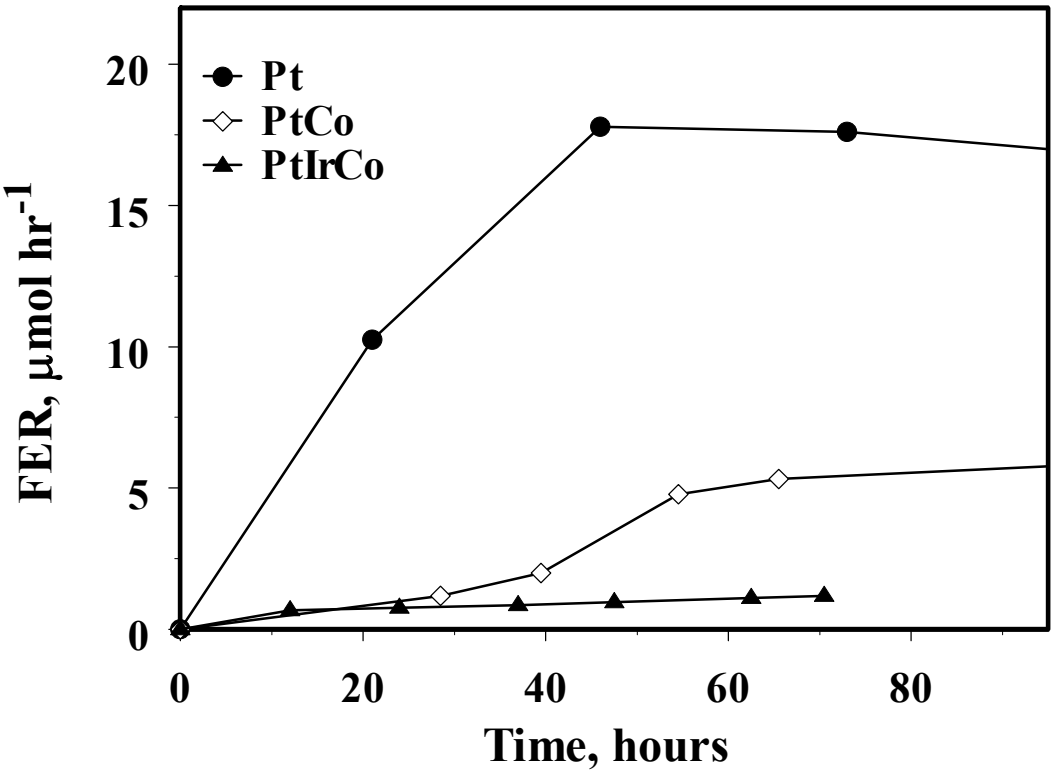

Figure 4-3. Fluorine emission rates (μmol hr^{-1}) measured as a function of time (hours) from the single sided MEAs. The cathode (O_2) had the catalyst and the substrate while anode had no catalyst or substrate. A potential of 600 mV vs. H_2 on Au was held on the cathode throughout the test.

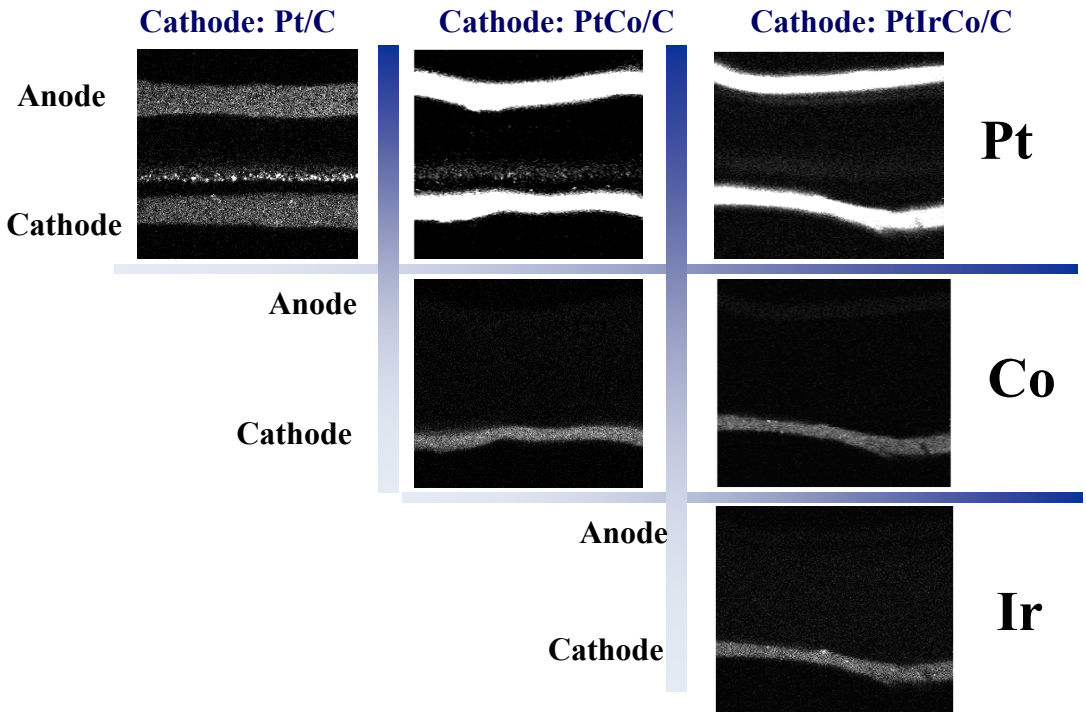

Figure 4-4. Electron microprobe analysis (EPMA) for elemental Pt, Co and Ir from the MEAs after 2800 cycles on cathode between 0.87 and 1.05 V vs. RHE (1 minute each) at 120 °C and 50%RH with H_2 on the anode and N_2 on the cathode.[22]

4.5 Conclusions

Though the alloys produce more hydrogen peroxide than Pt, their stability and lesser dissolution makes them better candidates to enhance membrane durability when operating in fuel cell conditions.

4.6. References

1. T. Okada, in *Handbook of Fuel Cells: Fundamentals, Technology, and Applications*, **3**, Chapter 37, W. Vielstich, A. Lamm and H. A. Gasteiger, Editors, John Wiley & Sons, New York, (2003).

2. D. Thompsett, in *Handbook of Fuel Cells: Fundamentals, Technology, and Applications*, **3**, Chapter 37, W. Vielstich, A. Lamm and H. A. Gasteiger, Editors, John Wiley & Sons, New York, NY (2003).

3. D. A. Landsman and F. J. Luczak, in *Handbook of Fuel Cells: Fundamentals, Technology, and Applications*, **4**, Chapter 65, W. Vielstich, A. Lamm and H. A. Gasteiger, Editors, John Wiley & Sons, New York, NY (2003).

4. N. M. Markovic, B. N. Grgur and P. N. Ross, *J. Physical Chemistry B*, **101**, 5405 (1997).

5. M. Watanabe, K. Tsurumi, T. Mizukami, T. Nakamura and P. Stonehart, *J. Electrochemical Society*, **141**, 2659 (1994).

6. S. Mukerjee and S. Srinivasan, *J. Electroanalytical Chemistry*, **357**, 201 (1993).

7. A. J. Appleby, *Energy*, **11**, 13 (1986).

8. J. C. Huang, R. K. Sen and E. Yeager, *J. Electrochemical Society*, **126**, 786 (1979).

9. V. Jalan and E. J. Taylor, *J. Electrochemical Society*, **130**, 2299 (1983).

10. V. Stamenkovic, T. J. Schmidt, P. N. Ross and N. M. Markovic, *J. Electroanalytical Chemistry*, **554**, 191 (2003).

11. V. Stamenkovic, T. J. Schmidt, P. N. Ross and N. M. Markovic, *J. Physical Chemistry B*, **106**, 11970 (2002).

12. J. St-Pierre, D. P. Wilkinson, S. Knights and M. L. Bos, *J. New Materials Electrochemical Systems*, **3**, 99 (2000).

13. T. R. Ralph and M. P. Hogarth, *Platinum Metals Review*, **46**, 3 (2002).

14. T. Okada, Y. Ayato, M. Yuasa and I. Sekine, *J. Physical Chemistry B*, **103**, 3315 (1999).

15. T. Okada and G. Xie, *Electrochimica Acta*, **43**, 3741 (1998).

16. M. Pourbaix, *Altas of Electrochemical Equilibrium in Aqueous Solutions*, Pergamon Press, New York, NY (1966).

17. P. Yu, M. Pemberton and P. Plasse, *Journal of Power Sources*, **144**, 11 (2005).

18. L. V. Protsailo, "Development of High Temperature Membranes and Improved Cathode Catalysts for PEM Fuel Cells" *DoE Hydrogen Program Review*, Arlington, VA, May 13-16, 2006.

19. V. Mittal, H. R. Kunz and J. M. Fenton, "Factors accelerating membrane degradation rate and underlying degradation mechanism in PEMFC", Abstract #1192, *208th Meeting of the Electrochemical Society*, Los Angeles, CA, October 16, 2005.

20. S. Cleghorn, J. Kolde and W. Liu, *Handbook of Fuel Cells*, **3**, 566 (2004).

21. V. A. Sethuraman, J. W. Weidner, A. T. Haug, S. Modi and L. V. Protsailo, "Effect of Humidity on the Durability of PEM Fuel Cells. II. H_2O_2 Kinetics on Pt Alloys", Abstract #451, *210th Meeting of the Electrochemical Society*, Cancun, Mexico, October 31, 2006.

22. A. T. Haug, L. V. Protsailo, S. Modi, V. A. Sethuraman and S. Motupally, "Characterization of Membranes and Catalysts for High Temperature PEM Fuel Cells", High Temperature Working Group (DoE DE-FC36-02AL), *210th Meeting of the Electrochemical Society,* Los Angeles, CA, October 16, 2005.

5. Effect of Di-phenyl Siloxane on Catalytic Activity of Pt/C

5.1 Abstract

The effect of silicone on the catalytic activity of Pt for oxygen reduction and hydrogen adsorption was studied using di-phenyl siloxane as a source compound at a rotating disc electrode (RDE). Di-phenyl siloxane did not affect the catalytic activity of Pt when it was injected into the electrolyte. However, it blocked the oxygen reduction reaction when it was premixed with the catalyst. Proton transport was not blocked in either case. We postulate that di-phenyl siloxane induces hydrophobicity and causes local water starvation thereby blocking oxygen transport. Hence, the slow leaching of silicone seals in a fuel cell could cause silicon deposition on the electrode, which will irreversibly degrade fuel cell performance by blocking oxygen transport to the catalyst sites.

[V. A. Sethuraman, J. W. Weidner, and L. V. Protsailo, "Effect of Di-phenyl Siloxane on the Catalytic Activity of Pt/C", manuscript to be submitted to *Electrochemical and Solid State Letters*, 2007]

5.2 Introduction

Proton exchange membrane fuel cells (PEMFC) are commonly configured into 'stacks', which comprises of multitude of single-cells arranged together as a single stack. In PEMFC stacks, sealing materials are required to separate the gas compartments from each other, to avoid mixing of the fuel (H_2) and the oxidant (O_2), and to prevent leakage and loss of fuel. They also serve additional functions such as electrical insulation and control of stack height. Silicone and silicon based elastomers are commonly used as sealing materials in PEMFC stack systems[1] due to their wide operating temperature (-40 to 300 °C), excellent hardness (20 to 60), stress relaxation (up to 25% force retained), good electrical resistivity (> 10^{14} Ωcm), and dielectric strength (15-17 kV/mm). Silicones also have excellent functional properties such as good pressure sealing ability (20-200 kPa), low swelling in PEMFC fluids (< 5%), and low permeability to fuel gases and coolants. However, currently used silicone based seals, gaskets and tubing materials fall short of the U. S. Department of Energy performance targets[2, 3]. Degraded or substandard seals might cause fuel leaks and may lead to reduced cell voltage due to mixed potential at the electrodes. In spite of this, there is not much in the literature either on the long term durability of sealing materials or their effect on the performance at such time-scales. Schulze et al.[4] noted alteration on the color of the membranes where the seal material was in contact after fuel cell operation. Using X-ray photoelectron spectroscopy (XPS), they detected residues of silicone on the surface of the membrane and catalysts. Using scanning electron microscope and energy dispersive X-ray (SEM/EDX) analysis, they observed enrichment of silicone residues on Pt. They speculated that the deposition

of Si on the catalyst may change the hydrophobic/hydrophilic characteristics of the electrodes.

In a fuel cell, slow leaching of silicone seals could cause silicone deposition on the electrode. In this work, the effect of such silicon deposition on the catalytic activity of Pt for oxygen reduction and hydrogen adsorption was studied using di-phenyl siloxane $[SiO(C_6H_5)_2]_4$ as a source compound at a rotating disc electrode (RDE).

5.3 Experimental

5.3.1. Rotating Disc Electrode (RDE)

The effect of di-phenyl siloxane on the catalytic activity of Pt/C was studied by means of RDE experimentation. For the measurements described in the RDE study, Pt/Vulcan XC-72 (20% Pt on Vulcan XC-72R carbon, Johnson Matthey Inc., PA) was used. The electrochemical measurements were conducted at room temperature in a standard electrochemical cell (RDE Cell®, Pine Instrument Company, NC) using a rotating disk electrode setup with a bi-potentiostat (Bi-Stat®, Princeton Applied Research Inc., TN) in conjunction with a rotation-control equipment (Pine Instrument Company, NC). EC-Lab® software (version 8.60, Bio-logic Science Instruments, France) was used to control the bi-potentiostat. Catalyst coated glassy carbon disc electrode (5 mm diameter, 0.1966 cm^2 area, DT21 Series, Pine Instrument Company, NC) was scanned between 0 – 1.2 V vs. SHE to represent potentials experienced by an electrode in fuel cell operating conditions. Potentials were determined using a Mercury-mercurous sulfate (Hg/Hg_2SO_4) reference electrode. All potentials in this study, however, refer to that of the standard hydrogen electrode (SHE). A high-surface area Pt cylindrical-mesh (5 mm

diameter, 50 mm length) attached to a Pt wire (0.5 mm thick, 5 mm length) was used as the counter electrode.

Catalyst coated glassy carbon electrodes were prepared as described by Schmidt et al.[5]. In short, suspensions of 1 mg Pt ml^{-1} were obtained by pulse-sonicating 20 mg Pt/Vulcan catalyst with 15 ml triple-distilled, ultrapure water (Millipore Corporation) in an ice bath (70% duty cycle, 60W, 15 minutes) and 5 ml diluted Nafion solution (5% aqueous solution, 1100 EW; Solution Technology Inc., Mendenhall, PA). Sonication was done using a Braun-Sonic U Type 853973/1 sonicator. Glassy carbon disc served as the substrate for the supported catalyst and was polished to a mirror finish (0.05 μm deagglomerated alumina, Buehler®) prior to catalyst coating. An aliquot of 14 μl catalyst suspension was pipetted onto the carbon substrate, which corresponded to a Pt loading of ~14.1 μg Pt cm^{-2}. After evaporation of water for 30 minutes in N_2 atmosphere (15 in-Hg, vacuum), the catalyst-Nafion® coated electrode was then immersed in deaerated (UHP Nitrogen, Praxair) 1 M Perchloric acid ($HClO_4$, 70%, Ultrapure Reagent Grade, J. T. Baker) for linear sweep voltammetry experiments. All solutions were prepared from ultrapure water (Millipore Inc., 18.2 MΩcm). Following three experiments were performed:

(a) No di-phenyl siloxane was present in the electrolyte. The linear sweep voltammogram obtained from this procedure became the baseline for comparison with those having Siloxane in the system.

(b) Di-phenyl siloxane was added to the electrolyte (0.5M $HClO_4$) prior to the ECA and ORR measurements. Two such experiments were performed each with a different concentration of di-phenyl siloxane namely 1μM and 10mM.

(c) In the third case di-phenyl siloxane was premixed with the catalyst such that the dispersion had 10 mM Siloxane in it.

5.4 Results and Discussion

Figure 5-1 shows polarization curves for the oxygen reduction reaction (ORR: $O_2 + 4H^+ + 4e^- \longrightarrow 2H_2O$) on a Pt/Vulcan XC-72R thin-film RDE in 0.5 M $HClO_4$ solution at 25 °C and 1 atm bubbled with O_2 with and without di-phenyl siloxane. The ORR current for the case with di-phenyl siloxane (1 μM and10 mM) in the electrolyte is the same as the no di-phenyl siloxane case. However, the ORR current decreased to very low values when di-phenyl siloxane was premixed in the ink or when siloxane was present in the electrode. Though the data showed in Figure 5-1 resulted from a negative sweep, similar trends were observed during the positive sweep as well, (i.e., very low ORR current with di-phenyl siloxane in the electrode).

Figure 5-2 shows polarization data with no oxygen in the electrolyte. There is no difference in the hydrogen adsorption ($Pt + 2H^+ + 2e^- \longrightarrow Pt - H_2$) peaks in the 25-400 mV potential window for these three cases. The area under this peak is normally used to calculate the electrochemical area (ECA) of Pt[6] and commonly serves as a tool to compare the catalytic activity of different catalysts for fuel cell applications. Since there is no difference in the ECA between the electrodes with and without siloxane, this indicates that proton transport to the catalyst was unaffected by the existence of di-phenyl siloxane either in the electrolyte or in the electrode.

What could possibly explain the behavior where the addition of an impurity blocked oxygen transport to the catalyst surface but had no influence on the proton transport? Oxygen diffuses through water channels to the catalyst surface whereas

protons hop via the sulfonic acid chains in the ionomer as well as through surface diffusion on carbon support. Siloxane deposition occurs on the catalyst in such a way that oxygen transport through water is blocked but proton transport through the ionomer is not. Since siloxane is hydrophobic, we postulate based on the data that it induces local hydrophobicity upon deposition and this hydrophobicity blocks oxygen transport. The ionomer channels could have been unaffected due to the deposition of di-phenyl siloxane on the catalyst.

In a fuel cell, degradation of seal materials and their slow leaching could result in their deposition on the electrode, which will irreversibly degrade fuel cell performance due to the following: (1) silicone induced local hydrophobicity could induce mechanical stresses and (2) local water starvation increases the acidity of the ionomer and accelerates chemical degradation via peroxy-radical attack. Further, the poisoned areas on the electrode will be unavailable to contribute to the fuel cell current. In the cathode, these areas will function as localized hydrogen pumps (under constant current operations) leading to parasitic losses to the power output. In the anode, if hydrogen supply to the catalyst sites is blocked, cell reversal will occur resulting in carbon corrosion on the corresponding area on the cathode[7]. These performance degradation and durability problems can result from any poisoning agent that induces hydrophobicity upon adsorption or deposition.

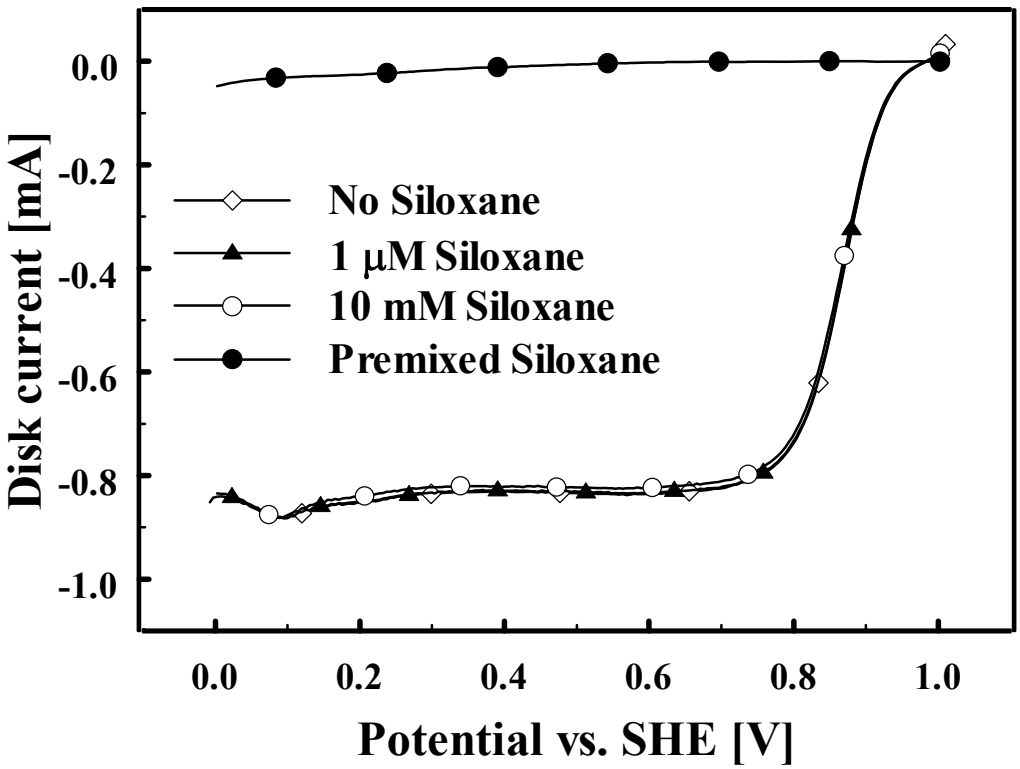

Figure 5-1. Disc currents in 0.5M $HClO_4$ at 1 atm, 25 °C and 1200 rpm with no di-phenyl siloxane (◊), 1 M di-phenyl siloxane (-▲-) in the electrolyte, 10 mM di-phenyl siloxane in the electrolyte (-o-), and 10 mM di-phenyl siloxane premixed in the electrolyte (-•-). Oxygen (UHP, Praxair) was bubbled through the electrolyte. The potential scan was started at 1.0 V vs. SHE and was swept cathodically at the rate of 5 mV s^{-1}.

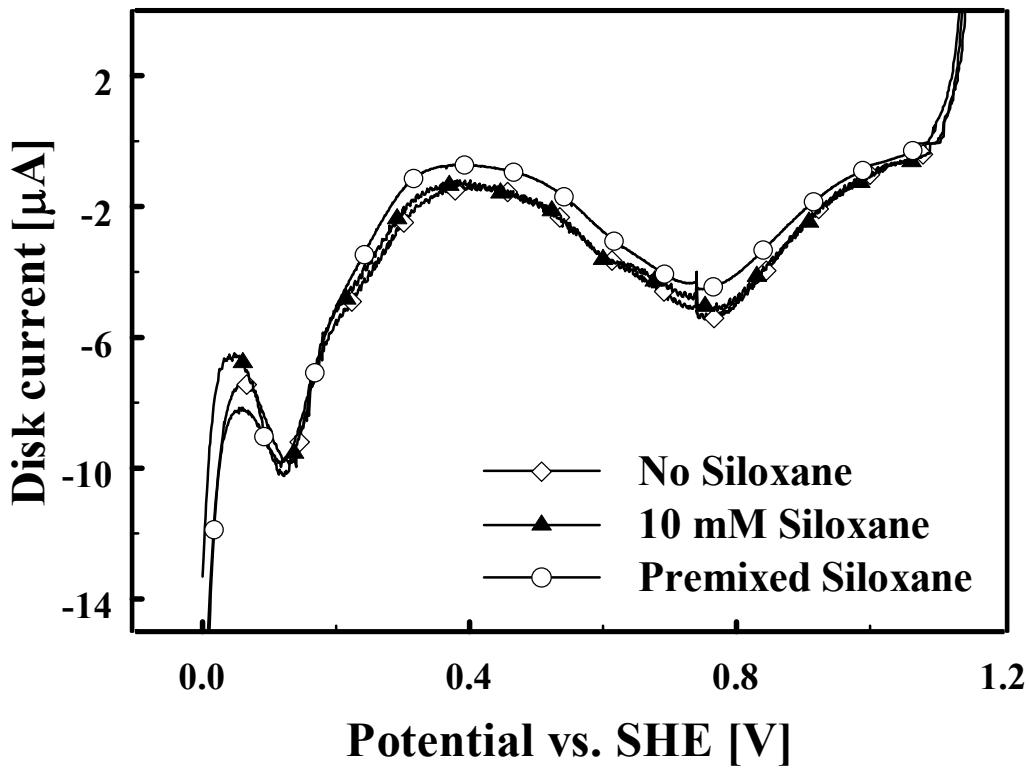

Figure 5-2. Disc currents in 0.5M $HClO_4$ at 1 atm, 25 °C and 1200 rpm for the three cases – No di-phenyl siloxane, di-phenyl siloxane in the electrolyte and di-phenyl siloxane premixed with the ink. Nitrogen (UHP, Praxair) was bubble though the electrolyte. The potential scan was started at 1.2 V vs. SHE and was swept cathodically at the rate of 5 mV s^{-1}.

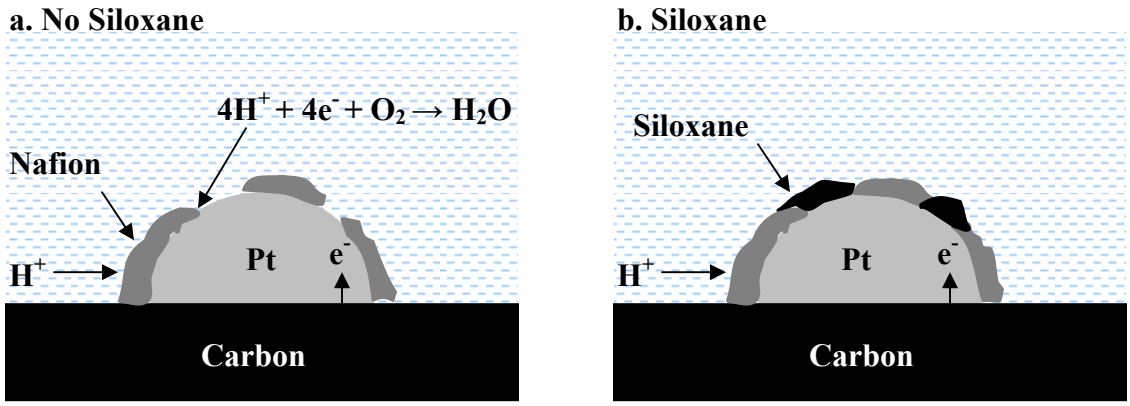

Figure 5-3. Schematic of the supported catalyst with and without diphenyl-siloxane on the catalyst particle.

5.5 Conclusions

Diphenyl-siloxane was used a source compound to understand the poisoning effect of the decomposition products of silicone seals over long-term fuel cell operation. Preliminary RDE data indicated that di-phenyl siloxane, when present in the electrode, blocked oxygen transport but did not hinder proton transport. Since oxygen transport occurs through aqueous media, we postulate that di-phenyl siloxane induced local water starvation upon deposition on catalyst sites which blocked oxygen transport to the catalyst sites. In a fuel cell, local water starvation could cause local mechanical stresses, increase local ionomer acidity and accelerate ionomer degradation via peroxy-radical attack. Local water starvation on the cathode side could block oxygen transport and degrade fuel cell performance.

5.6. References

1. L. Frisch, *Sealing Technology*, **93**, 7 (2001).

2. T. Clark in *DoE Hydrogen Program – FY 2004 Progress Report*, p. 493.

3. S. Motupally and T. D. Jarvi, Abstract #1167, 208th Meeting of the Electrochemical Society, Los Angeles, CA, October 16-21.

4. M. Schulze, T. Knöri, A. Schneider and E. Gülzow, *Journal of Power Sources*, **127**, 222 (2004).

5. T. J. Schmidt, H. A. Gasteiger, G. D. Stäb, P. M. Urban, D. M. Kolb and R. J. Behm, *J. Electrochem. Soc.,* **145**, 2354 (1998).

6 . S. Trasatti and O. A. Petrii, *Pure and Appl. Chem.,* **63**, 711 (1991).

7. C. A. Reiser, L. Bregoli, T. W. Patterson, J. S. Yi, J. D. Yang, M. L. Perry and T. D. Jarvi, *Electrochem. Solid State Letters*, **8**, A273 (2005).

6. Hydrogen Sulfide Kinetics on PEMFC Electrodes

6.1. Abstract

A concise mechanism for the poisoning kinetics of hydrogen sulfide (H_2S) on composite solid polymer electrolyte Pt (SPE-Pt) electrode is presented. The mechanism is validated experimentally by charge balances and theoretically by a model, which predicts the oxidation current as a function of the applied potential. H_2S dissociatively adsorbs onto SPE-Pt electrode as linear and bridge bonded sulfur (S) species and, under favorable potentials, undergoes electro-oxidation to sulfur and then to sulfur dioxide (SO2). A fraction of the adsorbed S species remains as 'hard-to-oxidize' adsorbents and causes irreversible loss of catalytic activity. Deactivation of bridge sites occurs first followed by the loss of linear sites.

[V. A. Sethuraman, L. A. Wise, S. Balasubramanian, and J. W. Weidner, "Hydrogen Sulfide Kinetics on PEM Fuel Cell Electrodes", *Electrochemical Society Transactions*, **1** (8), 111-130 (2006).]

6.2. Introduction

Though extensive research had been done on the issue of CO poisoning in polymer electrolyte membrane (PEM) fuel cells, there is much less in the literature on H_2S poisoning. Uribe *et al.*[1] showed that the poisoning effect due to H_2S is cumulative and irreversible. According to them, after H_2S poisoning, total recovery with neat hydrogen was not possible and a partial recovery was possible by a potential scan between 0 and 1.4 V vs. dynamic hydrogen electrode (DHE). Mohtadi *et al.*[2] found that the degree of recovery of a PEM fuel cell anode poisoned by H_2S depended on the degree of oxidation of two surface species observed in the cyclic voltammogram. Further they reported that the increase in Pt loading increased the partial recovery both with neat hydrogen and by a potential scan. Loučka[3], the first to study the kinetics of H_2S adsorption and oxidation on single crystal platinum electrodes in aqueous phase at 25 ºC, found that H_2S became completely dehydrogenated on adsorption and that the hydrogen thus formed became anodically oxidized at positive electrode potentials. Also, the charges for oxidation of adsorbed sulfur were too high to account for the oxidation of a mere monolayer of adsorbed sulfur. This was explained by the formation of a poorly reducible oxide on the electrode and not due to the presence of multiple layers of adsorbed sulfur atoms. Further, according to Loučka, complete removal by oxidation of adsorbed sulfur could not be attained by holding the poisoned Pt electrode at 1.6 V vs. DHE unless the degree of S coverage on the electrode was very low. Complete oxidation was reached only by periodic polarization to such positive potentials. Loučka proposed the following mechanism,

$$Pt - S + 3H_2O \leftrightarrow SO_3 + 6H^+ + 6e^- + Pt \quad \textbf{6-1}$$

$$Pt - S + 4H_2O \leftrightarrow SO_4^{2-} + 8H^+ + 6e^- + Pt \quad \textbf{6-2}$$

Najdekar *et al.*[4] attributed the formation of the poorly reducible oxide to the sulfidation of Pt electrode. They attributed the large oxidation peak in the 1.25-1.42V range to oxidation of platinum. They compared the oxidation and the reduction charges of each cycle of the cyclic voltammogram and postulated that platinum oxide reacted with sulfur released at the electrode surface with the regeneration of sulfide. Using potentiodynamic oxidation at elevated temperatures (i.e. >60 ºC), Contractor *et al.*[5] demonstrated the presence of two forms of chemisorbed sulfur distinguished by the number of platinum sites occupied per sulfur atom. Based on electrons per site (e.p.s.) calculations, they attributed the first peak to the oxidation of linear-bonded sulfur and the second peak to the oxidation of bridge-bonded sulfur. Pitara *et al.*[6] also confirmed this presence of two forms of chemisorbed sulfur. They reported that the adsorption of sulfur was sensitive to the nature of the platinum surface. While, one sulfur atom covered one Pt atom when H_2S was adsorbed on a smooth Pt atom in zero valence state, the charge of the adsorbed sulfur depended on the degree of its coverage on a rough platinum surface, ranging between 1.5 and 2 at low coverage to 1 at higher coverage. In another study[7], they showed that the sulfur species adsorbed on the surface of the platinum were likely to be composed of sulfur and sulfides.

Farooque *et al.* studied the oxidation of H_2S on a rotating tripolar wiper-blade electrode in the low potential region[8] (0-0.45V vs. SHE) and in the tafel region[9] (0.45-1.4V vs. SHE) and reported that at lower oxidation potentials, the anodic oxidation of H_2S followed a two-electron process to yield elemental sulfur, protons and electrons.

Using likelihood approach, a statistical tool to validate the most likely model from a set of contending models, they were able to prove that the low potential oxidation of H_2S most likely followed the mechanism given below,

$$Pt + H_2S \leftrightarrow Pt - H_2S_{ads} \quad \textbf{6-3}$$

$$Pt + SH^- \leftrightarrow Pt - SH_{ads} \quad \textbf{6-4}$$

$$Pt - H_2S_{ads} \rightarrow Pt - SH_{ads} + H^+ + e^- \quad \textbf{6-5}$$

$$Pt - SH_{ads} \rightarrow Pt - S_{ads} + H^+ + e^- \quad \textbf{6-6}$$

The chemical reactions 6-3 and 6-4 were faster than the electrochemical reactions 6-5 and 6-6. This confirmed the two-electron oxidation mechanism put forward by Loucka. Also, they reported that the oxidation of H_2S at higher potentials yielded colloidal sulfur. In their experiment, the wiper-blade electrode system continuously cleaned the surface by piperidine (a selective solvent for sulfur) to remove the colloidal sulfur formed. Since the electrode was always clean for further H_2S adsorption and oxidation, sulfur was the main product both in the lower and at the higher oxidation potentials.

H_2S poisoning studies have also been done for a variety of fuel cell systems. Uribe *et al.*[1] and Mohtadi *et al.*[2] studied the H_2S poisoning effects in a PEM fuel cell system. Chin *et al.*[10] investigated the poisoning effect of H_2S on the anodic oxidation of hydrogen on Pt in a 94 wt% phosphoric acid electrolyte fuel cell over a temperature range of 25 – 170 ºC. They reported that the extent of H_2S poisoning decreased with increasing temperature and increased with increasing electrode potential. Further, at sufficiently high anodic potentials, a layer of adsorbed elemental sulfur was found to form on the

electrode surface, which suppressed the formation of platinum oxide at the oxygen adsorption potentials. According to Kawase *et al.*[11], who studied the effect of H_2S on molten carbonate fuel cells, large voltage losses occurred after the cell was exposed to 5 ppm H_2S. They attributed this to the formation of SO_4^{2-} and S^{2-} on the nickel electrode.

Paál *et al.*[12] investigated gas phase H_2S adsorption on platinum in the presence of H_2. They were able to identify the presence of sulfide and sulfate species on the poisoned surface using XPS. Also, studies by Mathieu *et al.*[13] on gas phase chemisorption of H_2S on Pt showed that H_2S adsorbed dissociatively on Pt and the dissociation lead to adsorbed sulfur and gaseous hydrogen. While investigating the effects of sulfur poisoning on platinum supported on alumina, Chang *et al.*[14] found that the adsorbed sulfur induced Pt agglomeration by weakening the metal-support interaction and caused migration of Pt clusters in the process. Their observation was based on the size of Pt clusters measured before and after H_2S exposure.[15]

Donini *et al.*[16] described an electrochemical process for decomposing H_2S to produce hydrogen and sulfur. They used a divided electrolytic cell and a mixture of H_2S and volatile basic solution as the electrolyte to produce a polysulfide solution at the anode compartment. The polysulfide solution was then distilled to produce elemental sulfur. They later extended this invention to produce sulfur directly in a gas phase electrolysis process, where H_2S is oxidized at high potentials in a composite solid polymer electrolyte (CSPE)-Pt anode at elevated temperatures (>120 ºC).[17]

More recently, Wang *et al.*[18] developed an amperometric H_2S sensor based on its electrochemical oxidation route on a CSPE-Pt electrode. They found that the electro-oxidation products of H_2S depended on the local electrode potential at the time of

adsorption. Using XPS, they found that the main oxidation product was elemental sulfur at lower potentials and SO_4^{2-} at higher oxidation potentials. They reported that even at higher potentials, the elemental sulfur was difficult to remove from the surface of the electrode. This finding agrees with that of Loucka, Najdekar *et al.* and Contractor *et al.*. Further, they tested the durability of their H_2S sensor[19] and reported that the deposition of elemental sulfur on the CSPE-Pt electrode was the main factor affecting the life of the sensor. However, they reported that the tolerance levels of a CSPE-Pt electrode were significantly better than that of planar Pt electrodes and they attributed this to the highly porous nature of the former.

Following conclusions could be derived based on the above observations in the literature on the kinetics of H_2S adsorption and oxidation, both in liquid phase (planar electrodes[3, 4, 5, 6, 7, 8, 9] and CSPE-Pt electrodes[16]) and in gas phase (planar electrodes[10, 11, 12, 13, 14, 15] and CSPE-Pt electrodes[1, 2, 17, 18, 19]),

a. H_2S adsorption on Pt is dissociative producing elemental sulfur and hydrogen. The hydrogen thus formed undergoes oxidation at positive electrode potentials.
b. The sulfur thus formed strongly adsorbs to Pt. The adsorption results in linear-bonded sulfur species, Pt-S, and bridge-bonded sulfur species, $(Pt)_2$-S. The nature of adsorption is a strong function of temperature.
c. The Pt-S or $(Pt)_2$-S thus formed undergoes further oxidation at high electrode-potentials to yield SO_2 or SO_4^{2-}.
d. It takes several potential scans to completely clean the surface off of H_2S, S and their oxidation products.

e. In the process of H_2S and S adsorption and oxidation, a small percentage of the active catalyst sites are irreversibly lost due to the formation of an adsorbate that is difficult to oxidize or an oxide that is difficult to reduce.

f. Some of the explanations for the irreversible loss due to H_2S poisoning include sulfur induced Pt agglomeration, formation of platinum sulfides and oxides that are difficult to reduce and the migration of Pt clusters due to loss in the metal-support interaction.

Based on the above observations, a comprehensive list of reactions H_2S, as linear and bridge bonded species, can undergo on a CSPE-Pt electrode,

$$Pt + H_2S \leftrightarrow Pt - H_2S_{ads} \quad \textbf{6-7}$$

$$Pt - H_2S_{ads} \rightarrow Pt - SH_{ads} + H^+ + e^- \quad \textbf{6-8}$$

$$Pt - SH_{ads} \rightarrow Pt - S_{ads} + H^+ + e^- \quad \textbf{6-9}$$

$$2Pt + H_2S \leftrightarrow (Pt)_2 - H_2S_{ads} \quad \textbf{6-10}$$

$$2Pt - H_2S_{ads} \rightarrow (Pt)_2 - SH_{ads} + H^+ + e^- \quad \textbf{6-11}$$

$$2Pt - SH_{ads} \rightarrow (Pt)_2 - S_{ads} + H^+ + e^- \quad \textbf{6-12}$$

$$Pt - S_{ads} + 2H_2O \rightarrow SO_2 + 4H^+ + 4e^- + Pt \quad \textbf{6-13}$$

$$(Pt)_2 - S_{ads} + 2H_2O \rightarrow SO_2 + 4H^+ + 4e^- + 2Pt \quad \textbf{6-14}$$

$$Pt - S_{ads} + 3H_2O \rightarrow SO_3 + 6H^+ + 6e^- + Pt \quad \textbf{6-15}$$

$$(Pt)_2 - S_{ads} + 3H_2O \rightarrow SO_3 + 6H^+ + 6e^- + 2Pt \quad \textbf{6-16}$$

$$Pt - S_{ads} + 4H_2O \rightarrow SO_4^{2-} + 8H^+ + 8e^- + Pt \quad \textbf{6-17}$$

$$(Pt)_2 - S_{ads} + 4H_2O \rightarrow SO_4^{2-} + 8H^+ + 8e^- + 2Pt \quad \textbf{6-18}$$

Where reactions 6-7 and 6-10 are the adsorption and desorption of H_2S on Pt surface, and 6-8, 6-9, 6-11 and 6-12 represent the oxidation of the adsorbed H_2S resulting in sulfur adsorption. Reactions 6-13 through 6-18 represent the oxidation of adsorbed sulfur to SO_2, SO_3 and SO_4^{2-}. One of the main objectives of this article was to probe the multiple peaks obtained during the CV for the distribution of linear and bridge bonded S on the CSPE-Pt surface. Further charge balances are made to quantify the exact amount to different species formed during the electro-oxidation of H_2S adsorbed on the surface of the CSPE-Pt electrode.

6.3. Experimental

6.3.1. Fuel Cell

Pt catalyst ink with 75 wt% catalyst and 25 wt% Nafion® (dry solids content) was prepared with commercially available 40.2 wt% Pt on Vulcan XC-72 catalyst (E-TEK De Nora North America, NJ) and Perfluorosulfonic acid-PTFE copolymer (5% w/v, Alfa Aesar, MA). Isopropyl alcohol (99% v/v, VWR Scientific Products) was used as the thinning solvent. The ink was mixed properly for at least 8 hours. ELAT electrodes (E-TEK De Nora North America, NJ) coated with carbon on one side were used as gas diffusion layers (GDL). The GDLs were cut into 10 cm^2 pieces. Catalyst ink was then sprayed onto the GDLs, air dried for ½ hour and then dried at 383K for 10 minutes to evaporate any remaining solvent. The process was repeated until the target loading was achieved. The active area of the electrodes was 10 cm^2. Both the anode and the cathode

side had a loading of 0.5 mg/cm^2 of Pt. The catalyzed GDLs were then bonded to a pretreated Nafion® 112 membrane by hot pressing at 140 ºC for two minutes at 500 psig to make a membrane electrode assembly (MEA). The MEA was assembled into a fuel cell with single channel serpentine flow field plates bought from Fuel Cell Technologies. The cell was incubated at 70 °C and atmospheric pressure for at least 8 hours with 0.25 standard liters per minute (SLM) H_2 (UHP Hydrogen, Air products) and 0.18 SLM O_2 (UHP Oxygen, Air Products) on the anode and cathode side respectively. The temperature of the anode and the cathode humidity bottles were 80 °C and 70 °C respectively such that gases flowing through were fully humidified. Current - Voltage (VI) performance curves were recorded after incubation and compared with a baseline VI performance curve to confirm that the fuel cell is working properly.

6.3.2. Cyclic Voltammetry and Electrochemical Area

For initial characterization of the MEA, the cell was cooled down to 25 °C. N_2 at 0.10 SLM was fed through the anode side (henceforth called as the working electrode, WE) and H_2 at 0.05 SLM was fed through the cathode side of an open circuited cell. H_2 flowing over Pt/C acted as a dynamic hydrogen electrode (DHE) and hence all the potentials were referenced to this electrode. The open circuit potential was monitored while it decayed from the typical H_2/O_2 potential (~1.0 V vs. DHE) to the characteristic N_2/H_2 potential of ~0.085 V vs. DHE. N_2 flow was then switched to a flow of 476 ppm CO in N_2 with a total flow rate of 0.10 SLM for 300 seconds. This exposure and the resulting adsorption were found earlier to result in the maximum surface coverage of CO on Pt. N_2 flow was then restored to purge out CO present in the bulk of the flow channels. The cell was held at a constant potential of 50 mV for 25 seconds, which was

followed by cyclic voltammetry (CV) at a scan rate of 20 mV/s from 50 to 1150 mV and back to 50 mV vs. DHE. Experiments were conducted using a M263A potentiostat/galvanostat in conjunction with ECHEM software made by EG&G (Princeton Applied Research). The area under the CO oxidation peak, Q_{CO}, in the potential window 600 – 850 mV relative to the background current was used to calculate the amount of CO oxidized, which is then used to calculate the maximum active electrochemical area, Q_{max}. The voltammogram obtained from a CO covered electrode was baseline corrected and the two convoluted peaks were deconvoluted with a bimodal Gaussian distribution using commercially available Tablecurve2D® made by Systat®. The resulting fit was always with a R^2 greater than 0.98 and the deconvolution parameters were estimated for a 95% confidence interval. The bimodal Gaussian distribution equations, the deconvolution procedure and associated fitting parameters were discussed elsewhere.[20]

6.3.3. Adsorption

While the cell was still at 25 °C, N_2 flow on the WE was switched to a flow of 50 ppm H_2S in N_2 for 600 seconds. The total flow rate of this mixture was 0.10 SLM. This exposure and the resulting adsorption were found earlier to result in the maximum surface coverage of H_2S on Pt. N_2 flow was then restored to purge out H_2S present in the bulk of the tubing and flow channels. The cell was then held at a constant potential of 50 mV for 25 seconds followed by cyclic voltammetry (CV) at a scan rate of 5 mV/s from 50 to 1400 mV and back to 50 mV vs. DHE. The CV scans were repeated until no further oxidation peaks were noticed - *i.e.* until a CV cycle overlapped with a baseline CV

corresponding to a clean electrode. This experiment was repeated with conditioned fresh MEAs at eleven other temperatures in the 35-110 °C window.

6.3.4. Sequential adsorption and performance measurements

After a cell with a fresh MEA was conditioned at 70 °C and characterized for its true electrochemical area at 25 °C, it was taken back to 70 °C for sequential adsorption and performance measurements. The adsorption experiment like the one described before was done at 70 °C followed by a H_2/O_2 performance measurement. The cell was then cooled to 25 °C for ECA measurement using CO adsorption. This constituted one cycle. Such cycles were repeated until the cell lost more than half of its original active electrochemical area.

6.4. Theory

An electro-kinetic model is presented in conjunction with the data as a proof for the existence of one kind of reaction taking place on two kinds of adsorption sites, *i. e.* bridge and linear. This model assumes the following:

a. Mass transport of Pt sites and/or the adsorbed species were ignored.
b. Isothermal conditions exist and reaction heat was ignored.
c. Pt sites were assumed not to dissolve, migrate or ripen under the influence of the applied potential for the duration of the experiment. Though the applied potential routinely exceeded the equilibrium potential for Pt dissolution (~1.0V vs. DHE), this was a valid assumption because of the duration of the applied potential, which was of the order of few minutes as opposed to the time constant for Pt dissolution and migration which is at least two orders of magnitude higher. We confirmed

this by repeatedly scanning the electrode while observing ECA loss at regular intervals. No significant ECA loss was observed after 100 cycles.

d. Only the catalyst sites (Pt) participated in the reaction; the support (carbon) did not contribute to the oxidation current. We verified this by exposing H_2S to an uncatalyzed MEA followed by a potential scan at the rate of 5mV/s in the 50-1400mV vs. DHE window. No oxidation peaks and unusually high currents were observed.

e. Desorption of adsorbed species and the diffusion back to the bulk were ignored because our previous experiments suggested that desorption times were at least three orders of magnitude greater than those of adsorption. Further, the cell thickness (thickness of the porous electrode, l) was smaller than the diffusion layer thickness (if there was diffusion of desorbed H_2S within the pores), that is, $l << \sqrt{2D_{H_2S}t}$ for the given experimental time t.

f. N_2 flow in the bulk did not affect the kinetics of the adsorbed species

g. The concentration of the adsorbed species and Pt sites were assumed to be uniform [$C(x, t) = C(t)$ and $C_m(x, t) = C_m(t)$ *for* $0 \le x \le l$]

h. The degree to which adsorption equilibrium was attained before the start of the CV is assumed to be completely shifted towards adsorption, that is, no desorption was assumed to take place prior to and during the experiment.

i. Except for the surface coverage, the state of the electrode was assumed to be the same for all the experiments (CVs) when they were initiated.

j. No further adsorption was assumed to take place immediately after the initiation and during the CV experiment.

k. The oxidation products (CO_2, SO_2 etc.) formed during the experiment were assumed to be carried away by N_2 flowing in the bulk and that they do not affect the kinetics of the electro-oxidation reaction, that is, no lateral interactions occur between the adsorbed species and the oxidation products.

Equations for two scenarios are presented – one where multiple electro-oxidation reactions occur on one kind of sites and the other where one type of reaction occurs on different types of sites.

6.4.1. One kind of sites, multiple reactions

If H_2S adsorbs onto the Pt sites and under the influence of an applied potential E undergoes multiple electro-oxidation reactions, *1, 2,....., n*, the concentration of the sites can be expressed as,

$$C = C^0 e^{\left(-\frac{ART\left(\frac{k_1}{\alpha_1}+\frac{k_2}{\alpha_2}+...+\frac{k_n}{\alpha_n}\right)}{VF\upsilon} \right)} \qquad \textbf{6-19}$$

where C^0 is the initial concentration of Pt sites and k_n is the rate constant for the n^{th} electro-oxidation reaction which can be expressed as,

$$k_n = k_n^0 e^{\left(-\frac{\alpha_n F\left(E_n^0 - E\right)}{RT} \right)} \qquad \textbf{6-20}$$

where α_n is the transfer coefficient and E_n^0 is the equilibrium potential vs. DHE corresponding to the n^{th} electro-oxidation reaction and E is the applied potential vs. DHE. The oxidation current from this reaction is,

$$i_n = N_n FACk_n \qquad \textbf{6-21}$$

where N_n is the number of electrons transferred. The peak current, which occurs at $E_n^0 = E$ is given by,

$$i_n^p = N_n FAC^0 e^{\left(-\frac{ART\left(\frac{k_1^0}{\alpha_1} + \frac{k_2^0}{\alpha_2} + \ldots + \frac{k_n^0}{\alpha_n} \right)}{VF\upsilon} \right) k_n^0} \qquad \textbf{6-22}$$

The total current due to the oxidation of all adsorbed species is the summation of individual currents,

$$i = \sum_n i_n \qquad \textbf{6-23}$$

6.4.2. One reaction, multiple sites

If H_2S adsorbs onto the different kinds of Pt sites and under the influence of an applied potential *E,* undergoes one reaction pathway, the concentration of the of Pt sites of the m^{th} kind can be expressed as,

$$C_m = C_m^0 e^{\left(-\frac{ARTk}{VF\upsilon\alpha} \right)} \qquad \textbf{6-24}$$

where C_m^0 is initial concentration of the Pt sites of the m^{th} kind and *k* is the rate constant of the lone electro-oxidation reaction expressed as,

$$k = k^0 e^{\left(-\frac{\alpha F\left(E^0 - E\right)}{RT} \right)} \qquad \textbf{6-25}$$

where E^0 is the equilibrium potential vs. DHE. The oxidation current from this reaction is,

$$i_m = NFAC_m k \qquad \textbf{6-26}$$

where N is the number of electrons transferred in the reaction. The peak current, which occurs at $E^0 = E$ is given by,

$$i_m^p = NFAC_m^0 e^{\left(-\frac{ARTk^0}{VF\upsilon\alpha}\right)} k^0 \qquad \textbf{6-27}$$

The peak potential (obtained by differentiating 6-26 and setting the result to zero) occurs at,

$$E_m^p = E^0 - \frac{RT}{\alpha F}\ln\left(\frac{VF\upsilon\alpha}{ARTk^0}\right) \qquad \textbf{6-28}$$

The total current due to the oxidation of adsorbed species on all the sites is the summation of individual currents,

$$i = \sum_m i_m \qquad \textbf{6-29}$$

6.5. Results and Discussion

Figure 6-1 shows the first cycles of cyclic voltammograms obtained on a SPE-Pt electrode exposed to 50 ppm H_2S in N_2 for different temperatures. Data from higher temperature show two oxidation peaks corresponding to oxidation of species from two different types of sites. Though multiple potential sweeps were required to completely oxidize the adsorbed S from the SPE-Pt surface, the number of cycles decreased with temperature. At 110 °C, only one such potential sweep was required to completely oxidize all of the adsorbed S species. Further, the peak potential, E_P, for S oxidation

decreased with temperature. This was found to be the case for similar studies done on single crystal Pt in aqueous solutions. It is possible to estimate parameters such as k^0, C_l^0 and C_b^0 based on the peak current and peak potential values and such an attempt is presented elsewhere.

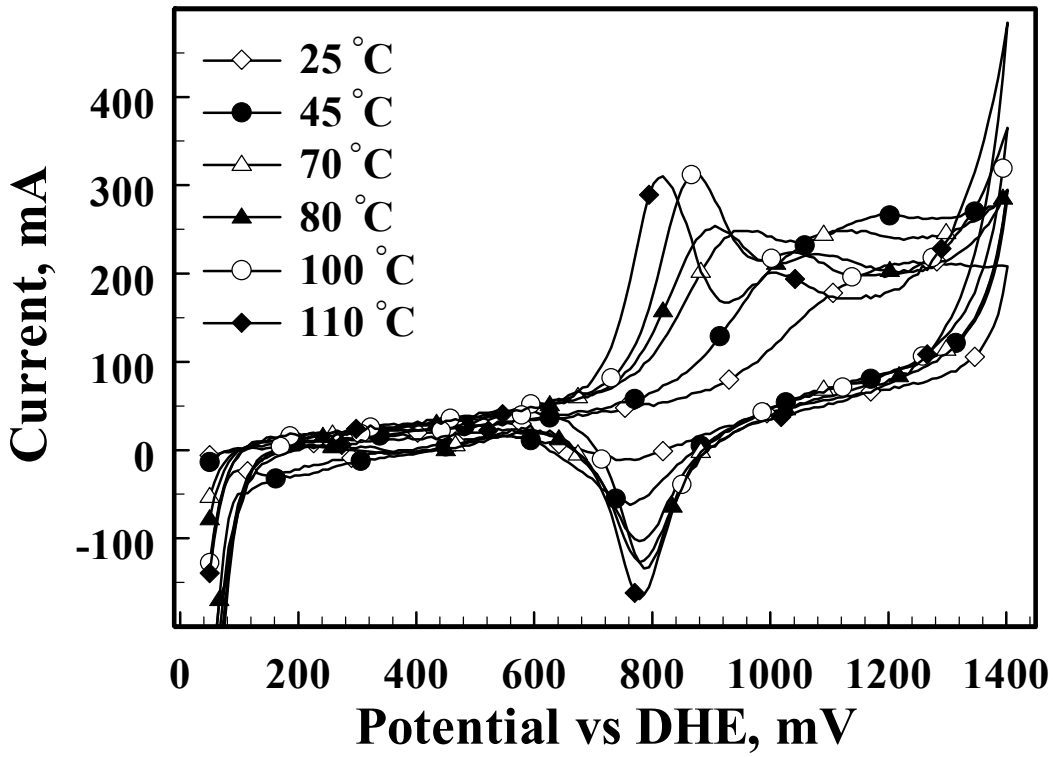

Figure 6-1. Cyclic voltammograms obtained from a 40% Pt supported on Vulcan XC-72R after exposure to 50 ppm H_2S in N_2 for 300s at different temperatures. CVs were conducted in N_2 30s after the gas feed was changed from H_2S in N_2 to N_2.

These oxidation curves were baseline-corrected, that is, the second cycle from the CV data was subtracted from the first cycle. For low temperature CV data where multiple scans were required to completely oxidize the adsorbed S to SO_2, subsequent cycles were baseline-corrected and added to the first baseline-corrected cyclic voltammogram, that is in general, $(n+1)^{th}$ cycle would be subtracted from the n^{th} cycle and the resulting data would be added to the first cycle. The area under each of the resulting baseline-corrected curves was deconvoluted using a bimodal Gaussian distribution. The area under the first peak contributes to oxidation charge Q_1 and the area under the second peak contributes to oxidation charge Q_2.

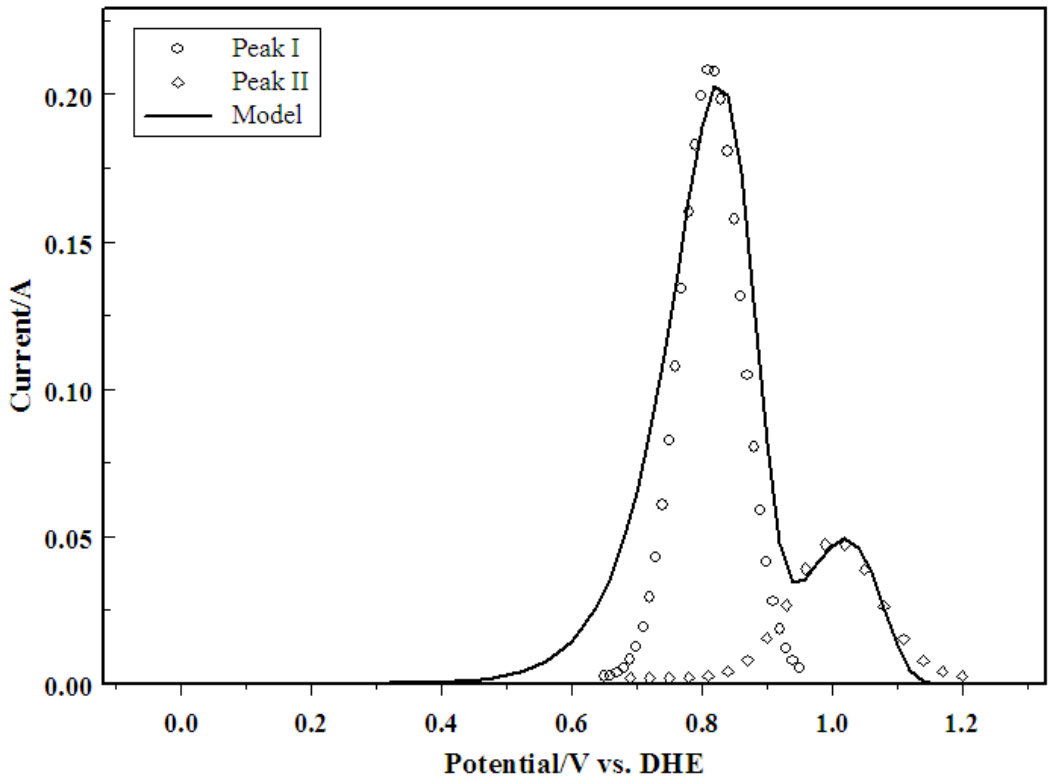

Figure 6-2. Data vs. model of a baseline corrected CV obtained from a 40% Pt supported on Vulcan XC-72R after exposure to 50 ppm H_2S in N_2 for 300s at 110 °C. Peaks I and II correspond to currents, respectively, due to the oxidation of bridge and linear bonded S species.

Figure 6-2 shows the data vs. model of a baseline corrected CV obtained from an adsorption experiment at 110 °C. The principal aim of this model was to prove that one type of reaction occurs on two types of sites. It is not hard to see that in the first case, where multiple reactions occur on one type of sites, the concentration of sites, defined by 6-19, decays with the applied potential as a single profile. Since the oxidation current is proportional to the concentration of sites, the current profiles for each of the reaction should have the same shape and fall on top of each other. Though each of the current profiles should have different peak currents, as defined by 6-22, they have the same peak potential. This type of behavior contradicts data, which clearly exhibits distinct peaks, indicating different energies of oxidation.

Figure 6-3 shows the number of electrons transferred per site (e. p. s) for different temperatures calculated from cyclic voltammogram data. Q_1 and Q_2 represent the oxidation charges of peaks I and II respectively. $(2Q_1+Q_2)/Q_{max}$ gives number of electrons transferred per site (e. p. s) if charge from peak I correspond to oxidation of bridge bonded species and charge from peak II correspond to oxidation of linearly bonded species. $(Q_1+2Q_2)/Q_{max}$ gives the e. p. s if charge from peak I correspond to oxidation of linearly bonded species and charge from peak II correspond to oxidation of bridge bonded species. Q_{max} is the charge obtained from a fresh electrode corresponding to an e. p. s. = 1. Q_{max} was calculated from CO adsorption and stripping at 25 °C, where adsorption was assumed to go to saturation. The number of electrons transferred per site was uniform ~6 for the case where the first peak was a result of bridge oxidation and the second, linear oxidation. The e. p. s was non-uniform for the other case. This concludes our discussion on mechanism validation, both theoretical and experimental.

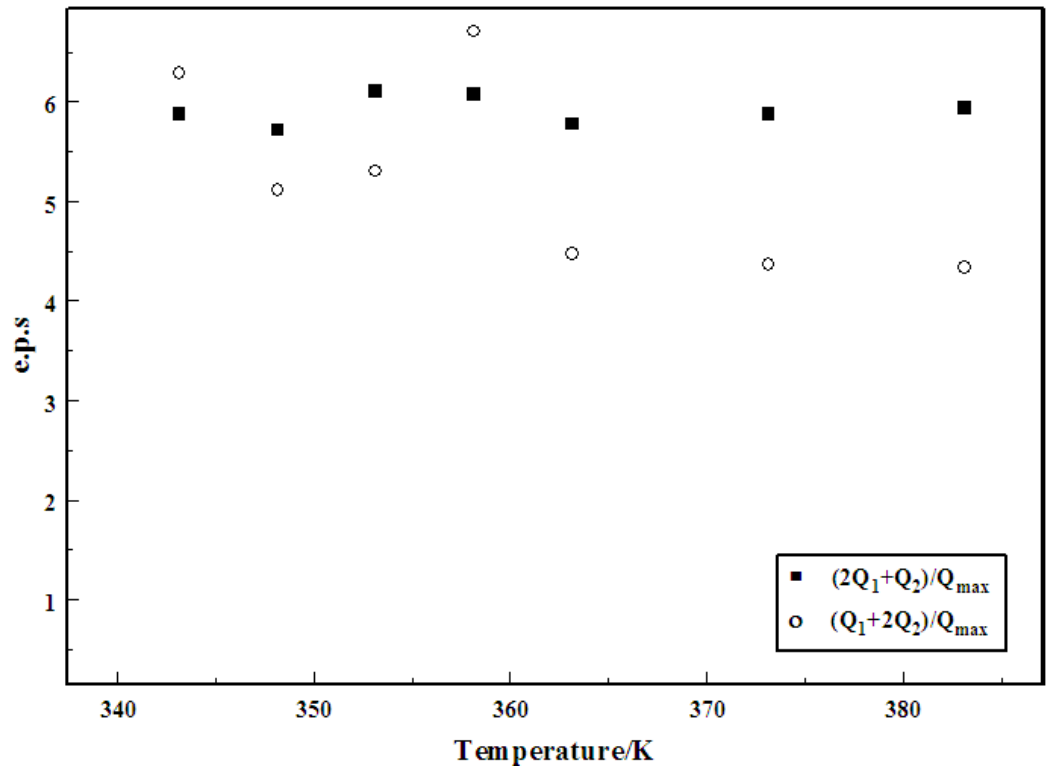

Figure 6-3. Electrons transferred per site (e. p. s) for different temperatures calculated from cyclic voltammogram data. Q_1 and Q_2 represent the oxidation charges of peaks I and II respectively. $(2Q_1+Q_2)/Q_{max}$ gives number of electrons transferred per site (e. p. s) if charge from peak I correspond to oxidation of bridge bonded species and charge from peak II correspond to oxidation of linearly bonded species. $(Q_1+2Q_2)/Q_{max}$ gives the e. p. s if charge from peak I correspond to oxidation of linearly bonded species and charge from peak II correspond to oxidation of bridge bonded species. Q_{max} is the charge obtained from a fresh electrode corresponding to an e. p. s. = 1.

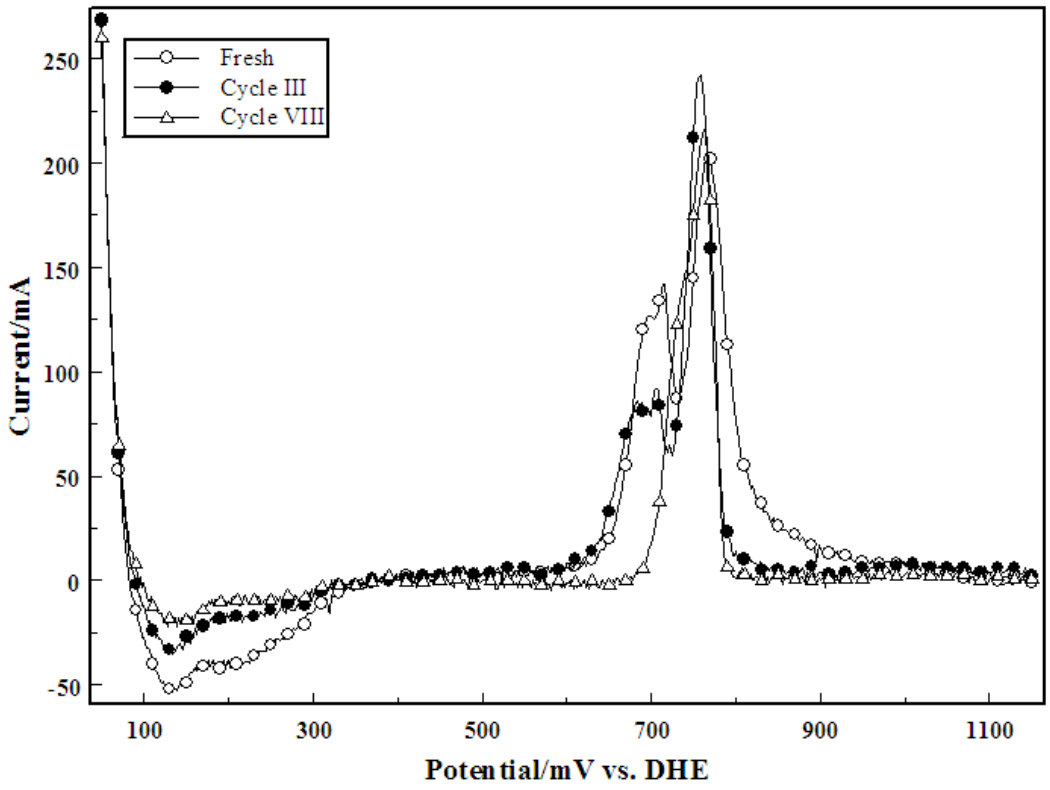

Figure 6-4. CVs obtained from a 40% Pt supported on Vulcan XC-72R after exposure to 0.1 SLM flow of 50 ppm CO in N_2 for 300s at 25 °C. These CVs were obtained on a fresh electrode, after three cycles and after eight cycles of H_2S adsorption and oxidation at 70 °C.

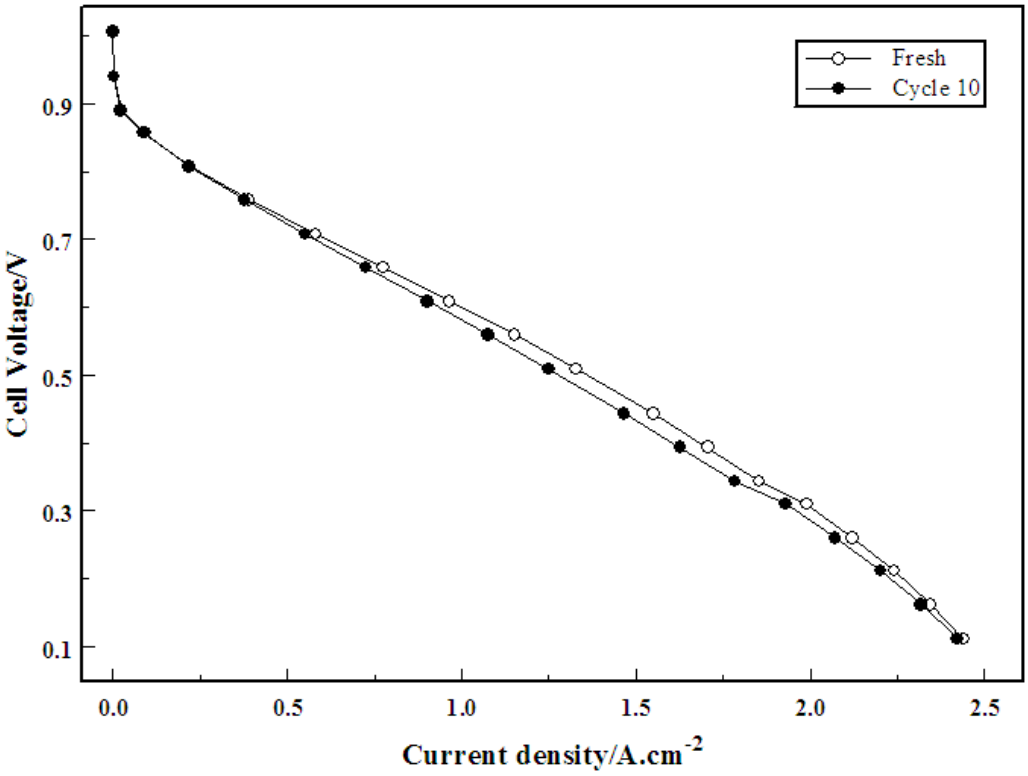

Figure 6-5. H_2/O_2 polarization curves at 70 °C and 1 atm pressure for a fresh electrode and after ten cycles of H_2S adsorption and oxidation.

Figure 6-4 shows the result of sequential adsorption and performance measurements at 70 °C. These baseline-corrected CVs were the result of CO adsorption and stripping experiments done at 25 °C on a fresh electrode and on electrodes with irreversible loss of catalytic activity induced by three and eight cycles of sequential H_2S adsorption and stripping at 70 °C. The amplitude of peak I decrease with increasing number of cycles, while the amplitude of peak II remains unchanged. Since peak II corresponds to oxidation due to bridge bonded species, the number of bridge sites decrease with increasing exposure to H_2S. It is interesting to note that H_2/O_2 performance curves at 70 °C on a fresh electrode and on an electrode after ten cycles of sequential H_2S adsorption and stripping, as shown in Figure 6-5, exhibit little or no change. However, there are subtle changes in the performance both in the kinetic region (Figure 6-6) as well as in the IR region (Figure 6-7). The performance in the IR region corresponds to the trend of sites lost. However, there is a slight increase in the performance in the kinetic region for cycle 4, where most of the bridge sites were lost and very little linear sites were lost. This is in accordance with the literature in that H_2 oxidation reaction is more facile on linear sites than on bridge sites.

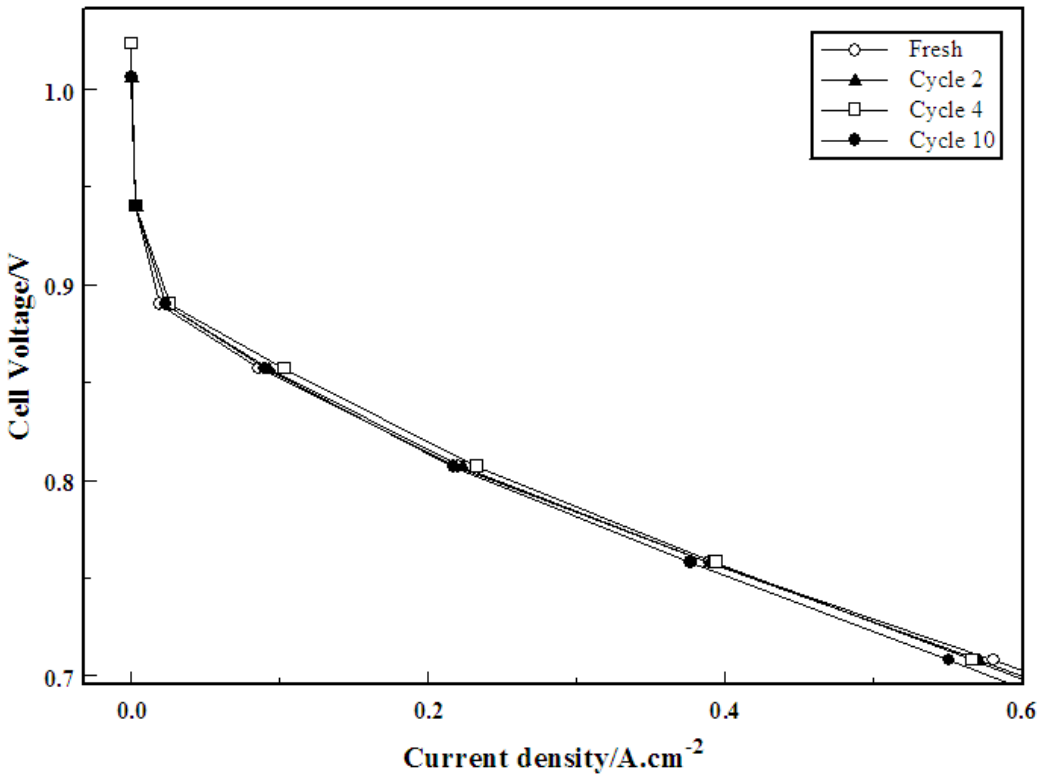

Figure 6-6 Kinetic region of H_2/O_2 polarization curves at 70 °C and 1 atm pressure for a fresh electrode and after two, four and ten cycles of H_2S adsorption and oxidation.

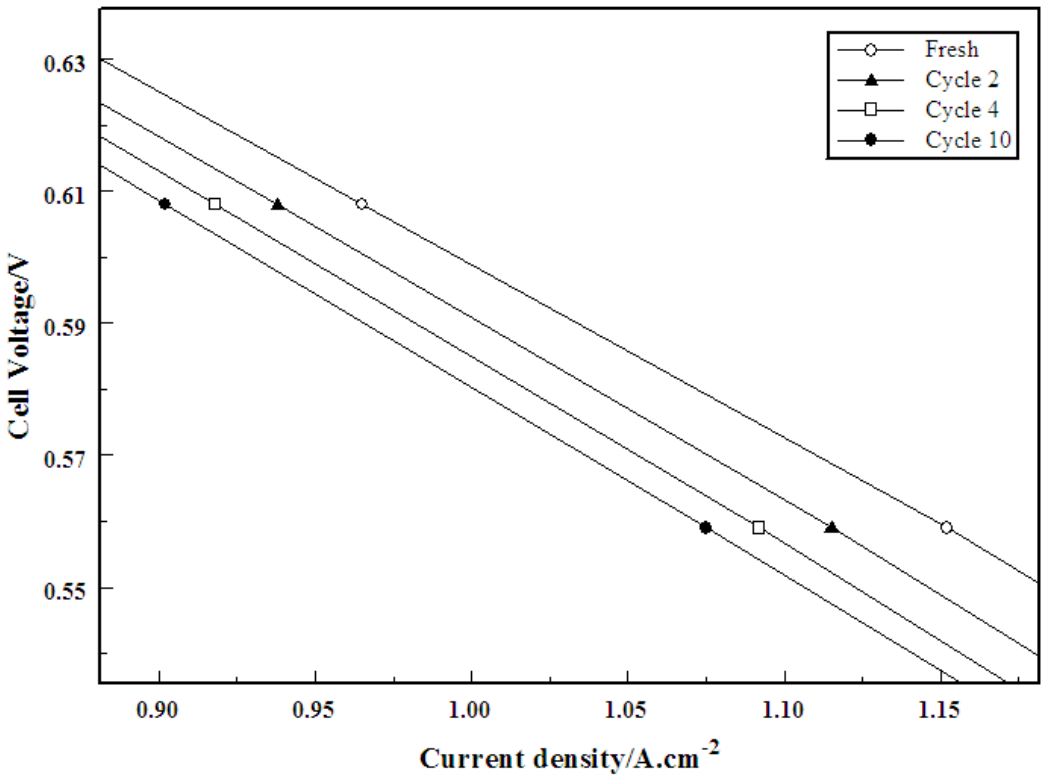

Figure 6-7. IR region of H_2/O_2 polarization curves at 70 °C and 1 atm pressure for a fresh electrode and after two, four and ten cycles of H_2S adsorption and oxidation.

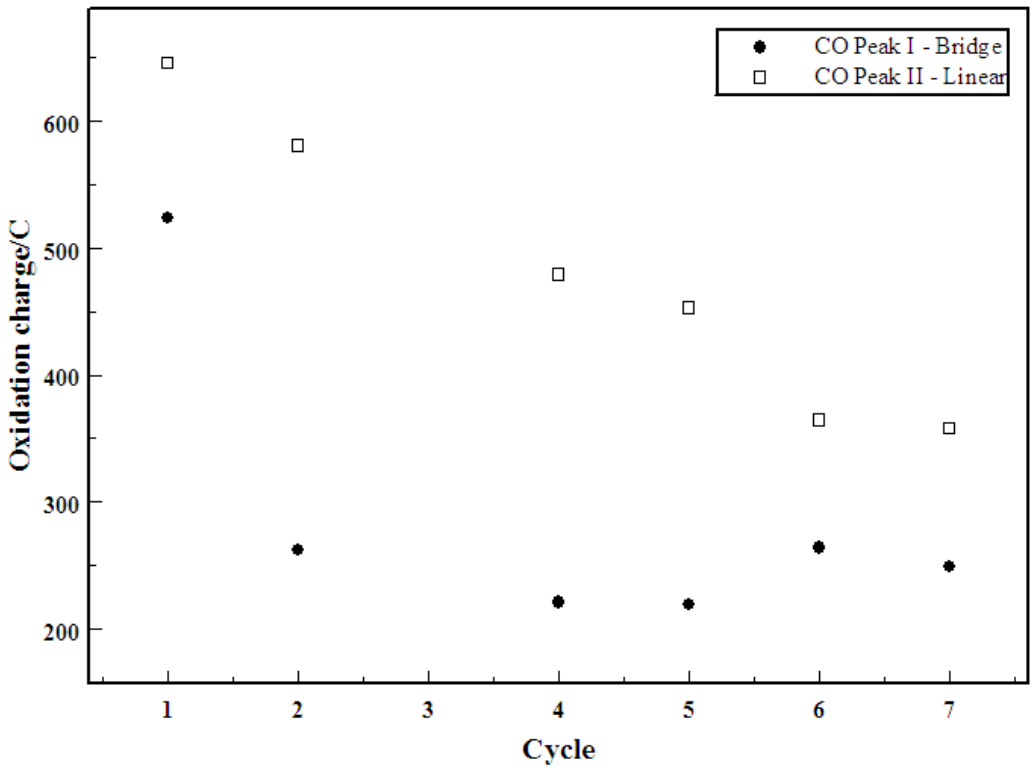

Figure 6-8. The loss of linear (peak II) and bridge (peak II) sites as a result of H_2S adsorption and oxidation cycles at 70 °C.

6.5. Conclusions

A concise mechanism for the kinetics of hydrogen sulfide on a CSPE-Pt electrode is presented. Unlike CO, H_2S causes irreversible loss of catalytic activity through S deposition, which is hard to oxidize.

List of Symbols

A	projected area of the porous electrode, cm^2
C	total concentration of catalyst sites, mol/cm^3
C^0	initial concentration of total catalyst sites, mol/cm^3
C_m^0	initial concentration of catalyst sites of m^{th} kind, mol/cm^3
D_{H_2S}	diffusion coefficient of H_2S in N_2, cm^2/s
E	applied potential, V
E^0	thermodynamic equilibrium potential vs. DHE, V
E_n^0	thermodynamic equilibrium potential vs. DHE for the n^{th} electro-oxidation reaction, V
E_m^p	peak potential corresponding to the electro-oxidation reaction occurring at sites of m^{th} kind, V
$e.p.s$	number of electrons transferred per Pt site
F	Faraday's constant, 96,487 C/equiv.
i	total electro-oxidation current, A
i_m	electro-oxidation current from sites of m^{th} kind, A
i_n	electro-oxidation current from n^{th} reaction, A
i_m^p	peak current corresponding to the electro-oxidation reaction occurring at sites of m^{th} kind, A
i_n^p	peak current corresponding to the n^{th} electro-oxidation reaction, A

k_n	electro-oxidation rate constant of n^{th} reaction, cm/s
k^0	equilibrium electro-oxidation rate constant, cm/s
k_n^0	equilibrium electro-oxidation rate constant of n^{th} reaction, cm/s
l	thickness of the porous electrode, cm
N	number of electrons transferred
N_n	number of electrons transferred in the n^{th} electro-oxidation reaction
Q_1	oxidation charge from peak I of a CV done on H_2S adsorbed electrode, mC
Q_2	oxidation charge from peak II of a CV done on H_2S adsorbed electrode, mC
Q_{CO}^b	oxidation charge from peak I of a CV done on CO adsorbed electrode, mC
Q_{CO}^l	oxidation charge from peak II of a CV done on CO adsorbed electrode, mC
Q_{max}	maximum oxidation charge calculated from a CV done on a CO adsorbed electrode, corresponding to an e.p.s = 1, mC
R	universal gas constant, 8.314 J/(mol K)
t	time, s
T	temperature, K
V	volume of the porous electrode, cm^3
x	distance coordinate in the X direction, cm
Greek	
α	transfer coefficient

α_n	transfer coefficient of n^{th} electro-oxidation reaction
v	sweep rate, V/s
Subscript	
1	peak I
2	peak II
CO	carbon monoxide
n	n^{th} electro-oxidation reaction
m	catalyst site of m^{th} kind
Superscript	
0	initial condition or standard state
b	bridge sites
l	linear sites
p	peak

Table 6-1. List of parameters used to fit the baseline corrected H_2S stripping voltammogram to the model.

Parameters	Value, units	Reference/Comments
A	10 cm^2	Measured
C_b^0	2.542 x 10^{-5} mol cm^{-3}	Estimated
C_l^0	7.208 x 10^{-6} mol cm^{-3}	Estimated
E_b^0	0.9 V vs. SHE*	Contractor *et al.*
E_l^0	1.1 V vs. SHE*	Contractor *et al.*
l	10^{-3} cm	Assumed
k_b^0	5.985 x 10^{-9} cm s^{-1}	Estimated
k_l^0	2.638 x 10^{-10} cm s^{-1}	Estimated
N	6 mole e^-/mole H_2S	Estimated
T	110 °C	Measured
α	0.5	Assumed
υ	0.005 V s^{-1}	Measured

* SHE – Standard Hydrogen Electrode

6.6. References

1. F. A. Uribe and T. A. Zawodzinski, Jr., Abstract #339, 200th Meeting of the Electrochemical Society, San Francisco, Fall 2001.
2. R. Mohtadi, W-K. Lee, S. Cowan, J. W. Van Zee and M. Murthy, *Electrochem. Solid State Letters,* **6,** A272 (2003).
3. T. Loučka, *J. Electroanal. Chem.,* **31,** 319 (1971).
4. E. Najdekar and E. Bishop, *J. Electroanal. Chem.,* **41**, 79 (1979).
5. A. Contractor and Hira Lal, *J. Electroanal. Chem.* **96**, 175 (1979).
6. E. Lamy-Pitara, L. Bencharif and J. Barbier, *Electrochemica Acta,* **30**, 971 (1985).
7. E. Lamy-Pitara, Y. Tainon, B. Beden and J. Barbier, *J. Electroanal. Chem.,* **279**, 291 (1990).
8. M. Farooque and T. Z. Fahidy, *J. Electrochem. Soc.,* **124**, 1191 (1977).
9. M. Farooque and T. Z. Fahidy, *J. Electrochem. Soc.,* **125**, 544 (1978).
10. D-T. Chin and P. D. Howard, *J. Electrochem. Soc.,* **133**, 2447 (1986).
11. M. Kawase, Y. Mugikura, and T. Watanabe, *J. Electrochem. Soc,* **147**, 1240 (2000).
12. Z. Paal, K. Matusek and M. Muhler, *Applied Catalysis,* **9**, 361 (1984).
13. M. Mathieu and M. Primet, *Applied Catalysis,* **9**, 361 (1984).
14. J. –R. Chang, S. –L. Chang and T. –B. Lin, *J. Catalysis,* **169**, 338 (1997).
15. J. –R. Chang and S. –L. Chang, *J. Catalysis,* **176**, 42 (1998).

16. J. C. Donini, S. Petrovic and E. A. Luinstra, *U. S. Patent* # 5,908,545 (1999).

17. J. C. Donini, K. T. Chuang, S. V. Slavov, A. R. Sanger and V. Stanic, *U. S. Patent* # 6,241,871 B1 (2001).

18. Y. Wang, H. Yan and E. Wang, *J. Electroanal. Chem.,* **497**, 163 (2001).

19. Y. Wang, H. Yan and E. Wang, *Sensors and Actuators B,* **87**, 115 (2002).

20. B. Lakshmanan, V. A. Sethuraman and J. W. Weidner, "Adsorption, Desorption and Rearrangement Kinetics of Linear and Bridge-bonded CO on Pt/C", to be submitted to *J. Electrochem. Soc*., (2006).

7. Future Work

7.1. Introduction

The exact nature of PEMFC degradation mechanism is not thoroughly understood and analyzed by the fuel cell community. The scope of this dissertation in terms of future research is to set the stage for such an effort. These are the suggested work that can immediately be built upon the data analyzed in this dissertation:

1. Understanding membrane degradation mechanism

By isolating the following processes that occur simultaneously, one can better understand the membrane degradation mechanism:

a. H_2O_2 formation at the anode and the cathode as a function of temperature, local potential and relative humidity for Pt and Pt alloys

b. H_2O_2 transport from the formation site into the membrane

c. Pt dissolution, passivation and transport into the membrane.

d. Formation of hydroxyl radicals and their effect on the ionomer and the membrane

e. Isolating the effects of potential, and the type of catalysts used on the durability of proton exchange membranes.

2. Catalyst design by understanding the roles played by the Pt (hkl) sites

Using H^+ as a probe molecule in conjunction with cyclic voltammetry, the distribution of Pt crystallites on supported Pt catalysts can be established. Using CO as a probe molecule, the distribution of linear and bridge sites can be established. Current catalyst manufacturers use trial and error method to synthesis supported catalysts for fuel cells. This technique can be used to analyze the surface of the synthesized catalysts pertinent to the fuel cell operation.

The durability aspects of these catalysts will be studied using potential cycling. For supported Pt catalysts, Pt (111) was found to be the least durable configuration followed by Pt (110) and Pt (100), the most durable. Previous work on Pt (hkl) electrodes by Markovic et al.[1] show that most of the peroxide generation was caused by Pt (111) surface and very little, if none, was due to the other two dominant phases. Not only is Pt (111) less durable it has almost 100% selectivity for catalyzing H_2O_2 formation. By eliminating this unwanted, unstable configuration, one can increase the durability and decrease the amount of catalyst presently used in fuel cells.

7.2. Objectives and Significance of Work

The objectives of the proposed work are

a. To establish a concrete mechanism for the degradation of proton exchange membrane electrode assembly

b. To isolate the various processes those contribute to such a mechanism

c. To design experiments to study each process independently and to estimate parameters as a function of temperature, potential and humidity pertinent to fuel cell operation

d. To use the parameters in developing a macroscopic membrane degradation model. This will act both as a screening tool to select new materials as well to estimate the lifetime and degradation characteristics of existing fuel cell MEAs.

7.3. Plan of Work

1. Isolating the effect of Pt alloys on membrane durability

In the durability studies with single sided MEAs, there are many variables that are interdependent on one another such as the local potential, the type of catalyst (Pt, Pt alloys etc),and the type of gas (H_2, O_2, N_2 etc). The following configurations (based on Pt/C catalyst) will be studied. The main indicator of degradation will be the amount of fluorine and hydrogen peroxide collected in the effluent water from both electrodes.

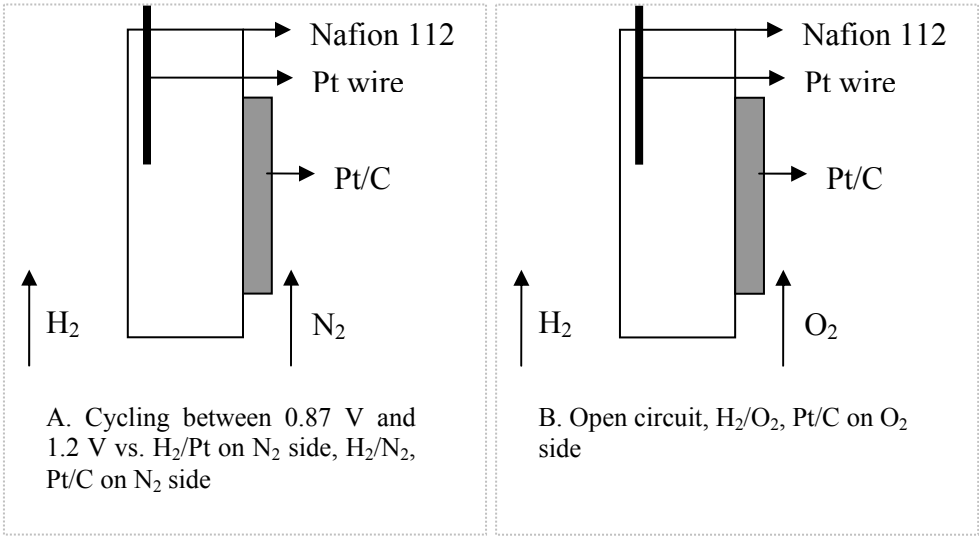

A. Cycling between 0.87 V and 1.2 V vs. H_2/Pt on N_2 side, H_2/N_2, Pt/C on N_2 side

B. Open circuit, H_2/O_2, Pt/C on O_2 side

Configuration A: Cycling the electrode between 0.87 V and 1.2 V vs. H_2/Pt with N_2 flowing over it causes Pt dissolution and re-precipitation on the support. The ECA change will be studied.

Configuration B: This is OCV decay experiment on a single sided MEA. Pt dissolution and passivation occurs. Migration into the membrane followed by chemical platinization may occur.

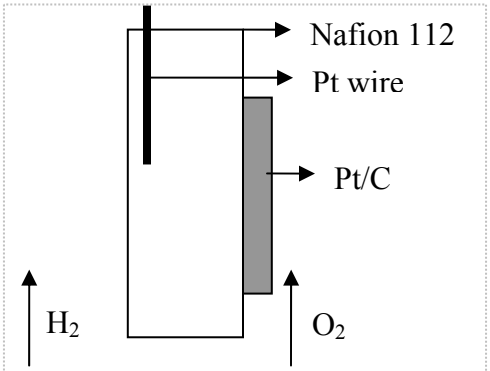

C. 0.6 V vs. H_2/Pt on O_2 side, H_2/O_2, Pt/C on O_2 side

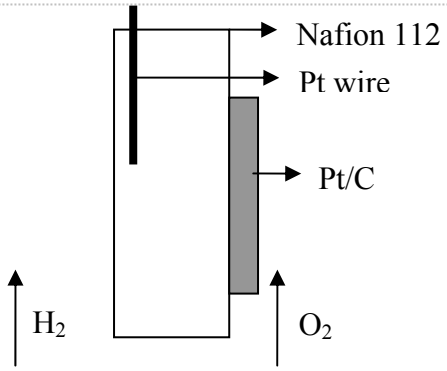

D. Cycling between OCV and 0.6 V vs. H_2/Pt on O_2 side, H_2/O_2, Pt/C on O_2 side

Configuration C: This is equivalent to applying a load on a single sided MEA. Since there is no anode to support hydrogen oxidation reaction, very low currents will be seen. The main objective is to form peroxide on the electrode on the O_2 side.

Configuration D: This is equivalent to load cycling test on a single sided MEA.

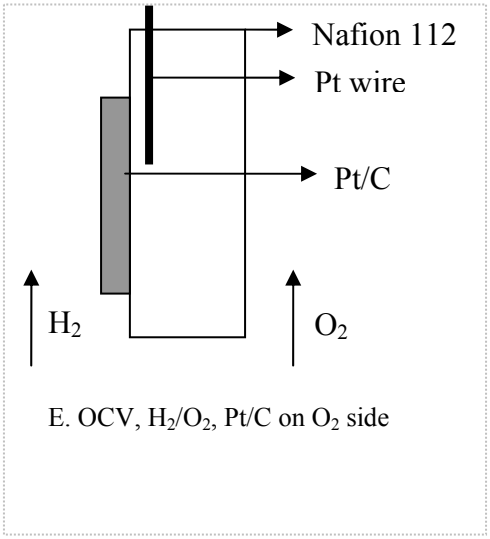

E. OCV, H_2/O_2, Pt/C on O_2 side

Configuration E: This configuration favors peroxide formation on the anode side.

These five configurations can be tested with Pt alloys catalysts also (PtCo/C, PtIrCo/C etc).

2. Using photo catalysts to generate hydroxyl radicals

TiO_2 generates highly active hydroxyl radicals in aqueous media in the presence of UV radiation. It is proposed to make single-sided MEAs with TiO2 catalysts suspended with Nafion® ionomer and a Nafion® 112 membrane and shine UV radiation using a solar-simulator in an aqueous media. This generates hydroxyl radicals in the membrane-TiO_2 electrode interface. TiO_2 loading on the electrode, the intensity and the duration of the UV radiation will be controlled. The water sample will then be analyzed for fluorine content.

This experiment will either prove or disprove the direct radical attack hypothesis currently speculated to play an important role in the membrane degradation mechanism by the fuel cell community.

7.4. References

1. N. M. Markovic, H. A. Gasteiger and P. N. Ross, *J. Electrochemical Society*, **144,** 1591 (1997).

Bibliography

Albery, W. J. and Hitchman, M. L., *Ring-Disc Electrodes*, Clarendon Press, Oxford (1971).

Appleby, A. J., *Energy*, **11**, 13 (1986).

Anderson, A. B. and Albu, T. V., *J. Electrochem. Soc.,* **147**, 4229 (2000).

Antoine, O. and Durand, R., *J. Applied Electrochemistry,* **30**, 839 (2000).

Balliet, R. J. and Reiser, C. A., *U. S. Pat. Appl.* 2004/0001980.

Balliet, R. J., Reiser, C. A., Patterson, T. W. and Perry, M. L., *U. S. Pat. Appl.* 2004/0126628.

Bekkedahl, T. A., Bregoli, L. J., Breault, R. D., Dykeman, E. A., Meyers, J. P., Patterson, T. W., Skiba, T., Vargas, C., Yang, D. and Yi, J. S., *U. S. Pat. Appl.* 2004/0081866.

Bett, J. A. S., Cipollini, N. E., Jarvi, T. D. and Breault, R. D., *U. S. Pat. Appl.* 2004/0126644.

Broka, K. and Ekdunge, P., *J. Appl. Electrochem.,* **27**, 117 (1997).

Campbell, C. J., and Laherrere, J. H., *Scientific American*, , p. 80, March 1998.

Chang, J. –R., Chang, S. –L. and Lin, T. –B., *J. Catalysis,* **169**, 338 (1997).

Chang, J. –R. and Chang, S. –L., *J. Catalysis,* **176**, 42 (1998).

Chin, D. –T. and Howard, P. D., *J. Electrochem. Soc.,* **133**, 2447 (1986).

Clark, T. in *DoE Hydrogen Program – FY 2004 Progress Report*, p. 493.

Claude, E., Addou, T., Latour, J.-M. and Aldebert, P., *J. Applied Electrochemistry*, **28**, 57 (1998).

Cleghorn, S., Kolde, J. and Liu, W., *Handbook of Fuel Cells*, **3**, 566 (2004).

Contractor, A. and Hira Lal, *J. Electroanal. Chem.* **96**, 175 (1979).

Curtin, D. E., Lousenberg, R. D., Henry, T. J., Tangeman, P. C. and Tisack, M. E., in *Proceedings of the 2nd European Polymer Electrolyte Fuel Cell Forum*, **1**, p. 25-35 (2003).

Curtin, D. E., Lousenberg, R. D., Henry, T. J., Tangeman, P. C. and Tisack, M. E., *J. Power Sources*, **131**, 41 (2004).

Damjanovic, A. and Hudson, G., *J. Electrochem. Soc.,* **135**, 2269 (1988).

Darling, R. and Meyers, J., *J. Electrochem. Soc.*, **150**, A1523 (2003).

Donini, J. C., Chuang, K. T., Slavov, S. V., Sanger, A. R. and Stanic, V., *U. S. Patent* # 6,241,871 B1 (2001).

Donini, J. C., Petrovic, S. and Luinstra, E. A., *U. S. Patent* # 5,908,545 (1999).

Dumais, J. J., Cholli, A. L., Jelinski, L. W., Hedrick, J. L. and McGrath, J. E., *Macromolecules*, **19**, 1884 (1986).

Enayetullah, M. A., DeVilbiss, T. D. and Bockris, J. O'M., *J. Electrochem. Soc.,* **136**, 3369 (1989).

Endoh, S., Terazono, S., Widjaja, H. and Takimoto, Y., *Electrochem. Solid State Letters,* **7**, A209 (2004).

Escobedo, G, Madden, T. H. and Moore, R. B., *DOE Hydrogen Program FY 2005 Progress Report*, 761, (2005).

Farooque, M. and Fahidy, T. Z., *J. Electrochem. Soc.,* **124**, 1191 (1977).

Farooque, M. and Fahidy, T. Z., *J. Electrochem. Soc.,* **125**, 544 (1978).

Fedkiw, P. S. and Her, W., *J. Electrochem. Soc.,* **136**, 899 (1989).

Ferreira, P. J., La O', G. J., Shao-Horn, Y., Morgan, D., Makharia, R., Kocha, S. and Gasteiger, H., *J. Electrochem. Soc.,* **152**, A2256 (2005).

Frisch, L., *Sealing Technology*, **93**, 7 (2001).

Fuller, T., *Ph. D. Dissertation*, University of California, Berkeley (1989).

Gevantman, L. H., in *CRC Handbook of Chemistry and Physics*, 79th Edition, Lide, D. R., Editor, p. 8-86, CRC Press, New York (1998-99).

Gu, T., Lee, W-k., Van Zee, J. W. and Murthy, M., *J. Electrochem. Soc.,* **151**, A2100 (2004).

Guo, Q., Sethuraman, V. A. and White, R. E., *J. Electrochem. Soc.,* **151**, A983 (2004).

Haug, A. T. and Protsailo, L. V., "Nafion® Oxygen Permeability at Elevated Temperature and Reduced Relative Humidity", manuscript submitted to *J. Electrochem. Soc.*, (2006).

Haug, A. T., Protsailo, L. V., Modi, S., Sethuraman, V. A. and Motupally, S., "Characterization of Membranes and Catalysts for High Temperature PEM Fuel Cells", High Temperature Working Group, October 2005, Los Angeles, CA (DoE DE-FC36-02AL).

Haug, A. T. and White, R. E., *J. Electrochem. Soc.,* **147**, 980 (2000).

Hickner, M. A., Ghassemi, H., Kim, Y. S., Einsla, B. R. and McGrath, J. E., *Chem. Rev.,* **104**, 4587 (2004).

Healy, J., Hayden, C., Xie, T., Olson, K., Waldo, R., Brundage, M. and Gasteiger, H., and J. Abbott, *Fuel Cells*, **5**, 302 (2004).

Huang, C., Tan, K. S., Lin, J. and Tan, K. L., *Chem. Phys. Letters,* **371**, 80 (2003).

Huang, J. C., Sen, R. K. and Yeager, E., *J. Electrochemical Society*, **126**, 786 (1979).

Jalan, V. and Taylor, E. J., *J. Electrochemical Society*, **130**, 2299 (1983).

Kawase, M., Mugikura, Y. and Watanabe, T., *J. Electrochem. Soc,* **147**, 1240 (2000).

Kerres, J. A., *J. Membrane Sci.,* **185**, 3 (2001).

Kocha, S. S., in *Handbook of Fuel Cells – Fundamentals, Technology and Applications, Fuel Cell Technology and Applications,* **3**, Chapter 43, Vielstich, W., Gasteiger, H. A. and Lamm, A., Editors, John Wiley and Sons, Ltd., West Sussex, England (2003).

Knights, S. D., Colbow, K. M., St-Pierre, J. and Wilkinson, D. P., *J. Power Sources*, **127**, 127 (2004).

Kyu, T. and Eisenberg, A., *Proceedings of the American Chemical Society,* Chapter 6 (1982).

LaConti, A. B., Hamdan, M. and McDonald, R. C., in *Handbook of Fuel Cells: Fundamentals, Technology and Applications*, **3**, Vielstich, W., Lamm, A. and Gasteiger, H. A., John Wiley and Sons, Ltd., New York (2003).

Lakshmanan, B., Sethuraman, V. A. and Weidner, J. W., "Adsorption, Desorption and Rearrangement Kinetics of Linear and Bridge Bonded CO on Pt/C", submitted to *J. Electrochem. Soc*., (2006).

Lamy-Pitara, E., Bencharif, L. and Barbier, J., *Electrochemica Acta,* **30**, 971 (1985)

Lamy-Pitara, E., Tainon, Y., Beden, B. and Barbier, J., *J. Electroanal. Chem.,* **279**, 291 (1990).

Landsman, D. A. and Luczak, F. J., in *Handbook of Fuel Cells: Fundamentals, Technology, and Applications*, **4**, Vielstich, W., Lamm, A. and Gasteiger, H. A., John Wiley and Sons, New York, Chapter 65 (2003).

Liu, R., Her, W-H. and Fedkiw, P. S., *J. Electrochem. Soc.,* **139**, 15 (1992).

Liu, W. and Zuckerbrod, D., *J. Electrochem. Soc.,* **152**, A1165 (2005).

Loučka, T., *J. Electroanal. Chem.,* **31,** 319 (1971).

MacDonald, R. C., Mittelsteadt, C. K. and Thompson, E. L., *Fuel Cells*, **4**, 208 (2004).

Markovic, N. M., Gasteiger, H. A. and Ross, P. N., *J. Electrochemical Society*, **144,** 1591 (1997).

Markovic, N. M., Grgur, B. N. and Ross, P. N., J. Physical Chemistry B, **101**, 5405 (1997).

Mathias, M. F., Makharia, R., Gasteiger, H. A., Conley, J. J., Fuller, T. J., Gittleman, C. J., Kocha, S. S., Miller, D. P., Mittelsteadt, C. K., Xie, T., Yan, S. G. and Yu, P. T., *Electrochem. Soc. Interface,* **14** (3), 24 (2005).

Mathieu, M. and Primet, M., *Applied Catalysis,* **9**, 361 (1984).

Mauritz, K. A. and Moore, R. B., *Chemical Reviews,* **104**, 4535 (2004).

Myers, J. P., "Development of High Temperature Membranes and Improved Cathode Catalysts", *DoE Hydrogen, Fuel Cells and Infrastructure Technologies Review*, May 2004.

Meyers, J. P. and Darling, R. M., *J. Electrochem. Soc.,* **153**, A1432 (2006).

Mittal, V., Kunz, H. R. and Fenton, J. M., "Factors accelerating membrane degradation rate and underlying degradation mechanism in PEMFC", Abstract #1192, *208th Meeting of the Electrochemical Society*, Los Angeles, CA, October 16, 2005.

Mohtadi, R., Lee, W-K., Cowan, S., Van Zee, J. W. and Murthy, M., *Electrochem. Solid State Letters,* **6,** A272 (2003).

Motupally, S. and Jarvi, T. D., Abstract #1167, *208th Meeting of the Electrochemical Society*, October 16-21, Los Angeles, CA.

Mukerjee, S. and Srinivasan, S., *J. Electroanalytical Chemistry*, **357**, 201 (1993).

Murthy, M., Esayian, M., Hobson, A., MacKenzie, S., Lee, W-K. and Van Zee, J. W., *J. Electrochem. Soc.,* **148**, A1141 (2001).

Murthy, M., Esayian, M., Lee, W-K. and Van Zee, J. W., *J. Electrochem. Soc.,* **150**, A29 (2003).

Murthi, V. S., Urian, R. C. and Mukerjee, S., *J. Phys. Chem. B*, **108**, 11011 (2004).

Najdekar, E. and Bishop, E., *J. Electroanal. Chem.,* **41**, 79 (1979).

Noshay, A. and Robeson, L. M., *J. Applied Polymer Science*, **20**, 1885, (1976).

Okada, T., in *Handbook of Fuel Cells: Fundamentals, Technology, and Applications*, **3**, Chapter 37, Vielstich, W., Gasteiger, H. A. and Lamm, A., Editors, John Wiley and Sons, Ltd., New York (2003).

Okada, T., Ayato, Y., Yuasa, M. and Sekine, I., *J. Phys. Chem. B*, **103**, 3315 (1999).

Okada, T. and Xie, G., *Electrochim. Acta*, **43**, 3741 (1998).

Paal, Z., Matusek, K. and Muhler, M., *Applied Catalysis,* **9**, 361 (1984).

Panchenko, A, *Dipl.-Chem.*, Institute für Phzsikalische Chemie der Universität Stuttgart, October 2004.

Paulus, U. A., Schmidt, T. J., Gasteiger, H. A. and Behm, R. J., *J. Electroanal. Chem.,* **495**, 134 (2001).

Paulus, U. A., Wokaun, A. A., Scherer, G. G., Schmidt, T. J., Stamenkovic, V., Markovic, N. M. and Ross, P. N., *Electrochim. Acta,* **47**, 3787 (2002).

Paulus, U. A., Wokaun, A. A., Scherer, G. G., Schmidt, T. J., Stamenkovic, V., Radmilovic, V., Markovic, N. M. and Ross, P. N., *J. Phys. Chem. B,* **106**, 4181 (2002).

Perry, R. H. and Green, D. W., *Perry's Chemical Engineer's Handbook*, 7th Edition, McGraw Hill (1997).

Pourbaix, M., *Atlas of Electrochemical Equilibria in Aqueous Solutions,* p. 453, National Association of Corrosion Engineers, Houston, Texas (1979).

Protsailo, L. V., "Development of High-Temperature Membranes and Improved Cathode Catalysts", *DoE Hydrogen Program FY 2005 Progress Report*, p. 743.

Protsailo, L. V., "Development of High Temperature Membranes and Improved Cathode Catalysts for PEM Fuel Cells", *DoE Hydrogen Program Review*, Arlington, VA, May 13-16 (2006).

Ralph, T. R. and Hogarth, M. P., *Platinum Met. Rev.*, **46**, 3 (2002).

Reid, R. C., Prausnitz, J. M. and Sherwood, T. K., *The Properties of Gases and Liquids*, McGraw Hill Inc., New York (1977).

Reiser, C. A., Bregoli, L., Patterson, T. W., Yi, J. S., Yang, J. D., Perry, M. L. and Jarvi, T. D., *Electrochem. Solid State Letters*, **8**, A273 (2005).

Reiser, C. A., Yang, D. and Sawyer, R., *U. S. Pat. Appl.* 2003/0134164.

Reiser, C. A., Yang, D. and Sawyer, R., *U. S. Pat. Appl.* 2003/0134165.

Reiser, C. A., Yang, D. and Sawyer, R., *U. S. Pat. Appl.* 2002/0076583.

Rotated Ring-Disk Electrodes: DT21 Series, Pine Instrument Company, Raleigh, NC 27617.

Sakai, T., Takenaka, H. and Torikai, E., *J. Electrochem. Soc.,* **133**, 88 (1986).

Schmidt, T. J., Gasteiger, H. A., Stäb, G. D., Urban, P. M., Kolb, D. M. and Behm, R. J., *J. Electrochem. Soc.,* **145**, 2354 (1998).

Schmidt, T. J., Paulus, U. A., Gasteiger, H. A. and Behm, R. J., *J. Electroanal. Chem.*, **508**, 41 (2002).

Schulze, M., Knöri, T., Schneider, A. and Gülzow, E., *Journal of Power Sources*, **127**, 222 (2004).

Sethuraman, V. A., Balasubramanian, S., Wise, L. A. and Weidner, J. W., *Electrochemical Society Transactions,* **1** (8), 111 (2006).

Sethuraman, V. A., Weidner, J. W., Haug, A. T., Motupally, S. and Protsailo, L. V., "Effect of Water Activity and Oxygen Concentration on H_2O_2 formation on Pt/C", submitted to *J. Electrochem. Soc.*, (2006).

Sethuraman, V. A., Weidner, J. W., Haug, A. T., Modi, S. and Protsailo, L. V., "Effect of Humidity on the Durability of PEM Fuel Cells. II. H_2O_2 Kinetics on Pt Alloys", Abstract #451, *210th Meeting of the Electrochemical Society*, Cancun, Mexico, October 31, 2006.

Sidik, R. A. and Anderson, A. B., *J. Electroanal. Chem.,* **528**, 69 (2002).

Soto, H. J., Lee, W-K., Van Zee, J. W. and Murthy, M., *Electrochem. Solid State Letters*, **6**, A133 (2003).

Stamenkovic, V., Schmidt, T. J., Ross, P. N. and Markovic, N. M., *J. Electroanalytical Chemistry*, **554**, 191 (2003).

Stamenkovic, V., Schmidt, T. J., Ross, P. N. and Markovic, N. M., *J. Physical Chemistry B*, **106**, 11970 (2002).

St-Pierre, J., Wilkinson, D. P., Knights, S. and Bos, M. L., *J. New Mater. Electrochem. Systems,* **3**, 99 (2000).

Takenaka, H., Torikai, E., Kawami, Y. and Wakabayashi, N., *Int. J. Hydrogen Energy*, **7**, 397 (1982).

Thompsett, D., in *Handbook of Fuel Cells: Fundamentals, Technology, and Applications*, **3**, Vielstich, W., Gasteiger, H. A. and Lamm, A., Editors, John Wiley and Sons, New York, Chapter 37 (2003).

Trasatti, S. and Petrii, O. A., *Pure and Appl. Chem.,* **63**, 711 (1991).

Uribe, F. A. and Zawodzinski, Jr., T. A., Abstract #339, *200th Meeting of the Electrochemical Society*, San Francisco, Fall 2001.

United States Department of Energy, Energy Efficiency and Renewable Energy: Hydrogen, Fuel Cells and Infrastructure Technologies Program, Website - http://www.eere.energy.gov/hydrogenandfuelcells/

Walling, C., *Accts. Chem. Research*, **8**, 125 (1975).

Wang, Y. and Balbuena, P. B., *J. Chem. Theory Comput.,* **1**, 935 (2005).

Wang, Y., Yan, H. and Wang, E., *J. Electroanal. Chem.,* **497**, 163 (2001).

Wang, Y., Yan, H. and Wang, E., *Sensors and Actuators B,* **87**, 115 (2002).

Wang, F., Hickner, M., Kim, Y. S., Zawodzinski, T. A. and McGrath, J. E., *J. Membrane Science*, **197**, 231 (2002).

Watanabe, M., Tsurumi, K., Mizukami, T., Nakamura, T. and Stonehart, P., *J. Electrochemical Society*, **141**, 2659 (1994).

Wilkie, C. A., Thomsen, J. R. and Mittleman, M. L., *J. Appl. Poly. Sci.*, **42**, 901 (1991).

Wilkinson, D. P. and St-Pierre. J., in *Handbook of Fuel Cells: Fundamentals, Technology, and Applications*, **3**, 647-663, Vielstich, W., Gasteiger, H. A. and Lamm, A., Editors, John Wiley and Sons, New York, (2003).

Wilson, M. S., Garzon, F. H., Sickafus, K. E. and Gottesfeld, S., *J. Electrochem. Soc.,* **140**, 2872 (1993).

Yang, D., Steinbugler, M. M., Sawyer, R. D., Van Dine, L. L. and Reiser, C. A., *U. S. Pat. Appl.* 2003/0129462.

Yeo, S. C. and Eisenberg, A., *J. Applied Polymer Sci.,* **21,** 875 (1977).

Yu, P., Pemberton, M., and Plasse, P., *Journal of Power Sources*, **144**, 11 (2005).

Zawodzinski, T., Neeman, M., Sillerud, L. and Gottesfeld, S., *J. Phys. Chem.,* **95**, 6040 (1991).

Zečević, S. K., Wainright, J. S., Litt, M. H., Gojković, S. Lj. and Savinell, R. F., *J. Electrochem. Soc.,* **144**, 2973 (1997).

Appendix A

MEA Fabrication and PEMFC Conditioning

Introduction

All methods described involve taking powdered catalyst (typically Pt, Ru or Pt:Ru on carbon), making it into an ink and then applying that ink onto a substrate (GDL or a decal). Several different variations are described here that can be used depending upon the type of MEAs you wish to make. These variations include making the inks in sodium or protonated form, using Pt, Ru, Pt:Ru, or some other catalyst, applying the ink to a Teflon decal or a gas diffusion layer (GDL), and applying the ink using paintbrush, airbrush, or Meyer rod. The MEA may be built using either a dry or wet membrane.

The goal in all cases is to make an MEA of the desired catalyst loading and uniform catalyst distribution and that gives highly reproducible performance. If an MEA using a membrane other than Nafion is used, the appropriate literature should be consulted concerning glass transition temperature, effects of wetting the membrane, appropriate chemicals for dissolving the membrane into solution (for catalyst inks), etc.

Materials Required

- 2 templates
- One 3.2 x 3.2 cm to cut the Teflon backings.
- One 6 x 6 cm to cut the Nafion 117 membranes
- Nafion 117

- Teflon coated fiberglass (made by laminating together 2 products Chemfab 10mil Premium and Flouroglass 6TB)
- NaOH
- Catalyst (20 % Pt/C from E-Tek)
- Nafion 112 solution (5%)
- Roller bar
- Stirring rod
- Stirring plate
- Airbrush
- Meyer Rod
- Carver Heated Press (Hydraulic Model #3925; Heater: 230V, 2.3kW, 13A)

Preliminaries - Coating Tools

One of three different tools may be used to coat the catalyst ink on the substrate: a paintbrush, airbrush, or Meyer Rod. All offer advantages and drawbacks. The paintbrush is simple to use and clean, however, it does not result in a uniform catalyst application. The paintbrush cannot be used on a GDL because the ink typically sinks in to the GDL to some extent, further preventing the user from ensuring uniformity of application.

The airbrush can be used to create far more uniform electrodes. It may be used on almost any substrate. And, unlike the other two methods, if the desired loading is not achieved on the first try, it may be used a second time. The drawbacks to using the airbrush are that it must be meticulously cleaned, replacement parts should be available

(hence buy a common product), and there is training required in order to determine the best ratio of ink to air, height at which the sprayer is held so as to avoid 'pooling' of the ink on the substrate. The sprayer must also be moved in a uniform manner over the substrate, introducing some non-uniformity in to the catalyst layer thickness.

The Meyer rod offers very good uniformity and reproducibility in applying catalyst inks. It can be used for any substrate. However, it can only be used once. If the loading is too low, an airbrush must be used to add additional catalyst. The correct bar (2 to 8 mm in thickness) must be known beforehand or determined. Another potential drawback is that often with high loadings on Teflon decals, cracking of the catalyst electrode will occur when the catalyst is applied in a single application. Despite these drawbacks, the Meyer rod offers a safe, simple method of applying uniform catalyst coatings.

It is recommended by the author that both a Meyer rod and airbrush be on hand during MEA preparation.

Preparing the Membranes

All Nafion membranes should be cut to the desired size. Most test cells are roughly 8 x 8 cm, so a membrane of 6 x 6 to 8 x 8 cm is sufficient. Cut membranes should be boiled for a minimum of 90 minutes in 1 N HNO_3/H_2SO_4 to ensure protonation. (Note: Only those membranes that are not in the protonated form already are recommended to be boiled in acid. If the membrane as received from the vendor is already in a protonated form, then this step may be skipped).[2] They should then be washed in DI water a minimum of 5 times before drying.

Should the MEA manufacture process be performed using inks and membranes in sodium form, the same process should be performed, except substituting 1 N NaOH for 1 N HSO_3/H_2SO_4. Unused membranes should be stored in DI water until time of use.

Decal/GDL preparation

The Teflon decal sheets are made by laminating together 2 products Chemfab 10mil Premium and Flouroglass 6TB. A dye is typically used to cut the sheets into appropriate sizes (5, 10, 25, 50 cm^2). A minimum of 8 Teflon squares should be cut, enough to make four MEAs. If applying catalyst to a GDL, there are several types of GDL to choose from (ETEK ELAT, Zoltek, Toray) that fall into two primary categories: papers and cloths. Both types of GDLs should have a microlayer of hydrophobic carbon on one side of the GDL. This is the side upon which the catalyst ink is applied. The microlayer offers a more uniform, less porous surface upon which to apply the catalyst. The GDL need not be cut into squares before ink is applied, rather it is more time efficient to apply the catalyst ink to a larger, single piece of GDL that after application and drying, may be cut into individual catalyzed GDLs.

Making the Ink

Obtain and label a small vial. Place a small magnetic stirrer into the vial. Obtain a Platinum/Carbon granular mixture (E-Tek, 20% Pt. by wt.), a solution of Nafion (Aldrich, 5 wt. %), Glycerol (Aldrich) and distilled water. Tare the small vial. Crease a weigh paper and place it on the scale. Tap out the goal weight (see Eq. 1) of Pt/C onto the paper. Place another weigh paper under the vial to catch any stray Pt/C. Then use the crease to slowly pour the mixture into the vial. Anything that misses the vial should be collected and tapped into the vial. Carefully flow an inert gas (nitrogen, argon etc) into

the glass vial to displace air. This is to avoid any unwanted combustion caused due to mixing an alcohol with an active catalyst in the presence of atmospheric oxygen. Caution should be used not to blow any catalyst powder off of the vial.[1] Nafion, water, and Glycerol should then be pipetted into the tarred vial until each reaches its goal weight. The Glycerol will take a big sopper because it is so thick. Try to keep the wrist steady while adding the solutions to avoid getting them on the outside of the vial or on the balance itself. After everything has been added place the ink on a magnetic stirrer for about 8 hours.

Painting/Coating

Prior to applying the ink, all substrates (decals, GDLs) must be weighed. The amount of dry catalyst-ink that must be applied to achieve the desired catalyst loading should also be calculated using the following formula:

$$\text{Goal}\left[\text{mg}\right] = \frac{\text{Target Loading}\left[\text{mg}/\text{cm}^2\right]}{\left(\frac{\text{Nafion wt. \%}}{100\%}\right)\left(\frac{\text{\% Pt on C}}{100\%}\right)} \times \text{Substrate Area}\left[\text{cm}^2\right] \qquad [0\text{-}1]$$

These numbers should be entered in to the MEA manufacture worksheet and can be used to determine whether more ink must be added.

A paintbrush, airbrush, or Meyer rod may be used to apply the ink. In interest of uniformity, as well for ease of application, the latter two tools should be used. Both an airbrush and Meyer rod board and rods may be bought for under $100.

The paintbrush is limited to use with the decals. When using the paintbrush, several layers may need to be applied to reach the desired loading. Each layer must be appropriately dried before subsequent loadings are applied.

Compressed air should not be used to spray the catalyst ink. An inert gas (nitrogen or argon) bottle may be used to spray the catalyst onto the GDLs. This is to avoid contamination from the compressed air (usually 'Industrial' quality) and to avoid Pt oxidation and combustion. When applying the ink to decals or GDLs, take care to not get ink on the backside of the substrate. This will increase overall loading, but the catalyst on the backside will work to produce current. In the case of decals, excess ink may be wiped from the backside. In the case of the GDLs, catalyst may be applied to a GDL larger than the final product, and then the edges containing catalyst on the backside may be trimmed off.

Drying

When using proton-based inks, the drying process is simple. Dry substrates at 105 – 110^{o}C for 10 minutes to remove all alcohols from the ink. Inks of sodium form contain glycerol, which evaporates only above roughly 160 ^{o}C at ambient pressure. These substrates may be dried in an oven at 110 ^{o}C initially for ~ 20-30 minutes, then at 180 ^{o}C for 10 minutes to remove any glycerol. Alternatively, place the dish in a vacuum oven and dried at lower temperatures 120-150 ^{o}C under vacuum. Close the purge valve and open the pressure valve so that the pressure rises to between 40-60 psi. At these temperatures, drying requires 30 – 60 minutes.

Loadings

At this point, the dried decals/GDLs must be weighed and catalyst loadings calculated. If the loadings are less than the goals, more ink may be applied through brushing or airbrushing.

Pressing

Three factors/variables that affect pressing are: Pressure (or force applied per unit GDL or decal area), temperature and membrane water content.

⇨ Pressure can exceed the recommended values as long as there are appropriate shims or gaskets to protect the MEA components from getting over-pressed.

⇨ Temperature and membrane water content are variables dependent on each other.

⇨ Presence of water affects the glass transition temperature of Nafion (T_g). The more the water, the lower is the glass transition temperature of Nafion. Pure water boils at 100 ^oC and completely dry Nafion phase-transitions at ~145 ^oC becoming more fluid above 165 ^oC. Depending on the water content, Nafion's T_g can be anywhere between these temperatures (i.e., 100 – 145 ^oC).

The two methods and the recommended pressing procedures are given below:

Decal transfer method

Assemble the decals, membrane (Nafion) and cover sheets/shims/gaskets (usually Teflon) as shown in Figure 0-1 between steel plates to be pressed in the hot press (Carver). Select Teflon or polyglass gaskets with same thickness as the decals. The decals and the gaskets/shims should not be compressible. It is preferable to have two thicker steel plates (1/2" thick recommended) with a socket/hole in one of them to host a thermocouple probe. Also, the steel plate dimensions should match the hot-plate (Carver) dimensions (6" by 6" for the current version in the lab-2B36) to avoid positioning problems. For the protonated case using decals, the press should be set to 155 ^oC (293 F). Make sure that the anode and cathode decals are aligned and in the center part of the steel plate and the membrane is relatively dry. For this decal transfer method, a pressure of 40

lbs/cm^2 should be used. Pressure can exceed up to 120% of the recommended value but not more than that. The MEA components should then be pressed for 2 minutes and quickly removed from the press. The time should be measured from the point when the steel plate reaches the set temperature, as read by the thermocouple, and not from when the steel plates are placed in the hot-press. For optimum transference, the MEA should be cooled under pressure (place between to flat metal weights, or something equivalent). After 5 minutes, remove assembly and place in freezer for further cooling. The freezer acts to further reduce the 'stickiness between the decals and the catalyst.

GDL method

Teflon or polyglass sheets with 80% thickness as the GDLs should be used as gaskets or shims. These materials should not be compressible/elastic. While assembling the membrane, GDLs (with catalyst), and Teflon gaskets, water maybe used to avoid Nafion-wrinkling. Using water introduces stickiness and helps one to align the components better. For the protonated case using GDLs, the press should be set to 145 ^{o}C (293 F). Pressing time should be 2 minutes from when the plates reach this temperature.

It is highly recommended that an O-ring be used along the edges of the steel plate. This o-ring in conjunction with a very thin Teflon sheet, the size of the steel plate (6" by 6"), on both sides helps keep the water (as steam) inside. Maintaining water helps protect the MEA from over-heating. The pressing time may be increased to as long as 15 minutes in this case. This process is sometimes referred to as *steam bonding*.

Summary

- In both cases (decal-transfer and GDL method) the membrane and ink should be in the same form (protonated or sodium).

- Ink on decals, Ink and Nafion in sodium form: press with membrane **dry** at 165^{o}C for 2 minutes at 40 lbs/cm^{2}.
- Ink on decals, Ink and Nafion in protonated form: press with membrane **dry** at 155^{o}C for 2 minutes at 40 lbs/cm^{2}.
- [2]Ink on GDLs, Ink and Nafion in proton form: press with membrane ***wet*** at 145^{o}C for 2 minutes at minimal pressure (25 lbs or less per cm^{2}). Using excess pressure will crush the GDL and compromise its hydrophobicity. No excess cooling needed because no peeling is needed when applying catalyst to GDLs.
- Alternate membrane: Pressing temperature must be varied to exceed glass transition temperature, but not cause permanent damage to the membrane (loss of mass).

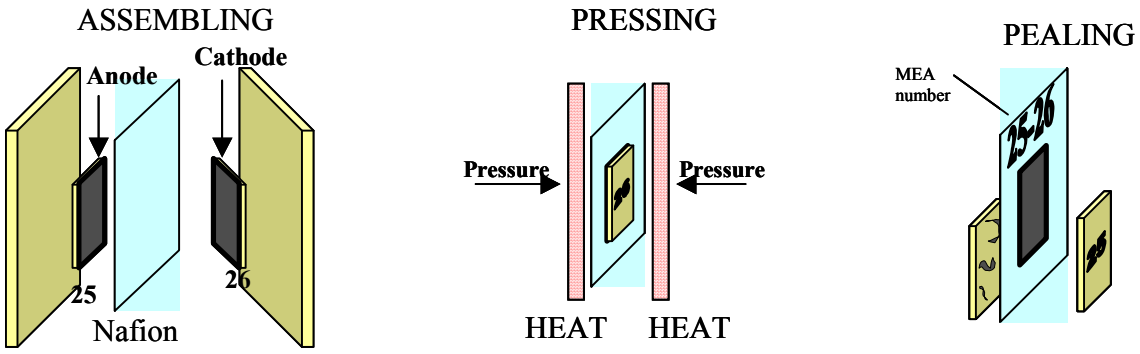

Figure 0-1 The electrodes are painted and the MEA is assembled as shown in (a). The assembly is then pressed under heat (b) for 15 minutes. After cooling, the Teflon blanks are pealed from the MEA in (c). The numbering of the electrodes (25 and 26) is intended to show the labeling scheme of each MEA. Combining electrodes #25 and #26 on the membrane results in MEA #25-26.

Peeling the Blanks

Remove the top cover sheet from the membrane. Slowly, peel the Teflon square back from the membrane by curling it backward with the thumb and forefinger. Do not pull the blank off; instead curl it back so that a greater transfer of ink to the Nafion membrane will occur. Peel at alternating corners until the blank has been totally removed from the membrane. Repeat the peeling process with the second blank, being even more careful to touch the membrane as little as possible. Weigh the blanks and compute the percent transference using the following formula:

$$\text{Transference} = \frac{\text{Mass}_{\text{Teflon+catalyst}} - \text{Mass}_{\text{Teflon blank after pressing}}}{\text{Mass}_{\text{Teflon+catalyst}} - \text{Mass}_{\text{Empty Teflon blank}}} \qquad [0\text{-}2]$$

Transferences of much les than 95% are generally unacceptable as they lead to non-uniform ness of the electrode.

Re-protonation

Fully manufactured MEA in sodium form must be re-protonated. This is generally done by placing the MEA in 1 N Nitric acid solution set just below boiling (a strong boil may dislodge some catalyst). It should be boiled for a minimum of 90 minutes. After the boiling, the membrane is rinsed several times with DI water, and then dried.

Storing

Unused MEAs may be stored in Ziplock bags in DI water (to keep the membranes wrinkle-free and humidified).

Appendix B

Distribution of Linear and Bridge Sites Using CO Stripping

CO adsorption followed by stripping it by means of a cyclic voltammogram constitutes this experiment. Flow 50 SCCM H_2 on the cathode side and 100 SCCM N_2 on the anode side. Switch the N_2 flow to 500 ppm CO in N_2 (same flow rate). CO and N_2 have the same molecular mass and hence the same density. Therefore 'gas cal factors' in the mass flow controllers need not be changed. Flow CO in N_2 for as long as it takes to completely saturate the surface. The algorithm to measure the saturation time is given at the end of this appendix.

Complete saturation is impossible because there is always chemical desorption. Hence perform this experiment at room temperature where CO desorption is minimal (or assume zero desorption). Once the surface is completely saturated with CO, switch the gas flow back to N_2 and wait for the bulk to clear up. Perform a CV (same protocol as in ECA) and observe the dual peaks on the first cycle and no peaks on subsequent cycles. Subtract cycle two from cycle one. This results in a "baseline-corrected" CV. This baseline corrected CV is used in conjunction with TableCurve2D to deconvolute the two observed peaks.

Algorithm to measure time for CO to saturate the surface

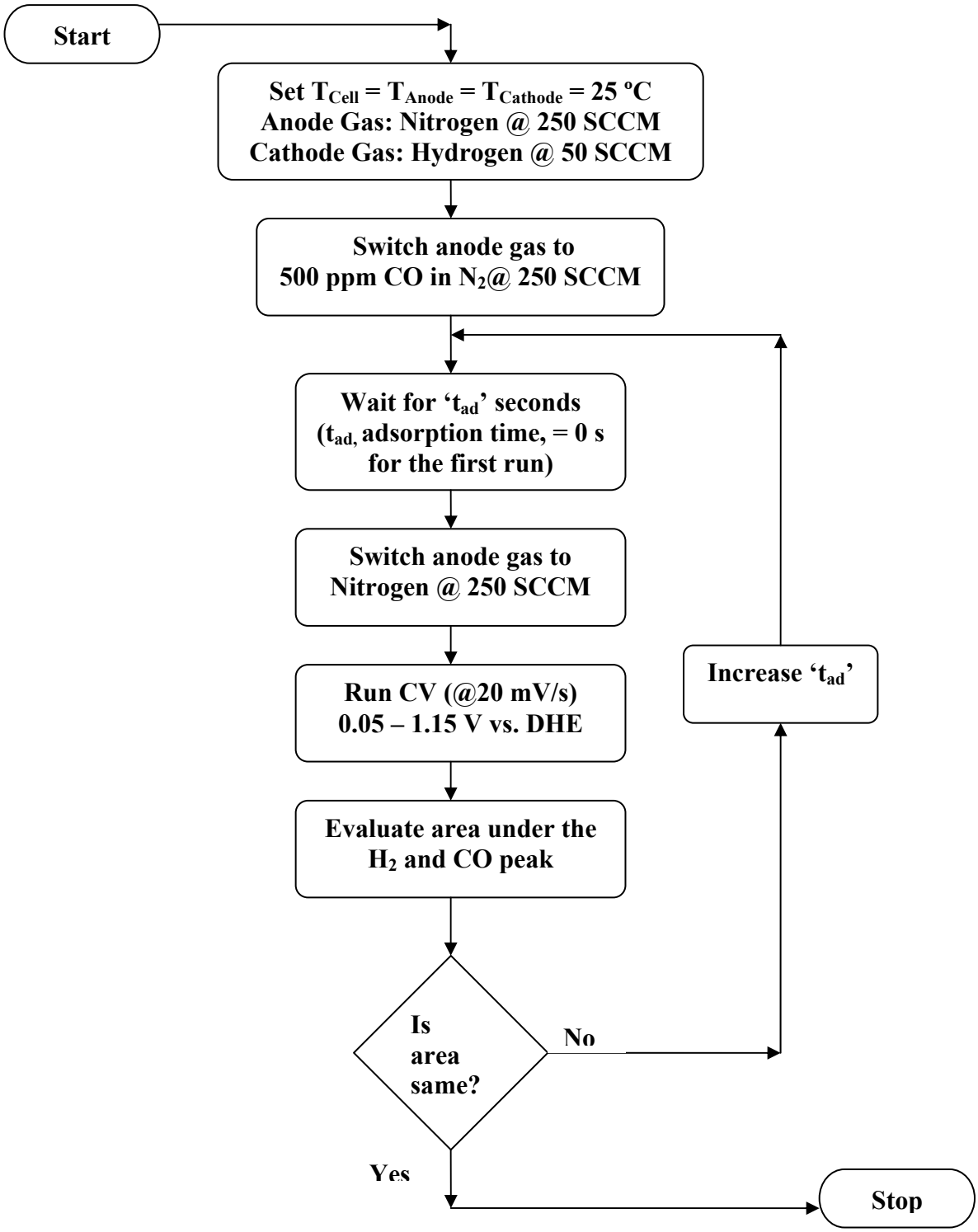

The following publications resulted from this dissertation (*in reverse chronological order*):

1. **V.A. Sethuraman**, J.W. Weidner. Analysis of Sulfur Poisoning on a PEM Fuel Cell Electrode. *Electrochimica Acta*, 55 (20), 5683-5694, 2010.
   DOI: 10.1016/j.electacta.2010.05.004

2. **V.A. Sethuraman**, J.W. Weidner, A.T. Haug, M. Pemberton, L.V. Protsailo. Importance of Catalyst Stability *vis-à-vis* Hydrogen Peroxide Formation Rates in PEM Fuel Cell Electrodes. *Electrochimica Acta,* 54 (23), 5571-5582, 2009.
   DOI: 10.1016/j.electacta.2009.04.062

3. **V.A. Sethuraman**, J.W. Weidner, A.T. Haug, L.V. Protsailo. Durability of Perfluorosulfonic Acid and Hydrocarbon Membranes. *Journal of The Electrochemical Society*, 155 (2), B119-B124, 2008.
   DOI: 10.1149/1.2806798

4. **V.A. Sethuraman**, J.W. Weidner, A.T. Haug, S. Motupally, L.V. Protsailo. Hydrogen Peroxide Formation Rates in a PEMFC Anode and Cathode. *Journal of The Electrochemical Society*, 155 (1), B50-B57, 2008.
   DOI: 10.1149/1.2801980

5. **V.A. Sethuraman**, J.W. Weidner, L.V. Protsailo. Effect of Di-phenyl Siloxane on the Catalytic Activity of Pt on Carbon. *Electrochemical and Solid-State Letters*, 10 (12), B207-B209, 2007.
   DOI: 10.1149/1.2787870